Approximation and interpolation of divergence free flows

Raúl F. Tempone

Montevideo, 1999

Master thesis dissertation
Advisor: Professor Jesper Oppelstrup[1]
Facultad de Ingeniería. Universidad de la República
Instituto de Matemáticas y Estadística Rafael Laguardia (IMERL)

[1]Numerical Analysis and Computing Science, The Royal Institute of technology (KTH), Stockholm

Abstract

In many applications like meteorology, atmospheric pollution studies, eolic energy prospection, estimation of instantaneous velocity fields, etc., one faces the problem of estimating a velocity field that is assumed to be incompressible. Very often the available data contains just a few and sparse velocity measurements and may be some boundary conditions imposed by solid boundaries. This inverse problem is studied here, and a new method to provide a numerical solution is presented. It is based on the Fourier transform, and allows to include the incompressibility constraint in a simple way, leading to an unconstrained least squares formulation, usually ill-posed.

The Tikhonov regularization is applied to stabilize the solution, as well as to provide some smoothness in the estimated flow. As a consequence, the numerical solution will generally approximate the measurements up to a threshold given by the size of the regularization parameter. Moreover, if the available velocity measurements come from a smooth velocity field then the numerical solution can be usually constructed using just a small number of Fourier terms.

The choice of the regularization parameter is done using the L curve method, balancing the perturbation and regularization contributions to the error.

Perturbation bounds (i.e.), bounds for the condition number of the matrix from the Least Squares formulation are included.

Numerical experiments with test problems and real data from the southern part of Uruguay are carried out. In addition, the results are compared with related work and the results are satisfactory.

Keywords: Incompressible flow, Mass consistent models, Inverse problems, Ill-posed problems, Regularization methods.

AMS subject classification: 65F20, 65F30, 76D99, 35R25.

Acknowledgments

I would like to thank:

My advisor Jesper Oppelstrup, for sharing his expertise and enthusiasm and for his never ending support.

Members of the numerical analysis group at C2M2, NADA for creating a nice and stimulating atmosphere to work in.

Carlos López Vázquez for posing the problem and kindly giving all the data for the Uruguayan case.

Those in the Facultad de Ingeniería who made this Master career a reality.

My wife Roxana for her love and encouragement in all times.

This work was partially supported by the Swedish Institute, and the Comisión Sectorial de Investigación Científica (CSIC) from Universidad de la República. Those grants are gratefully acknowledged.

Contents

1 Introduction **4**
- 1.1 Inverse problems . . . 4
- 1.2 Ill-posed problems . . . 5
- 1.3 Regularization methods . . . 6
- 1.4 Flow estimation . . . 6
- 1.5 Outline of the thesis . . . 7

2 Background **11**
- 2.1 Variational formulations on flow estimation . . . 11
- 2.2 Regularization . . . 15
  - 2.2.1 Singular Value Decomposition . . . 15
  - 2.2.2 Generalized Singular Value Decomposition . . . 17
  - 2.2.3 The L curve . . . 20
  - 2.2.4 Regularization methods . . . 23
  - 2.2.5 Choice of the regularization parameter. . . . 28

3 Formulation **29**
- 3.1 Basis functions . . . 31
- 3.2 Number of variables involved . . . 32
- 3.3 Size of the computational domain . . . 33
- 3.4 Some implementation issues . . . 34
  - 3.4.1 Formulation of the problem in real arithmetic . . . 34
  - 3.4.2 Treatment of the constraints . . . 34

4 Numerical examples **37**
- 4.1 Model problems . . . 38
  - 4.1.1 2D flow around a circular tube . . . 38
  - 4.1.2 2D flow over a ramp . . . 45
  - 4.1.3 Comparison with exact solution . . . 51
  - 4.1.4 2D Rankine vortex inside a tube . . . 53
- 4.2 Wind field in the southern zone of Uruguay . . . 59
  - 4.2.1 Comparison with the results from [35] . . . 64
- 4.3 Effect of the parameters . . . 67
  - 4.3.1 Experiments with noise in the data . . . 69

5 Conclusions **73**

A Singular values estimates **75**

B Convergence as $\epsilon_r \to 0^+$ **82**

C Reduction to the 2D case for flat topology **88**

D Other results in the Uruguayan case **89**
D.0.2 Flow results 89

Chapter 1

Introduction

This Master thesis considers the problem of finding a suitable mass consistent (i.e.), a divergence free velocity field given a finite number of measurements, and possibly, some boundary conditions. This is a *flow estimation* problem, which belongs to the family of *Inverse problems*, and in addition it is *Ill-posed*. To treat this last feature, we use a *regularization method* widely known as the Tikhonov regularization. In this introduction we try to clarify what we understand by this concepts, as well as give a brief outline of the work.

1.1 Inverse problems

In practical applications, the interpretation of experimental data yields important information. Some physical quantities do not render an easy way to be measured, and their effect is what we can only see. Beside this, linking the effect with the causes we usually have a mathematical model, which may be derived from physical laws or other sources. We now recall what a direct problem means: given a total description of the causes find the effect. On the other hand, finding the solution of an inverse problem involves determining unknown causes based on observation of their effects.

One can intuitively understand what the solution of a common inverse problem in human vision involves. When we see, we derive the size, the shape, the surface finish and the structure of an object from the scattering and absorption of the light perceived by the eye. As simple as it may seem, it involves a complex eye structure and the ability of the brain to process such information. This ability improves during learning processes, and it is necessary to use it with the information offered by the eyes to obtain good results.

There are different kind of Inverse problems. For example, some of them seek initial conditions in a known dynamical system, given its evolution during a certain period of time. A simple example is the cannon ball problem. The cannon man has to determine the shooting angle in order to hit a given target at a given position. Related to this are the boundary inverse problems, where we

want to find some missing boundary condition given the evolution of a system, possibly governed by a Partial Differential Equation (PDE). The inverse heat equation problem is a famous example, where we want to determine the income surface heat flux, given the evolution of the temperature profile inside a body.

Others are the classical parameter estimation, known as coefficient inverse problem. Linked with this is the kind of problem we deal with in this work. Given the observations, and a parametric model to explain them, the task is to find the parameters in some optimal way. For more examples of engineering applications from inverse problems see [1].

1.2 Ill-posed problems

Ill-posed problems appear frequently in science and engineering. Their theory is well developed in the literature [20], and still very much alive among various research groups. This sort of problems is usually related with three main difficulties:

1. The condition number of the problem is large.
2. Solving a "nearby" well conditioned problem derived from the first does not necessarily lead to an useful solution.
3. Care must be taken when imposing additional constraints.

The concept of ill-posedness goes back to Hadamard in the beginning of the twentieth century [14]. Shortly, the definition says that a problem is *ill-posed* if its solution is not unique or if it does not depend continuously on the data. This means that a tiny perturbation in the data may lead to a large change in the solution. It is widely known that nature offers a non ending source of perturbations, so we can hardly expect to compute with reasonable accuracy the solution of an ill-posed problem unless we add more information to determine the solution. Hadamard believed that ill-posed problems were rare in nature, somewhat artificial, but that is not the case. There is an enormous amount of applications, ranging from integral equations, image processing, tomography technology, astronomy, seismology, to atmospheric flow estimation.

For finite dimensional problems, the definition of ill-posedness becomes wider, allowing highly sensitive problems; but with continuous dependence of the solution with respect to the data. The classical example, which is also related with the subject of this thesis is the linear least squares problem

$$\min_x \|Ax - b\|_2, \qquad A \in \mathbb{R}^{m\times n} \tag{1.1}$$

Here we can say that problem (1.1) is *ill-posed* if the singular values of the matrix A decay "gradually" to zero and the ratio between the largest and the smallest singular value is large. The latter implies that the matrix A is ill conditioned, which means that the solution is very sensitive to perturbations. Typical examples of finite dimensional ill-posed problems are obtained from the

discretization of infinite dimensional ill-posed problems like partial differential equations and integral equations. We now remark what we said before about the computability of the solution of an ill-posed problem. The fact that a problem is ill-posed does not necessarily imply that we cannot compute an useful solution, but that we must be careful when designing the numerical method to find it.

1.3 Regularization methods

The main difficulty we face when solving an ill-posed problem is that its solution is essentially indeterminate. This indetermination happens in the subspace associated with small singular values, where any small perturbation, coming from data errors or roundoff error during computations is highly amplified.

Numerical regularization theory pursues to provide efficient and numerically stable methods for including proper side constraints, in order to achieve stabilized and at the same time valuable solutions.

A classical tool in this area is the Tikhonov regularization [33]. Keeping in mind the linear least squares problem (1.1), the Tikhonov regularization defines the regularized solution as the optimum of the following weighted problem:

$$x(\epsilon) = argmin \left\{ \|Ax - b\|_2^2 + \epsilon \|Bx\|_2^2 \right\} \tag{1.2}$$

where B is a linear operator. In addition, the null spaces of A and B intersect trivially. Intuitively, one can see that the term $\|Bx\|_2^2$ introduces more information into the problem. Its importance is weighted by a positive regularization parameter ϵ. The reader will realize that once we regularize with a strictly positive ϵ we lose the possibility of attaining $\|Ax - b\|_2 = 0$. However, by doing so we improve the stability of the problem. Typically, the operator B is the identity, or some difference discretization of a derivative operator. The choice of the B operator is motivated either by requiring small size in the solution or a smooth solution. When $B = I$ it is said that (1.2) is in *standard form*.
A large value of ϵ will favour the regularization term in the minimization, offering a large residual and a small value of $\|Bx\|_2$. The opposite behaviour, with small residual and large $\|Bx\|_2$ begins to dominate as we shrink the regularization parameter. A good regularization will offer a sufficiently small residual, and at the same time the obtained solution will be close to the solution of the unperturbed underlying problem. On the other hand, the regularization parameter governs the sensitivity of the regularized solution. Shrinking the regularization effect makes the problem more sensitive.

As the reader may have already guessed, the actual choice of the regularization parameter plays an important role in this subject. There are many methods for doing so, which will be discussed later on.

1.4 Flow estimation

In some applications like weather prediction, advection diffusion of pollutants in the atmosphere, eolic energy prospections or instantaneous velocity field estima-

tion, we face the problem of estimating a velocity field from given measurements. In Uruguay, the problem of eolic energy prospection has been analyzed by many people. As an example, the National Direction of Energy carried out site measurements in several points of the country. Nevertheless, it is uneconomical to do massive measurements all over the territory, so a common problem is to "extend" a few number of measurements, usually coming from metereological stations, in order to generate a flow approximation defined in all the territory. This problem belongs to the so called inverse problems, which are usually challengly ill-posed, since in general the amount of available data is not enough to determine a well defined solution. Therefore, it is important to incorporate as much as possible of the physical information we have a priori, like boundary conditions and when it is possible, the incompressibility property of the flow.

Flow estimation in the Uruguayan case has been already considered by Carlos López [35] following the work of Sherman [31] and Sasaki [30]. In that work the estimated flow is obtained roughly by first interpolating the data and then making a weighted L^2 projection of the interpolant onto a subspace of incompressible flows. The projection is carried out using a dual problem whose solution is under certain hypothesis the multiplier associated with the incompressibility constraint. The numerical technique includes various kind of interpolation and the solution of the stationary heat equation using finite elements.

In the present work we use a different formulation, based on the Fourier transform, which allows to substitute the incompressibility constraint without introducing a Dual Problem. The numerical technique is basically a Tikhonov regularization implemented as an unconstrained least squares problem.

1.5 Outline of the thesis

As we said before, this thesis considers the problem of finding a suitable mass consistent (i.e.), a divergence free velocity field, given a finite number of measurements, and possibly, some boundary conditions. With respect to our work, the approximate field that we propose is *a linear combination of fields which automatically satisfy the incompressibility relation* $u_x + v_y = 0$. The construction of such fields is based on the Fourier transform, which is able to handle the incompressibility constraint in a simple way.

The mentioned superposition is computed to meet the data set and the boundary conditions, which are enforced as equations to fulfill "inside" the computational domain. That computational domain is chosen as a square containing all the data locations, as sketched in Figure 1.1. Beside this, we impose periodic boundary conditions in the boundary of the computational domain. The data fitting problem is posed as an unconstrained linear least squares problem. We have chosen a Tikhonov regularization [33] to ensure some smoothness in the approximation and at the same time to stabilize the problem. Therefore, we are able to bound and control the matrix condition number of the least squares problem, roughly in terms of a regularization parameter and the dimension of the Fourier subspace where we seek the solution. Moreover, the

regularized solution depends smoothly on the regularization parameter, and we are able to make extrapolations. This unregularized limit will interpolate the data whenever this is possible (i.e.) when we allow a sufficiently large number of frequencies in the solution. However, when we allow data contaminated with errors, there exist different criteria for choosing the regularization parameter. Some of them, in particular the L curve method, are discussed in this work. It relates the noise present in the data with the actual amount of regularization.

The number of Fourier components needed will depend in general on the smoothness of the flow we want to represent. Thus, for smooth flows, the numerical solution will contain just a few terms.

Here we have been working with two dimensional examples, but the technique can be extended to higher dimensions in a straightforward way. As an example of a real 2D problem, in Figure 1.1 we show the data from six weather stations in Uruguay, while computational results can be seen in Figure 1.2. To compute the solutions of the different cases we have developed a Matlab [27] code, which can handle both data points and slip boundary conditions, as well as an analysis of the effect of the regularization parameters.

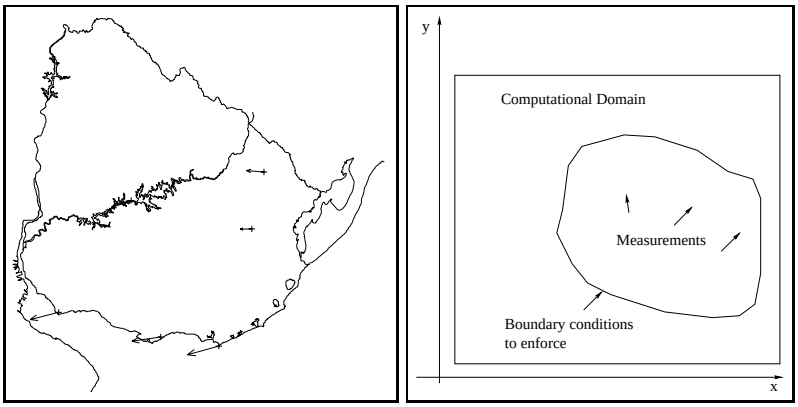

Figure 1.1: Left: Data for one wind field case in the southern part of Uruguay Right:The computational domain contains all the data point locations and the boundaries where we want to impose slip boundary conditions. In addition, periodic boundary conditions are imposed at the boundary of the computational domain

The thesis work is organized as follows: First, in Chapter 2 we make a short overview of related work on mass consistent flow estimation. The great majority are based on extending the given data to the whole domain by a suitable interpolation, and then fitting an incompressible flow to the interpolated flow. However, care must be taken when imposing Boundary Conditions in the formulation.

In addition, we comment some regularization techniques, introducing also the singular value (SVD) decomposition and its generalization, the Generalized Singular Value Decomposition (GSVD) [12] , which are basic tools for this

purpose. The account of regularization techniques that we offer there follows Hansen's work. Sensitivity of the solution with respect to perturbations is an important issue, and its analysis can be done with the aid of the mentioned factorizations. For this reason, the condition number of the formulated problem is analyzed in Appendix A, yielding perturbation bounds for the solution (i.e.), bounds that link data perturbations with perturbations in the solution. These are related the size of the regularization parameter. There is also a geometric interpretation of a necessary condition for the regularization operator B in the Tikhonov regularization. The proofs were done independently from Hansen [15], since the author was not aware of that work. Here the arguments rely on the SVD decomposition, whereas the bounds in [15] are based on the Generalized Singular Value Decomposition [12].

By means of the sensitivity analysis one can see that in presence of perturbed data there is no point in shrinking too much the regularization parameter. In section 2.2.2. as well as in Appendix B, we consider the effect of the regularization parameter, introducing also the use of the extrapolation with respect to this parameter. This leads to an optimal value for the regularization parameter, which is a standard problem in the area of numerical regularization. In Chapter 3 we offer the mathematical formulation and in Section 3.4 we present briefly some implementation issues.

Then, we apply the method to some model problems, some of them with known solution, as well as a real data case, coming from the wind field estimation problem in the southern zone of Uruguay. The results of this last case is compared with those offered by López Vázquez [35], showing satisfactory levels of agreement even with much less freedom degrees.

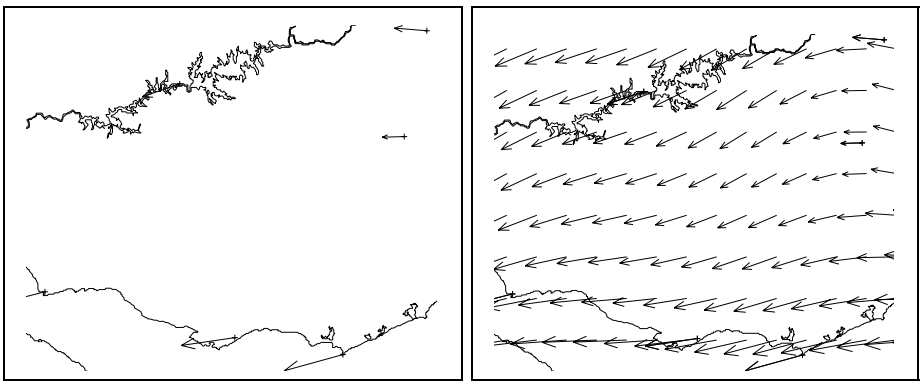

Figure 1.2: A closer look to the example presented in Figure 1.1.
Left: Zoomed view of available data. Right: Computational results.

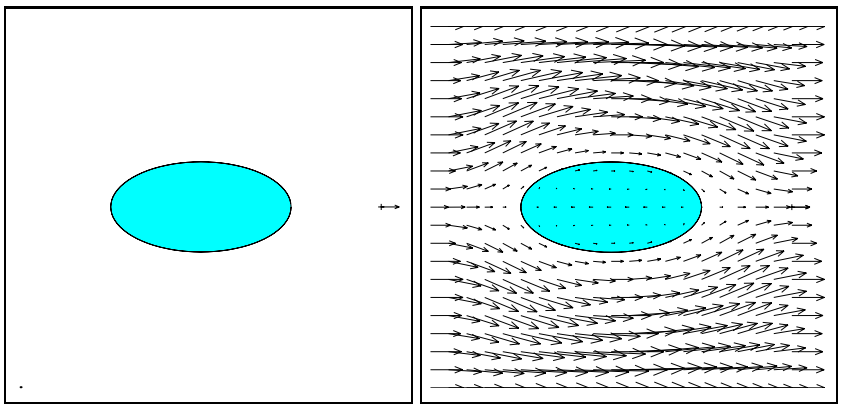

Figure 1.3: Another example of velocity field estimation. Now there exist also boundary conditions.
Left: Available Data: There is only one velocity measurement, and the flow cannot traspass the given ellipse. Right: Computational Results with the proposed method.

Chapter 2

Background

2.1 Variational formulations on flow estimation

The purpose of this section is to comment shortly other works on mass consistent velocity field estimation. Most of them follow Sasaki [30], and are based on extending the available data

$$\varphi(P_i) = \bar{\varphi}_i, \quad for \quad i = 1 \dots N_d$$

to the whole domain by a suitable interpolation, and then fitting an incompressible flow to the extended flow by minimizing a weighted L^2 norm of their difference.

Let $\hat{\varphi} : D \subset \mathbb{R}^d \to \mathbb{R}^d$ be a flow obtained by (e.g.) interpolation of the data, and φ the desired approximate flow. Sasaki [30] proposed to take φ as the solution of

$$\begin{cases} \min J(\varphi) = \int_D \frac{1}{2} \|\alpha(\varphi - \hat{\varphi})\|_2^2 dx \\ s.t. \\ \nabla \cdot \varphi = 0, \quad in \ D \end{cases} \tag{2.1}$$

In the above, α denotes a scaling diagonal matrix with strictly positive weights. A Lagrangian relaxation of the incompressibility constraint

$$\nabla . \varphi = 0 \tag{2.2}$$

gives the relaxed subproblem

$$\Phi(\lambda) = \min_{\varphi} J_\lambda(\varphi) = \int_D \left(\frac{1}{2} \|\alpha(\varphi - \hat{\varphi})\|_2^2 + \lambda \nabla \cdot \varphi \right) dx$$

where $\lambda : D_c \to \mathbb{R}$ is a dual function. The corresponding dual problem can be then defined as

$$\max_{\lambda} \Phi(\lambda)$$

Since problem (2.1) is strictly convex, it can be assured that once we find the optimal Lagrange multiplier associated with the incompressibility constraint λ^* the estimated flow can be obtained from the solution of

$$\varphi = arg \min_{\psi} J_{\lambda^*}(\psi)$$

Actually, one may also want the approximate flow φ to satisfy boundary conditions, such as a slip boundary condition at a solid wall, on a certain subset of ∂D. That can be expressed as

$$(\varphi, n) = 0, \text{ on } \partial D_1 \subset \partial D \tag{2.3}$$

where $(.,.) : \mathbb{R}^d \times \mathbb{R}^d \to \mathbb{R}$ is the usual inner product in $\mathbb{R}^d$. Then, both constraints (2.2) and (2.3) are relaxed to find the Euler-Lagrange equation. This is done by introducing the multipliers λ for (2.2) and μ for (2.3) respectively. Thus, the functional for the relaxed problem is

$$J_{\lambda,\mu}(\varphi) = \int_D \left(\frac{1}{2} \|\alpha(\varphi - \hat{\varphi})\|^2 + \lambda \nabla . \varphi \right) dx + \int_{\partial D_1} \mu(\varphi, n) ds$$

The first variation for this functional yields

$$\int_D \left(\alpha^2(\varphi - \hat{\varphi}) - \nabla\lambda, h \right) dx + \int_{\partial D_2} \lambda(h, n) ds + \int_{\partial D_1} (\mu + \lambda)(h, n) ds = 0$$

where $h : D \to \mathbb{R}^d$ denotes a perturbation to the original flow and $\partial D_1, \partial D_2$ is a disjoint partition of the boundary ∂D. Therefore, since h is arbitrary we obtain the conditions

$$\begin{aligned} \alpha^2(\varphi - \hat{\varphi}) - \nabla\lambda = 0, \text{ on } D \\ \lambda + \mu = 0, \text{ on } \partial D_1 \text{ (Solid Wall)} \\ \lambda = 0, \text{ on } \partial D_2 \text{ (Free Boundary)} \end{aligned}$$

In other approaches (see for example [13], [25], [26], [31], [34] and [35]), a boundary condition for the Lagrange multiplier λ

$$\frac{\partial \lambda}{\partial n} = (\nabla\lambda, n) = 0, \text{ on } \partial D_1 \tag{2.4}$$

is introduced as a way to enforce the slip constraint $(\varphi, n) = 0$ (2.3). The reader will realize that (2.4) is not a natural boundary condition for the minimization of the functional, since it implies

$$(\alpha^2(\varphi - \hat{\varphi}), n) = (\nabla\lambda, n) = 0, \text{ on } \partial D_1 \tag{2.5}$$

which clearly does not guarantee (2.3) in general, unless all the diagonal elements of α are equal (which is not the case in those approaches) and the interpolant flow $\hat{\varphi}$ fulfills $(\hat{\varphi}, n) = 0$. It is our impression that the use of such boundary condition may introduce spurious solutions (i.e.), λ obtained in this way will not be the desired Lagrange multiplier.

Using boundary condition (2.4), they first solve the problem

$$\begin{cases} -\nabla.\hat{\varphi} = \nabla.(\alpha^{-2}\nabla\lambda), \text{ on } D \\ \lambda = 0, \text{ on } \partial D_2 \\ \frac{\partial\lambda}{\partial n} = 0, \text{ on } \partial D_1 \end{cases} \tag{2.6}$$

for the incompressibility multiplier λ and after that obtain an approximation for the flow φ in terms of λ and the interpolated flow $\hat{\varphi}$

$$\varphi = \hat{\varphi} + \alpha^{-2}\nabla\lambda \tag{2.7}$$

Observe that problem (2.6) can be seen as a stationary heat equation,with λ playing the role of the temperature field. This fact makes the approach followed in [35] easy to implement, since for the heat equation there exist software that handles even complicated geometry.

In order to avoid the undesired boundary condition in (2.6) and find the right one for λ, it is enough to use (2.7), yielding

$$0 = (\varphi, n) = (\widehat{\varphi}, n) + (\alpha^{-2}\nabla\lambda, n), \text{ on } \partial D_1$$

which gives $(\alpha^{-2}\nabla\lambda, n) = -(\widehat{\varphi}, n)$, on ∂D_1, as the boundary condition to be applied in (2.6).

In our proposal this boundary condition problem does not appear, since we are able to substitute directly the incompressibility constraints obtaining an unconstrained formulation, which does not need the auxiliary problem for λ .

There are other formulations inspired in the work of Sasaki [30], but based on an integrated version of the continuity equation along the vertical axis, like those presented in [5],[8],[9]. The variables are mean values of the horizontal velocities within some mixing zone, and the vertical velocity at the top of the top boundary. Therefore, the continuity equation reads

$$h_t + (hu)_x + (hv)_y + w = 0 \tag{2.8}$$

where
$h = h(x, y, t)$ is the inversion height of the inversion base above topography, $u = u(x, y, t)$ and $v = v(x, y, t)$ are horizontal components of the mean velocity within the mixing zone, and $w = w(x, y, t)$ is a vertical outflow velocity through the top boundary.

If we denote $\varphi = \begin{pmatrix} U \\ V \\ w \end{pmatrix} = \begin{pmatrix} hu \\ hv \\ w \end{pmatrix}$ then the corresponding relaxed functional to be minimized for every time t is

$$\Phi(\lambda;t) = \min_{\varphi} J_{\lambda;t}(\varphi) = \int_D \left(\frac{1}{2} \|\alpha(\varphi - \hat{\varphi})\|_2^2 + \lambda \left(h_t + U_x + V_y + w \right) \right) dx$$

where $\lambda : D_c \to \mathbb{R}$ is a dual function. After carrying out the first variation we arrive to the Euler Lagrange equations

$$\begin{aligned} U - \hat{U} &= \lambda_x / \alpha_1^2, \\ V - \hat{V} &= \lambda_y / \alpha_1^2, \\ w - \hat{w} &= \lambda / \alpha_2^2, \end{aligned}$$

Applying the above relations together with (2.8) yields the following partial differential equation for λ

$$\nabla \cdot \left(\frac{1}{\alpha_1^2} \nabla \lambda \right) + \lambda / \alpha_2^2 + h_t + \nabla \cdot \hat{\varphi} = 0$$

with identical boundary conditions as in (2.6). Although the Euler Lagrange equations may look similar to those derived before in (2.6) such formulations do not exhibit problems with slip boundary conditions. However, this averaged formulation is not capable to compute three dimensional effects of the flow.

Another method, due to Liu and Goodin[23] is based on a linear iterative procedure. In that algorithm the measured wind values are held fixed while adjacent values are adjusted in order to reduce the divergence at every point. Once converged, the velocity field will satisfy a discretized version of

$$(hu)_x + (hv)_y = 0 \tag{2.9}$$

If we let h be a constant value, then the simplest version of this procedure, which contains the key idea of the method, can be described as follows: Let U^n, V^n denote vectors containing the mesh values of the estimated velocities at the nth iteration. Thus, a discretized divergence at every interior mesh point is computed by

$$D^n = \begin{pmatrix} \frac{E_{\Delta x} - E_{\Delta x}^{-1}}{2\Delta x} & \frac{E_{\Delta y} - E_{\Delta y}^{-1}}{2\Delta y} \end{pmatrix} \begin{pmatrix} U^n \\ V^n \end{pmatrix}$$

where $E_{\Delta x}, E_{\Delta y}$ denote the classical shift operators in x and y directions. After that, the velocity components are updated as shown below

$$\begin{pmatrix} U^{n+1} \\ V^{n+1} \end{pmatrix} = \begin{pmatrix} U^n \\ V^n \end{pmatrix} + \begin{pmatrix} F_{\Delta x} \\ F_{\Delta y} \end{pmatrix} D^n = \begin{pmatrix} U^n \\ V^n \end{pmatrix} + \begin{pmatrix} F_{\Delta x} \\ F_{\Delta y} \end{pmatrix} \begin{pmatrix} \frac{E_{\Delta x} - E_{\Delta x}^{-1}}{2\Delta x} & \frac{E_{\Delta y} - E_{\Delta y}^{-1}}{2\Delta y} \end{pmatrix} \begin{pmatrix} U^n \\ V^n \end{pmatrix}$$

where $F_{\Delta x}, F_{\Delta y}$ are constant diagonal matrices. If one value comes from a measurement point then it is kept fixed along the iterations, and its corresponding entry in the F matrix will be zero. For the remaining values, the entries of these matrices are chosen by consistency considerations.

A study of the convergence with respect to the number of iterations is included. However, since the only physical equation considered is (2.9) and no regularization has been done the numerical results, apart from being sensitive with respect to the initial iteration field are also very sensitive to perturbations, looking wiggly and unnecessarily complex.

On the other hand, our formulation is motivated by the alternative problem:

$$\begin{cases} \min \int_{D_c} J_r(\varphi) \\ s.t. \\ \nabla.\varphi = 0, \ on \ D \\ \varphi = \bar{\varphi}|_{observed\ points} \\ (\varphi, n) = 0, \ on \ \partial D_1 \end{cases} \tag{2.10}$$

where the functional $J_r(\varphi)$ to minimize will assure uniqueness and some smoothness of our approximation. However, the interpolation formulation (2.10) is not useful in presence of data errors, since it is very sensitive. Therefore, we keep it in mind as the underlying unperturbed problem, solving a regularized version of it.

In accordance with regular practice in inverse problems, this is just one way of choosing one solution from the set of those which satisfy the natural constraints of the problem, and its quality will be studied in what follows. The intuitive idea behind, is to strongly respect the original data, and at the same time to obtain a smooth incompressible flow.

2.2 Regularization

2.2.1 Singular Value Decomposition

Before we enter into the description of the different regularization approaches we quote the celebrated singular value decomposition ([12], Theorem 2.5.1, page71). This decomposition can be used to solve the least squares problem, as well as to analyze the sensitivity of its solution.

Theorem 1 *Let $A \in \mathbb{R}^{m\times n}$ be a real rectangular matrix then there exist orthogonal matrices*

$$U = [u_1, \ldots, u_m] \in \mathbb{R}^{m\times m} \quad and \quad V = [v_1, \ldots, v_n] \in \mathbb{R}^{n\times n}$$

such that

$$U^T A V = \Sigma = diag(\sigma_1, \ldots, \sigma_q) \in \mathbb{R}^{m\times n}, \quad with \ q = \min(m, n)$$

and $\sigma_1 \geq \sigma_2 \geq \ldots \geq \sigma_q \geq 0$

□

In the present work, we deal with least squares formulations where we have

$m \geq n$. The numbers σ_i are called the *singular values* of the matrix A, while the vectors u_i, v_i are known as the left and right singular vectors respectively. The matrix A can be expanded in a neat way using the SVD decomposition as follows:

$$A = U_r \Sigma_r V_r^T = \sum_{i=1}^{r} \sigma_i \; u_i \; v_i^T$$

where the number $r \leq q$ denotes the rank of A (i.e.), $\sigma_r \neq 0, \quad \sigma_{r+1} = 0$.

In the case of discrete ill posed problems, there is a characteristic feature in the set of singular values: they decay gradually to zero. As we increase the dimension of the problem, the smallest singular value becomes closer to zero, and the number of relatively small singular values increase.

The SVD gives very useful information about the ill conditioning of the matrix A. In fact, the 2-norm condition number can be computed as

$$\kappa_2(A) = \frac{\sigma_1}{\sigma_r} = \|A\|_2 \|A^I\|_2$$

where A^I denotes the pseudo inverse of the matrix A. For more information about the definition of the pseudo inverse see [12], page 243. When we multiply A times a vector x the components of x associated with small singular values, often associated with high frequency, are dampened out by σ_i as follows:

$$Ax = \sum_{i=1}^{r} \sigma_i \; (v_i^T x) u_i$$

Conversely, when we face the problem of reconstructing x from the vector $b = Ax$ it is intuitive to expect that small perturbations in b may lead to great changes in x if they happen in the subspace associated with small singular values. The fact that usually the errors in the data appear as high frequency linked with small singular values tells us that unless we prevent it, those errors will be magnified in x.

In the next paragraph, we assume that there are no exactly zero singular values (i.e.), that A is full column rank. With this assumption, the solution is unique, and we are able to carry out a perturbation analysis without introducing further information. This assumption is natural in regular practice, since roundoff or other sources of error makes hard to obtain exactly zero singular values. Using the SVD it is easy to show that the solution of the linear least squares problem (1.1) reads

$$x_{LSQ} = \sum_{i=1}^{n} \frac{u_i^T b}{\sigma_i} \; v_i \tag{2.11}$$

which clearly shows the amplification effect of the small singular values on the solution x_{LSQ}. Moreover, we can see by direct perturbation of the data vector b how the worst case associated with the condition number of A appears:

Let us choose $b = \sigma_1 u_1$. Since (2.11) holds and from the fact that the matrix V is orthogonal we obtain $x = v_1$. On the other hand, if we perturb

b with $\delta b = \sigma_n u_n$ the corresponding perturbation in the solution is $\delta x = v_n$. Thus, the quotient of the relative perturbations of solution and data is

$$\frac{\frac{||\delta x||_2}{||x||_2}}{\frac{||\delta b||_2}{||b||_2}} = \frac{\sigma_1}{\sigma_n} = \kappa_2(A) \tag{2.12}$$

More generally, when perturbations in the matrix A are allowed, a standard perturbation bound for the full rank least squares problem (1.1) (see [2], Theorem 5.5) is given by

$$\|x - \hat{x}\| \leq \frac{\kappa_2(A)}{1 - \kappa_2(A)\frac{\|\delta A\|}{\|A\|}} \left(\frac{\|\delta A\|}{\|A\|}\|x\| + \frac{\|\delta b\|}{\|A\|} + \kappa_2(A)\frac{\|\delta A\|}{\|A\|}\frac{\|r\|}{\|A\|} \right) \tag{2.13}$$

where the condition number $\kappa_2(A)$ still amplifies the perturbations in the data. In the above, $r = Ax - b$, $\|.\| = \|.\|_2$ and $\|A^I\|\|\delta A\| = \kappa_2(A)\frac{\|\delta A\|}{\|A\|} < 1$. Observe that when the residual r is nonzero there is also a perturbation which is amplified by $\kappa_2^2(A)$. This makes things much more sensitive for ill-posed problems.

Since the Fourier coefficients of the right hand side $u_i^T b$ do not shrink to zero but keep above some threshold due to the presence of errors in b the solution is dominated by small singular values, usually looking completely random. At this point, regularization problems can be stated as eliminating, or filtering out the undesired contributions corresponding to small singular values. What really matters for the filtering to work is to have a sufficiently fast decay in the Fourier coefficients of the unperturbed right hand side. To illustrate the need for this, let us consider the singular value decomposition of a compact operator $K(s,t) = \sum_{i=1}^{\infty} \sigma_i u_i(s) v_i(t)$ and the problem $\inf_{f \in L^2} \|Kf - g\|_{L^2}$, where the right hand side g can be written as $g(s) = \sum_{i=1}^{\infty} \beta_i u_i(s)$. Then, if we want f to be square integrable the necessary and sufficient condition is

$$\sum_{i=1}^{\infty} \left(\frac{(u_i^T g)}{\sigma_i} \right)^2 < \infty, \quad \sigma_i > 0 \tag{2.14}$$

Therefore, the quotient $\frac{(u_i^T g)}{\sigma_i}$ must decay sufficiently fast to zero for a square integrable solution to exist. The above condition is known as the Picard Condition [17]. The discrete version of this, due to P. C. Hansen[17], can be expressed by means of the Generalized Singular Value Decomposition, as will be seen below.

2.2.2 Generalized Singular Value Decomposition

The Generalized Singular Value Decomposition (GSVD) of the matrix pair (A, B) is a generalization of the SVD decomposition of the matrix A. It is used here to analyze the dependence of the regularized solution with respect to the regularization parameter, as well as to provide sensitivity bounds for the solution.

Theorem 2 *Let $A \in \mathbb{R}^{m\times n}$, $B \in \mathbb{R}^{p\times n}$ with $m \geq n \geq p$. Moreover, assume that rank $\left(\begin{bmatrix} A \\ B \end{bmatrix}\right) = n$ and denote $q = rank(B) \leq p$. Then, the GSVD is a decomposition of the form*

$$A = U \begin{pmatrix} \Sigma & 0 \\ 0 & I_{n-q} \end{pmatrix} X^{-1}, \qquad B = V \ (\mathcal{M}, 0) \ X^{-1}, \tag{2.15}$$

where $U \in \mathbb{R}^{m\times n}$ and $V \in \mathbb{R}^{q\times q}$ have orthogonal columns (i.e), $U^T U = I_n$ and $V^T V = I_q$. The matrix $X \in \mathbb{R}^{n\times n}$ is non singular, and Σ and $\mathcal{M}$ are $q \times q$ diagonal matrices: $\Sigma = diag(\sigma_1, \ldots, \sigma_q)$, $\mathcal{M} = diag(\mu_1, \ldots, \mu_q)$. Furthermore, the diagonal entries of Σ and $\mathcal{M}$ can be ordered in the following way

$$0 \leq \sigma_1 \leq \ldots \leq \sigma_q \leq 1, \qquad 1 \geq \mu_1 \geq \ldots \geq \mu_q \geq 0$$

and normalized such that

$$\sigma_i^2 + \mu_i^2 = 1, \quad for\ i = 1 \ldots q$$

Furthermore, the singular values of the matrix X^{-1} equal the singular values of the matrix $\begin{bmatrix} A \\ B \end{bmatrix}$

The generalized singular values γ_i *of the matrix pair (A, B) are defined as the quotients*

$$\gamma_i = \sigma_i/\mu_i, \quad for\ i = 1, \ldots, q$$

and they appear in non-decreasing order.

□

For a proof see Björck [3], theorem 4.2.2, page 157.
Observe that the above decomposition can be written as

$$\begin{aligned} A &= \textstyle\sum_{i=1}^{q} u_i \sigma_i y_i^T + \sum_{i=q+1}^{n} u_i y_i^T \\ B &= \textstyle\sum_{i=1}^{q} v_i \mu_i y_i^T \end{aligned} \tag{2.16}$$

where the vectors y_i^T denote the rows of X^{-1} (i.e.), $y_i^T x_j = \begin{cases} 1 & if\ i = j \\ 0 & otherwise \end{cases}$

It is easy to see from (2.16) that the last $n - q$ columns of the matrix X are basis vectors of the null space of B. On the other hand, if $rank(A) < n$ then $\sigma_i = 0$ for $1 \leq i \leq dim(ker(A))$ and the corresponding columns of X make a basis of the null space of A. Therefore, the columns of the matrix X contain enough information to characterize the null spaces of both A and B. This tells us that if the angle between the subspaces ker(A) and ker(B) is small, the matrix X will be near singular and its condition number large.

Here is worth to realize that by an abuse of notation, the matrices U, V, Σ have the same name as those appearing in the SVD of A (theorem 1), but in

general they are not the same. In particular, when $B = I_n$ the generalized singular values coincide, up to a permutation, with the usual singular values, as well as U, V are identical to the U, V from the SVD up to a column permutation. In general, the Singular Values will not coincide with their corresponding generalized Singular Values, but when the matrix $\|B^I\|_2$ is small they are closely related, being of the same order of magnitude [16].

As mentioned in the previous subsection, there exist a discrete version of the Picard condition that is needed to obtain useful results from regularization[17]. Basically, it says that if the Fourier coefficients $|u_i^T b|$ of the *unperturbed right hand side* decay faster than the generalized singular values γ_i then the regularized solution $x(\epsilon)$ approximately exhibits the same properties as the exact solution of the unperturbed problem. The decay in the Fourier coefficients need not be monotonic as long as, *on the average*, is faster than γ_i. This, if $\|B^I\|_2$ is relatively small, can also be written in terms of the usual singular values of the matrix A. On the other hand, it is not needed to check the discrete Picard condition for all the generalized singular values. Instead, it is only needed to so if they are numerically nonzero (i.e.), above a threshold related with the error level in A. This of course is of no practical use as long as we need the unperturbed right hand side to verify the property. However, as Hansen points out, if the underlying problem satisfies the Picard condition then one can often make the regularized perturbed version to satisfy the Picard condition.

As a direct application of this decomposition to perturbation analysis in the Tikhonov regularization (1.2) we include a result from [15].

Theorem 3 *Let δA and δb denote perturbations of A and b respectively, and let $\hat{x}(\epsilon)$ denote the perturbed regularized solution of*

$$\min \|(A + \delta A)\hat{x} - (b + \delta b)\|_2^2 + \epsilon \|Bx\|_2^2$$

Then, if $0 < \epsilon \leq 1$ and the intersection of the null spaces of A and B is trivial (i.e.), $\begin{bmatrix} A \\ \sqrt{\epsilon}B \end{bmatrix}$ is full column rank

$$\|x(\epsilon) - \hat{x}(\epsilon)\| \leq \frac{\kappa_\epsilon}{1 - \kappa_\epsilon \frac{\|\delta A\|}{\|A\|}} \left((1 + \kappa_2(X)) \frac{\|\delta A\|}{\|A\|} \|x(\epsilon)\| + \frac{\|\delta b\|}{\|A\|} + \kappa_\epsilon \frac{\|\delta A\|}{\|A\|} \frac{\|r_\epsilon\|}{\|A\|} \right)$$

where $\kappa_\epsilon = \|A\|\|X\|/\sqrt{\epsilon}$.
Moreover, if $q = n$ and the matrix B is nonsingular the following sharper bound holds

$$\|x(\epsilon) - \hat{x}(\epsilon)\| \leq \frac{\hat{\kappa}_\epsilon}{1 - \hat{\kappa}_\epsilon \frac{\|\delta A\|}{\|A\|}} \left((1 + \kappa_2(B)) \frac{\|\delta A\|}{\|A\|} \|x(\epsilon)\| + \frac{\|\delta b\|}{\|A\|} + \hat{\kappa}_\epsilon \frac{\|\delta A\|}{\|A\|} \frac{\|r_\epsilon\|}{\|A\|} \right)$$

where now $\hat{\kappa}_\epsilon = \|A\|\|B^{-1}\|/\sqrt{\epsilon}$

□

Using the GSVD decomposition, the Tikhonov regularized solution can be written as:

$$x(\epsilon) = X \begin{pmatrix} \left(\Sigma^2 + \epsilon M^2\right)^{-1} \Sigma & 0 \\ 0 & I_{n-q} \end{pmatrix} U^T b = \sum_{i=1}^{q} \frac{\gamma_i^2}{\gamma_i^2 + \epsilon} \frac{u_i^T b}{\sigma_i} x_i + \sum_{i=q+1}^{n} (u_i^T b) x_i \tag{2.17}$$

where $x_i, i = 1, \ldots, n$ denote the columns of the matrix X. This expansion looks similar as what we did with the SVD in the full rank case. Nevertheless, here we can observe the dampening effect of the so called "filter factors"

$$f_i = \frac{\gamma_i^2}{\gamma_i^2 + \epsilon}$$

that "filters out" the contributions to $x(\epsilon)$ corresponding to small γ_i (i.e.), less than $\sqrt{\epsilon}$.

In addition, it can be checked that

$$\|Bx(\epsilon)\|_2^2 = \sum_{i=1}^{q} \left(\frac{\gamma_i^2}{\gamma_i^2 + \epsilon} \frac{u_i^T b}{\sigma_i} \right)^2 \tag{2.18}$$

$$\|r(\epsilon)\|_2^2 = \|Ax(\epsilon) - b\|_2^2 = \sum_{\{i: 1 \le i \le q, \gamma_i > 0\}} \left(\frac{\epsilon}{\gamma_i^2 + \epsilon} u_i^T b \right)^2 + \|r(0)\|_2^2 \tag{2.19}$$

where $r(0)$ is that component of the right hand side b which is outside the range of A. Its norm is sometimes called *incompatibility measure*.

2.2.3 The L curve

The L curve method is a classic graphical tool to analyze regularization problems. It was first introduced by Lawson and Hanson [22] and Miller [28]. The name refers to its shape, and it is used to choose the value of the regularization parameter. In double logarithmic scale, the norm of the regularization term $\|Bx(\epsilon)\|_2$ is plotted against the residual $\|Ax(\epsilon) - b\|_2$ as shown in Figure 2.1. The vertical part of the curve corresponds to small values of the regularization parameter, where $\|Bx(\epsilon)\|_2$ is very sensitive with respect to the regularization parameter. On the other hand, the horizontal part of the curve corresponds to large values of the regularization parameter, where the residual $\|Ax(\epsilon) - b\|_2$ is the sensitive term.

The following theorem from [19] yields the monotonicity property of the L curve, as well as another characterization of its points.

Theorem 4 *Let $x(\epsilon)$ denote the solution of $\min \|Ax-b\|_2^2 + \epsilon \|Bx\|^2$. Then $\|Bx(\epsilon)\|_2$ is monotonically decreasing function of $\|Ax(\epsilon)\|_2$ and any point (δ_1, δ_2) on the curve $(\|Ax(\epsilon)-b\|, \|Bx(\epsilon)\|)$ is a solution of the following two inequality constrained least squares problems:*

$$\delta_1 = \min \|Ax-b\|_2 \text{ subject to } \|Bx\|_2 \leq \delta_2, \qquad 0 \leq \delta_2 \leq \|Bx(0)\|_2 \tag{2.20}$$

$$\delta_2 = \min \|Bx\|_2 \text{ subject to } \|Ax-b\|_2 \leq \delta_1 \qquad \|r(0)\| \leq \delta_1 \leq \|r(\infty)\|_2 \tag{2.21}$$

□

To see the solution dependence more carefully, let x denote the exact solution to the unregularized problem with the exact right hand side b. Then, let e be a perturbation in the right hand side and denote by $\hat{x}(\epsilon)$ the solution of the regularized problem corresponding to the perturbed right hand side $\hat{b} = b + e$. Direct application of (2.17) yields

$$\hat{x}(\epsilon) - x = \underbrace{\left(\sum_{i=1}^{q} f_i \frac{u_i^T e}{\sigma_i} x_i + \sum_{i=q+1}^{n} (u_i^T e) x_i \right)}_{\text{perturbation error}} + \underbrace{\sum_{i=1}^{q} (f_i - 1) \frac{u_i^T b}{\sigma_i} x_i}_{\text{regularization error}} \tag{2.22}$$

where $f_i = \frac{\gamma_i^2}{\gamma_i^2 + \epsilon}$ are the Tikhonov's filter factors. Now, we will motivate the dependence of the solution with respect to ϵ specially for small singular values, that is $\gamma_i << 1$.

For large values of ϵ (i.e.), $\epsilon >> \gamma_i^2$ we have

$$f_i \frac{u_i^T e}{\sigma_i} = \frac{\gamma_i^2}{\gamma_i^2 + \epsilon} \frac{u_i^T e}{\sigma_i} \approx \frac{\gamma_i^2}{\epsilon} \frac{u_i^T e}{\sigma_i} = \frac{1}{\sqrt{\epsilon}} \frac{\gamma_i}{\sqrt{\epsilon}} \sqrt{\gamma_i^2 + 1}\ u_i^T e \tag{2.23}$$

which means that the contribution corresponding to small generalized singular values in the perturbation error is filtered up to $\mathcal{O}\left(\frac{1}{\sqrt{\epsilon}}\right)$.
At the same time, the contribution to the regularization error is large,

$$(f_i - 1) \frac{u_i^T b}{\sigma_i} \approx -\frac{u_i^T b}{\sigma_i} = \mathcal{O}\left(\frac{1}{\gamma_i}\right)$$

On the other hand, when we consider small values of the regularization parameter (i.e.), $\epsilon << \gamma_i^2$ the total error is made of a large perturbation error and a small regularization one, as can be seen in the next equations

$$\text{Contribution to Perturbation error: } f_i \frac{u_i^T e}{\sigma_i} \approx \frac{u_i^T e}{\sigma_i} = \mathcal{O}\left(\frac{1}{\gamma_i}\right)$$

Contribution to Regularization error: $\left|(f_i - 1)\frac{u_i^T b}{\sigma_i}\right| \approx \left|\frac{\epsilon}{\gamma_i^2}\frac{u_i^T b}{\sigma_i}\right| << \left|\frac{u_i^T e}{\sigma_i}\right|$

Equation (2.23) is related with theorem 3 since it shows that as the regularization parameter shrinks to zero perturbations corresponding to small generalized singular values are amplified by $\mathcal{O}(\frac{1}{\sqrt{\epsilon}})$ For values of ϵ ranging in between, there is a small region where the perturbation error and the regularization one balance to give a minimum total error contribution. That corresponds to the vicinity of the corner of the L curve. In [19] a characterization is given to provide conditions for using the L curve. If the b Fourier components $u_i^T b$ associated with small singular values decay sufficiently fast and the perturbation in the right hand side is not large then the L curve can be used to determine a sensible regularized solution. That solution corresponds to the corner of the L curve, which also determines the choice of ϵ. The corner of the L curve is defined as the point with maximum curvature. Since we only have a finite number of points in the L curve, a spline interpolation is recommended to define the corner numerically [19].

If b has a non negligible contribution in the subspace of small singular values then it is very difficult to find the corresponding x, since the amplified harmful perturbations in such subspace cannot be separated from the desired solution.

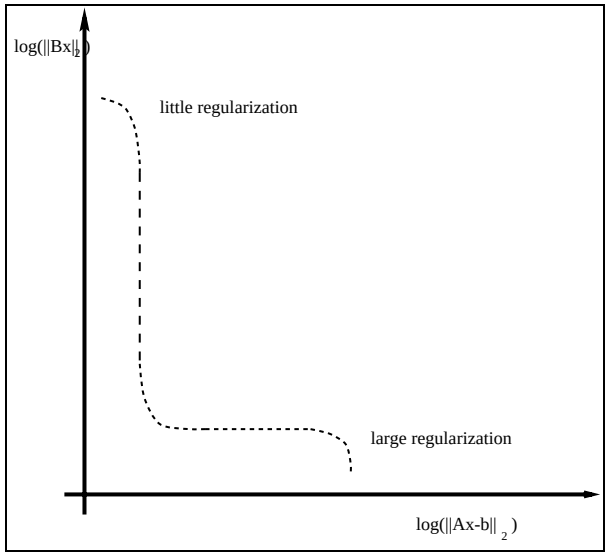

Figure 2.1: The L curve.

The L curve can be used for Tikhonov regularizations, where the regularization parameter varies continuously, but also with discrete regularization parameter, like in the Truncated SVD method and others.

2.2.4 Regularization methods

Regularization methods can be classified in terms of the numerical method that is used to obtain the solution. Following this line, there exist direct and iterative regularization methods. Our aim is not to give an extensive enumeration of all such methods, but to describe some basic techniques. This description will hopefully give a framework where the Tikhonov regularization applied in this work will fit. This is a direct regularization method, defined by the least squares problem as mentioned in (1.2).

$$\min \|Ax - b\|_2^2 + \epsilon \|Bx\|_2^2 = \min \left\| \begin{pmatrix} A \\ \sqrt{\epsilon} B \end{pmatrix} x - \begin{pmatrix} b \\ 0 \end{pmatrix} \right\|_2$$

The regularized solution is unique whenever the null spaces of A and B intersect trivially. That will be one of our basic assumptions throughout the work. Its numerical solution can be computed in many ways, like direct solution of the sparse normal equations

$$(A^T A + \epsilon B^T B) x(\epsilon) = A^T b$$

or using the QR factorization of $\begin{pmatrix} \sqrt{\epsilon} B \\ A \end{pmatrix}$. Since both of these methods require to redo all computations every time require a computation with a different value of ϵ they are not very attractive.

Another possibility is to compute the GSVD of the matrix pair (A,B) once and then compute Tikhonov's filter factors every time that ϵ changes, obtaining $x(\epsilon)$ from equation (2.17).

Finally, there is a method proposed by L. Eldén [7] that begins by transforming the problem into standard form obtaining

$$\min \|\bar{A}\bar{x} - \bar{b}\|_2^2 + \epsilon \|\bar{x}\|_2^2 = \|Ax - b\|_2^2 + \epsilon \|Bx\|_2^2$$

where $\|\bar{x}\|_2^2 = \|Bx\|_2^2$ and $\|\bar{A}\bar{x} - \bar{b}\|_2^2 = \|Ax - b\|_2^2$.

After this, applying orthogonal transformations $\bar{U}$ and $\bar{V}$ to the matrix $\bar{A}$ arrives to an upper bidiagonal matrix $\begin{pmatrix} \bar{A}_b \\ 0 \end{pmatrix} = \bar{V} \bar{A} \bar{U}^T$. Therefore,

$$\begin{aligned} &\min \left\| \begin{pmatrix} A \\ \sqrt{\epsilon} B \end{pmatrix} x - \begin{pmatrix} b \\ 0 \end{pmatrix} \right\|_2 = \min \left\| \begin{pmatrix} \bar{A} \\ \sqrt{\epsilon} I \end{pmatrix} \bar{x} - \begin{pmatrix} \bar{b} \\ 0 \end{pmatrix} \right\|_2 = \\ &\min \left\| \begin{pmatrix} \bar{A}_b \\ 0 \\ \sqrt{\epsilon} I \end{pmatrix} y - \begin{pmatrix} c_1 \\ c_2 \\ 0 \end{pmatrix} \right\|_2 = \|c_2\|_2^2 + \min_y \left\| \begin{pmatrix} \bar{A}_b \\ \sqrt{\epsilon} I \end{pmatrix} y - \begin{pmatrix} c_1 \\ 0 \end{pmatrix} \right\|_2 \end{aligned} \tag{2.24}$$

where $y = \bar{V}^T \bar{x}$, $\begin{pmatrix} c_1 \\ c_2 \end{pmatrix} = \bar{U}^T \bar{b}$.

Now there exist two possibilities: either we use Givens rotations to annihilate $\sqrt{\epsilon}I$ using $\bar{A}_b$ by means of Eldén's algorithm [7] or we recognize that y in (2.24) is the solution of the linear system

$$\begin{pmatrix} I & \bar{A}_{bid} \\ \bar{A}_{bid}^T & \epsilon I \end{pmatrix} \begin{pmatrix} r_1 \\ y \end{pmatrix} = \begin{pmatrix} c_1 \\ 0 \end{pmatrix} \tag{2.25}$$

which can be transformed into a symmetric tridiagonal and indefinite system by a suitable symmetric reordering columns and rows [10]. Although both possibilities can be computed with approximately $20n$ flops for every new value of ϵ Eldén's transform is more robust since it is based in orthogonal transformations.

At the end, the desired solution x is obtained by transforming back to the original formulation.

Another direct method is the least squares with a quadratic constraint. Its formulation is fairly close to the Tikhonov regularization, as mentioned before in theorem 4. There are two versions

$$\begin{array}{lll} \min \|Ax-b\|_2 & subject\ to & \|Bx\|_2 \leq \delta_1 \\ \min \|Bx\|_2 & subject\ to & \|Ax-b\|_2 \leq \delta_2 \end{array} \tag{2.26}$$

where δ_1 and δ_2 are suitable positive parameters that play the same role as the regularization parameter in the Tikhonov regularization.

To solve the first problem, first the unconstrained least squares solution x_{LSQ} is found. Then, if $\|Bx_{LSQ}\|_2 \leq \delta_1$ it is accepted as the solution. Otherwise, the solution solves the equality constrained problem

$$\min \|Ax-b\|_2 \quad subject\ to \quad \|Bx\|_2 = \delta_1 \tag{2.27}$$

A suitable method to solve (2.27) is based on a Lagrangian relaxation of the equality constraint $\|Bx\|_2^2 = \delta_1^2$. This yields a smooth one dimensional dual problem with an unconstrained LSQ as subproblem.

Two regularization methods with discrete regularization parameter are the Truncated SVD (TSVD) method [18] and the Modified Truncated SVD (MTSVD) [21]. Basically, they regularize by annihilation of the contribution coming from small singular values. The original ill conditioned matrix

$$A = \sum_{i=1}^{r} \sigma_i \ u_i \ v_i^T$$

is replaced in the TSVD method by a *truncated* rank deficient matrix

$$A_k = \sum_{i=1}^{k} \sigma_i \ u_i \ v_i^T$$

Moreover, A_k is the closest matrix to A among those of rank k ([12],theorem 2.5.2, page 73) (i.e.),

$$\sigma_{k+1} = \|A - A_k\|_2 = min\,\{\|A - B_k\|_2 : rank(B_k) = k\} \tag{2.28}$$

This choice yields the solution

$$x_k = A_k^I b = \sum_{i=1}^{k} \frac{u_i^T b}{\sigma_i} v_i$$

that is less sensitive to data perturbations than the unregularized solution. Its condition number is $\frac{\sigma_1}{\sigma_k}$ which is smaller than the original one introduced in equation (2.12). This is similar to a Tikhonov regularization with $B = I$. The difference lies on the filter factors. Here they are chosen by $f_i = \begin{cases} 1, & for\ 1 \le i \le k \\ 0, & Otherwise, \end{cases}$ offering a sudden "cutoff" at k while in Tikhonov's they decay gradually with $f_i = \frac{\sigma_i^2}{\sigma_i^2 + \epsilon}$. Beside this, if $\sqrt{\epsilon} \approx \sigma_k$ then the sensitivity of the Tikhonov solution and the TSVD solution will be similar.

The replacement of the matrix A by A_k is motivated by the fact that those components of the solution associated with large singular values are untouched, while those related with small ones do not appear. In addition, the truncated approximation A_k is much better conditioned than the original matrix A. It is clear that in order to define the method completely, we have to give a choice of the "numerical rank" k. The notion of numerical δ-rank reflects the error level in the data and depends on a tolerance. We say that a matrix has δ-rank equal to k if

$$k = \min\{rank(B) : \|A - B\|_2 \le \delta\}, \quad \text{where } \delta > 0 \text{ is a given constant}$$

From (2.28) we can see that A has δ-rank k if

$$\sigma_1 \ge \ldots \ge \sigma_r \ge \delta \ge \sigma_{r+1} \ge \ldots \ge \sigma_n$$

The definition is satisfactory whenever the spectrum of singular values has clear gap. In that case it is fairly straightforward how to proceed, since the numerical rank can be defined as the number of singular values above the gap. Unfortunately, that is not the usual case with inverse problems, and is a clear sign of ill-conditioning. Usually we have a "continuously" decaying diagram, and the choice is far from straightforward. A "rule of thumb" is given in [2](page 511). If we assume that $|e_{ij}| \le e$ then it is suggested to take $\delta = (mn)^{1/2} \cdot e$ However, it is advisable to use it only when the norms of the columns of A are of the same order.

There is another way to characterize the regularized solution of the TSVD method. It is the solution the following constrained LSQ problem

$$\min \|x\|_2 \quad subject\ to \quad \min \|A_k x - b\|_2 \tag{2.29}$$

Based on the same kind of ideas, the *modified TSVD* (MTSVD)[21] introduces the need for minimizing $\|Bx\|_2$ leading to

$$\min \|Bx\|_2 \quad subject\ to \quad \min \|A_k x - b\|_2 \tag{2.30}$$

Observe that (2.30) is closely related with the constrained least squares formulation of Tikhonov regularization (2.26). Since the condition $\min \|A_k x - b\|_2$ still holds the solution of (2.30) is obtained by adding a correction in the null space of A_k to x_k, the solution of the TSVD method (2.29), as follows:

$x_{B,k} = x_k + \delta x_B$, where

$$\delta x_B = \sum_{i=k+1}^{n} z_i v_i = V_{k+1} z \in \ker(A)$$

The correction is then chosen to minimize

$$\|Bx\|_2 = \|Bx_k + B\delta x_B\|_2 = \|Bx_k + BV_{k+1} z\|_2$$

yielding

$$x_{B,k} = x_k - V_{k+1}(BV_{k+1})^I x_k$$

All these formulations with truncated matrices can also be generalized using the GSVD to give the Truncated Generalized Singular Value Decomposition (TGSVD)[16]. A truncation is done in the generalized singular values, and the corresponding solution is given by

$$x_{B,k} = \sum_{i=q-k+1}^{q} \frac{u_i^T b}{\sigma_i} x_i + \sum_{i=q+1}^{n} (u_i^T b) x_i$$

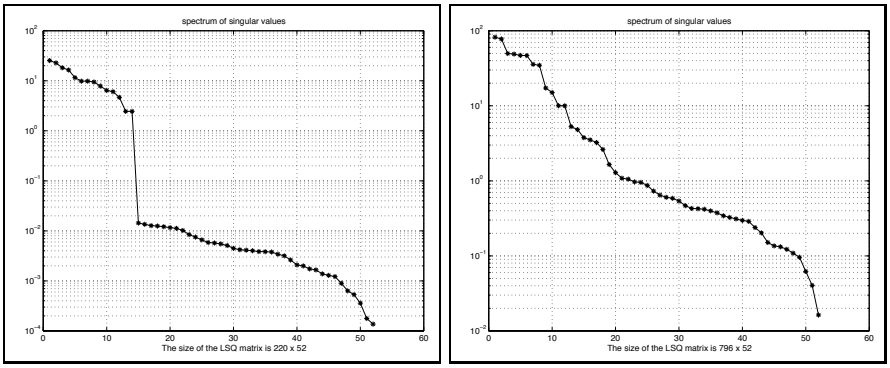

Figure 2.2: Two singular values diagrams. On the left, we see a case with a distinct gap and well defined numerical rank, coming from an example with real data from the Uruguayan case. On the right, another example from a model problem where the definition of the numerical rank is less clear.

Again, this implies a sudden cutoff in the GSV spectrum.

Instead of directly annihilation of the small singular values, there exist the possibility to damp their effect, but with filter factors different from those appearing in Tikhonov's regularization.

That is carried out by the *damped SVD* method [6], which regularizes the solution by means of the filter factors: $f_i = \begin{cases} \frac{\sigma_i}{\sigma_i+\sqrt{\epsilon}} & if\ B = I \\ \frac{\gamma_i}{\gamma_i+\sqrt{\epsilon}} & if\ B \neq I \end{cases}$ It can be observed that the decay of the filter factors is slower than in Tikhonov's regularization, therefore the damped GSVD offers less regularization.

When both the coefficient matrix A and the right hand side b are contaminated with errors an appropriate formulation is the *total least squares method* (TLS) ([12], page 576):

$$\min_{\tilde{A},\tilde{b},x} \|(A,b) - (\tilde{A},\tilde{b})\|_F \quad subject\ to \quad \tilde{b} = \tilde{A}x$$

In this case, Tikhonov regularization can be applied following [10]:

$$\min_{\tilde{A},\tilde{b},x} \|(A,b) - (\tilde{A},\tilde{b})\|_F \quad subject\ to \quad \tilde{b} = \tilde{A}x, \quad \|Bx\|_2 \leq \delta_1 \tag{2.31}$$

where δ is a positive constant. As observed in [10] the solution of (2.31) is closely related to the solution of (1.2) since it solves the equation

$$(A^T A + \lambda_I I_n + \lambda_B B^T B)x = A^T b$$

where the parameters $\lambda_I < 0,\ \lambda_B > 0$ satisfy

$$\begin{aligned} \lambda_I &= -\tfrac{\|b-Ax\|_2^2}{1+\|x\|_2^2} \\ \lambda_B &= \mu(1 + \|x\|_2^2) \\ \lambda_B \delta_1^2 &= b^T(b - Ax) + \lambda_I \end{aligned}$$

Here μ is the Lagrange multiplier associated with the norm constraint in (2.31).

On the other hand, *iterative regularization methods* are devised for large structured problems, and an efficient implementation must take care of the sparsity of the matrices involved in the problem. As an example of such methods, the conjugate gradient method is a classical method for minimizing a quadratic form with positive definite matrix coefficient, or equivalently, to solve a linear system of equations whose coefficient matrix is symmetric and positive definite. In this setting, it is applied to the unregularized normal equations. The regularization comes from the known fact that as the iterations proceed, the low frequency components converge first, offering a smooth solution that becomes more and more wiggly as the iterations proceed. Therefore, is the number of iterations which plays the role of regularization parameter.

2.2.5 Choice of the regularization parameter.

The goal of a sensible choice of the regularization parameter is to compensate the contributions of the *perturbation error*, which is due to errors in the data of the problem, and the *regularization error* in the regularized solution.

As P.C. Hansen points out, the strategies can be classified in those which make use of $\|e\|_2$, the error level present in the data, and those which do not, making the choice based on a posteriori information.

Among the first class is the *discrepancy principle*. If the ill-posed problem is consistent (i.e.), has zero incompatibility measure, it says that it does not pay to fit the data with a residual which is less than the data error. The regularized solution x_{reg} then solves

$$\|Ax_{reg} - b\|_2 = \|e\|_2$$

Naturally, this method relies on a good estimate of data errors, and when that happens, its solution is close to the one offered by the L curve method.

Finally, the L curve method is the most used method among those which do not make use of an a priori estimate of the data errors. This method has already been described in 2.2.3.

Chapter 3

Formulation

As we said before, our task is to provide an incompressible velocity field that fulfills a finite number of data measurements up to a certain regularization threshold and possibly, some slip boundary conditions.

The construction of such estimated flow is based on a finite superposition of incompressible velocity fields.

Let (u_i, v_i) be the velocity measurements at the station points

$$P_i = (x_i, y_i) \in D, \ with \ 1 \leq i \leq N_d$$

where D denotes the physical domain. In order to make easier the presentation of the equations and without any lose of generality, we assume that $D \subset [0, 2\pi]^2 = D_c$. The notation D_c stands for the computational domain, where we embed our solution.

Now consider a finite dimensional vector subspace in the space of complex valued and square integrable functions $L^2_{[0,2\pi]^2}$, spanned by a basis

$$\{\phi_{\eta,\xi}(x,y)\}_{|\eta| \leq \eta_{max}, |\xi| \leq \xi_{max}}, \text{ with } \phi_{\eta,\xi} : D_c \subset \mathbb{R}^2 \mapsto \mathbb{C}$$

With this notation, we propose to take the estimated flow as

$$\varphi(x,y) = [U(x,y) \quad V(x,y)] = \sum_{\eta,\xi} C_{\eta,\xi} \ \phi_{\eta,\xi}(x,y), \tag{3.1}$$

where $C_{\eta,\xi} = \left[\hat{U}_{\eta,\xi} \quad \hat{V}_{\eta,\xi}\right]$ arises for a vector of complex coefficients.

Some of the equations that will determine the coefficients $C_{\eta,\xi}$ come from the desired interpolation property $\varphi(P_i) = \hat{\varphi}(P_i)$, yielding

$$\sum_{\eta,\xi} C_{\eta,\xi} \phi_{\eta,\xi}(x_i, y_i) = (u_i, v_i), \ for \ 1 \leq i \leq N_d \tag{3.2}$$

In this context, a natural choice is to try to fulfill (3.2) using least squares as follows

$$\min_{\mathbf{C}} f_d(\mathbf{C}) = \frac{1}{N_d} \sum_{1 \le i \le N_d} \left\| \sum_{\eta,\xi} C_{\eta,\xi} \phi_{\eta,\xi}(x_i, y_i) - (u_i, v_i) \right\|_2^2, \tag{3.3}$$

where $\mathbf{C}$ is the complex valued vector made of the blocks

$$C_{\eta,\xi} = \begin{bmatrix} \hat{U}_{\eta,\xi} & \hat{V}_{\eta,\xi} \end{bmatrix}$$

It is useful to observe that after reordering the variables we can think of $\mathbf{C}$ as made of two blocks $\mathbf{C} = \begin{bmatrix} \hat{\mathbf{U}} & \hat{\mathbf{V}} \end{bmatrix}$ each of them containing the coefficients for the ansatz of $U(x, y)$ and $V(x, y)$ respectively.

There are also boundary conditions (B.C.) that we may want to impose to our approximation. In order to introduce them in the formulation we first discretize the boundary ∂D_1 into a finite set of points distributed by the arclength:

$$P_h = (x_h, y_h), \ for \ 1 \le h \le N_b$$

After that, the B.C. at the discretized boundary are considered as extra equations to fulfill. We treat one basic linear boundary condition, which models the in viscid flow at a solid wall (i.e.) $(n(P), \varphi(P))|_{\text{solid wall}} = 0$ where $n(P) = [n_x(P) \ n_y(P)]$ is the inwards normal direction to the boundary.

Using the basis functions $\phi_{\eta,\xi}$ we can rewrite the slip condition, arriving to

$$\begin{aligned} &(n(x_h, y_h), \sum_{\eta,\xi} C_{\eta,\xi} \ \phi_{\eta,\xi}(x_h, y_h)) = \\ &= \sum_{\eta,\xi} (n(x_h, y_h), C_{\eta,\xi}) \ \phi_{\eta,\xi}(x_h, y_h) = \\ &= \sum_{\eta,\xi} (n_x(x_h, y_h) \ \hat{U}_{\eta,\xi} + n_y(x_h, y_h) \ \hat{V}_{\eta,\xi}) \ \phi_{\eta,\xi}(x_h, y_h) = 0, \\ &\qquad for \ 1 \le h \le N_b, \ (x_h, y_h) \in \partial D_1 \end{aligned} \tag{3.4}$$

As we did with (3.2), we treat (3.4) in least squares sense. The contribution of the boundary conditions is called $f_b(\mathbf{C})$ and reads

$$\begin{aligned} f_b(\mathbf{C}) = \tfrac{1}{N_b} \ \textstyle\sum_h \left| \sum_{\eta,\xi} (C_{\eta,\xi}, n(x_h, y_h)) \phi_{\eta,\xi}(x_h, y_h) \right|^2 = \\ \tfrac{1}{length(\partial D_1)} \int_{\partial D_1} |(\ n(P(s)), \varphi(P(s)) \ )|^2 \, ds + \mathcal{O}(\tfrac{1}{N_b}) \end{aligned} \tag{3.5}$$

This is a natural choice, since the boundary data is as useful as the flow data, and sometimes contains less error.

A Tikhonov's regularization term $\epsilon_r f_r(\mathbf{C})$ is added to ensure a unique solution to the Linear Least Squares (LSQ) problem. It stabilizes the problem and works as a low pass filter, smoothing the solution. That smoothing is obtained

by penalizing higher frequencies with larger terms. The regularization term can be expressed as

$$\epsilon_r f_r(\mathbf{C}) = \epsilon_r/2 \sum_{\eta,\xi} \left(|\hat{U}_{\eta,\xi}|^2 + |\hat{V}_{\eta,\xi}|^2 \right) (|\eta|^{2p} + |\xi|^{2p}) =$$
$$= \epsilon_r/2 \left(\|\widetilde{B}_1 \hat{\mathbf{U}}\|_2^2 + \|\widetilde{B}_1 \hat{\mathbf{V}}\|_2^2 \right) = \epsilon_r/2 \ \|\widetilde{B}\mathbf{C}\|_2^2$$

We have introduced the notation $\widetilde{B}_1 = diag(\sqrt{|\eta|^{2p} + |\xi|^{2p}})$ and

$$\widetilde{B} = \begin{bmatrix} \widetilde{B}_1 & 0 \\ 0 & \widetilde{B}_1 \end{bmatrix}$$

After choosing our basis functions the parameter p will control the smoothness degree in the solution.

Finally, the optimal weights $C_{\eta,\xi}$ are found as the solution of

$$\min_{\mathbf{C}} f_d(\mathbf{C}) + f_b(\mathbf{C}) + \epsilon_r f_r(\mathbf{C}) \tag{3.6}$$

3.1 Basis functions

Until now, we have based our construction on the fact that a family of divergence free flows was available. Here we offer explicit details about how such construction can be accomplished. A practical approach would require that $\phi_{\eta,\xi}(x,y)$ should be easy to construct. Furthermore, we would like to have good convergence properties when we increase η_{max} and ξ_{max}, in the L^2 norm sense for example. So we begin our construction with the well known Fourier basis for L^2. Assuming that we work on the computational domain $D = [0, 2\pi]^2$, then our choice for $\phi_{\eta,\xi}(x,y)$ is $\phi_{\eta,\xi}(x,y) = e^{i\eta x} e^{i\xi y}$ where the wavenumbers η, ξ are integers. The flow representation will be

$$\varphi(x,y) = [u(x,y), v(x,y)]$$
$$u(x,y) = \sum \hat{U}_{\eta,\xi} \ e^{i\eta x} e^{i\xi y}$$
$$v(x,y) = \sum \hat{V}_{\eta,\xi} \ e^{i\eta x} e^{i\xi y}$$

Our task is then to find the subspace of fields that fulfill $u_x + v_y = 0$. Now is when the fact that $\phi_{\eta,\xi}(x,y) = e^{i\eta x} e^{i\xi y}{}_{\eta,\xi \in \mathbb{Z}}$ are eigenvectors of any derivative operator becomes extremely useful, because the incompressibility condition can be expressed as:

$$\eta \ \hat{U}_{\eta,\xi} + \ \xi \hat{V}_{\eta,\xi} = 0, \quad \text{for all} \quad \eta, \xi \tag{3.7}$$

which is a linear constraint involving Fourier coefficients of the same wavenumber on different flow components. Since (3.7) has such a simple structure we can make direct substitution arriving to an unconstrained formulation, that fits

nicely into the Tikhonov's regularization framework. Thus, whenever $\xi \neq 0$ we may think of $\hat{U}_{\eta,\xi}$ as independent variables and write $\hat{V}_{\eta,\xi} = -\eta/\xi\ \hat{U}_{\eta,\xi},\ \ \xi \neq 0$. When $\xi = 0$ we keep $\hat{V}_{\eta,0}$ as free variables and get also that $\hat{U}_{\eta,0} = 0,\ \eta \neq 0$. For the same reason, it is easy to see that $\hat{U}_{0,0}$ is another free variable. So far, we are able to span a vector subspace of divergence free flows, based on the Fourier basis of the whole space. Furthermore, since we want to consider just real valued flows, there are other constraints to be imposed:

$$\bar{\hat{U}}_{-\eta,-\xi} = \hat{U}_{\eta,\xi},\ \forall\ |\eta| \leq \eta_{max}, |\xi| \leq \xi_{max} \tag{3.8}$$

where the bar denotes the complex conjugate, and

$$\bar{\hat{V}}_{-\eta,-\xi} = \hat{V}_{\eta,\xi}\ \forall\ |\eta| \leq \eta_{max}, |\xi| \leq \xi_{max} \tag{3.9}$$

Observe that (3.8) and (3.9) are linear constraints if written in terms of the real and imaginary parts of the coefficients separately.
Summing up, when we express all the equations in terms of the real and imaginary parts of the desired quantities, (3.6) becomes a linearly constrained least squares problem.

$$\begin{cases} \min_{\mathbf{C}} f_d(\mathbf{C}) + f_b(\mathbf{C}) + \epsilon_r f_r(\mathbf{C}) \\ \text{subject to} \\ \eta\ \hat{U}_{\eta,\xi} + \ \xi \hat{V}_{\eta,\xi} = 0,\ \forall\ \ |\eta| \leq \eta_{max}, |\xi| \leq \xi_{max} \\ Re\left(\hat{U}_{-\eta,-\xi}\right) = Re\left(\hat{U}_{\eta,\xi}\right),\ \forall\ \ |\eta| \leq \eta_{max}, |\xi| \leq \xi_{max} \\ Im\left(\hat{U}_{-\eta,-\xi}\right) = -Im\left(\hat{U}_{\eta,\xi}\right),\ \forall\ \ |\eta| \leq \eta_{max}, |\xi| \leq \xi_{max} \end{cases} \tag{3.10}$$

By Parseval's identity, the regularization term can be written for integer values of p as

$$\epsilon_r f_r(\mathbf{C}) = \epsilon_r/2 \int_{D_c} \left\{ \left(\frac{\partial^p u}{\partial x^p}\right)^2 + \left(\frac{\partial^p u}{\partial y^p}\right)^2 + \left(\frac{\partial^p v}{\partial x^p}\right)^2 + \left(\frac{\partial^p v}{\partial y^p}\right)^2 \right\} dx$$

which says that we are looking into the space of functions with square integrable pth derivative. That makes the connection to Sobolev spaces and explains how the smoothness of the approximate flow depends on p [11]. Although due to numerical reasons p must be kept relatively small, it has to be large enough to assure the continuity of the solution flow when we allow infinitely many frequencies to appear in the solution (i.e.), $\eta_{max} = \xi_{max} = +\infty$. The minimum value for p depends on the number of dimensions of the space that contains the data which in this case is 2. Observe that without continuity in the solution, pointwise interpolation conditions (3.2) that we want to impose do not make any sense.

3.2 Number of variables involved

This section is devoted to offer an estimate of how many freedom degrees are really present in the solution after imposing the incompressibility constraint.

That will give us an idea of for example how many interpolation conditions can be imposed given once we fix the number of frequencies in the solution. Initially, with no constraints we have $2(2\eta_{max}+1)(2\xi_{max}+1)$ complex variables $\left(\hat{U}_{\eta,\xi}, \hat{V}_{\eta,\xi}\right)$ in the problem. The $(2\eta_{max}+1)(2\xi_{max}+1)-1$ incompressibility constraints (3.7) approximately halve the degrees of freedom. Notice that the incompressibility condition for $\eta = \xi = 0$ gives just a trivial identity $0 = 0$. Beside this, observe that if the free variables are chosen to generate a real flow, then (3.7) will automatically keep that constraint for the dependent variables. This means that we only have to ensure (3.8) and (3.9) just on our free variables. That leaves $2(2\eta_{max}\xi_{max} + \eta_{max} + \xi_{max} + 1)$ free real variables in our system. The last result is obtained by considering the real and imaginary part of each "free" component as independent. A special case occurs again for $\eta = \xi = 0$, where just the real part is nonzero. Suppose now that we have N_d data points and N_b points in the solid wall boundary (denoted by ∂D_1), and we want to know how many Fourier modes we need in the solution in order to be able to interpolate them. The number of Fourier modes present in the solution is $N_f = (2\eta_{max}+1)(2\xi_{max}+1)$, and there are $\mathcal{N} = 2(2\eta_{max}\xi_{max}+\eta_{max}+\xi_{max}+1)$ degrees of freedom so we need to have

$$N_d + N_b/2 \leq 2\eta_{max}\xi_{max} + \eta_{max} + \xi_{max} + 1$$

For the particular case that we take $n_f = \eta_{max} = \xi_{max}$ we have

$$N_d + N_b/2 \leq (n_f+1)^2 + n_f^2 < 2(n_f+1)^2$$

so it is enough to take $n_f > \max(0, \sqrt{\frac{N_d+N_b/2}{2}} - 1)$ to be able to interpolate all the data points. In general, we shall not take n_f large enough to ensure interpolation, since small residuals can be achieved with smaller values.

3.3 Size of the computational domain

We shall now consider how large the computational domain should be compared to the physical one. On one hand, one would like to have it as large as possible, to diminish the effect of the "unnatural" periodic boundary conditions. To offer a crude example of such requirement, suppose that the physical domain is a square, with different prescribed velocities on 2 opposite sides. If the computational domain is just a bit larger than the physical one the periodic extension will be seen as "almost" discontinuous. This will imply that the solution may exhibit the oscillatory behaviour known as Gibb's phenomenon ([32], page 272) and furthermore, contain a lot of high frequency, which is undesirable if one wants low values of η_{max}, ξ_{max} to be able to represent the solution. On the other hand, it is not advisable for the computational domain to be very large because the data will contain only relatively high modes since all the variations are contained in relatively little space. That also implies large values of η_{max}, ξ_{max} to be able to represent the solution. Therefore, we have a trade

off. Here we have taken the size of the computational domain to be twice of the size of the physical one. From the computational results, it seems to be enough. Numerical experiments related with this fact can be observed in section 4.3.

3.4 Some implementation issues

3.4.1 Formulation of the problem in real arithmetic

As seen before in section 3, the problem (3.10) was formulated in the complex space. Now we want to perform our computations with real numbers, so we proceed in the usual way (see [4]). If we have a linear system of equations with complex numbers, $Mf = g$ then it is equivalent to

$$\begin{bmatrix} M_R & -M_I \\ M_I & M_R \end{bmatrix} \begin{bmatrix} f_R \\ f_I \end{bmatrix} = \begin{bmatrix} g_R \\ g_I \end{bmatrix}$$

where the subindex $._R$ denotes the real part and the subindex $._I$ denotes the imaginary part of each quantity. Therefore, from now on we shall work only with real variables and express all the equations in terms of them. The vector $\mathbf{C} = \begin{bmatrix} \hat{\mathbf{U}} & \hat{\mathbf{V}} \end{bmatrix}$ will be then treated by blocks as

$$x = \begin{bmatrix} \mathbf{C}_R & \mathbf{C}_I \end{bmatrix} = \begin{bmatrix} \hat{\mathbf{U}}_R & \hat{\mathbf{U}}_I & \hat{\mathbf{V}}_R & \hat{\mathbf{V}}_I \end{bmatrix}$$

3.4.2 Treatment of the constraints

The real valued version of problem (3.10) defined in section 3 reformulated in terms of real variables as seen in section 3.4.1 can be expressed as a linearly constrained Least Squares problem with the following structure:

$$\begin{cases} \min_x \left\| \begin{bmatrix} A \\ \sqrt{\epsilon_r} B \end{bmatrix} [x] - \begin{bmatrix} b \\ 0 \end{bmatrix} \right\|_2^2 = \|Ax - b\|_2^2 + \epsilon_r \|Bx\|_2^2 \\ s.t. \\ Hx = 0 \end{cases} \tag{3.11}$$

where H denotes the matrix for the homogeneous linear constraints (3.7), (3.8) and (3.9). As observed before in 3.1 the structure of the matrix H is so simple that allows us to perform direct substitution of the variables in order to obtain an unconstrained problem with less variables. To state this in a more direct way, let us write our constraints $Hx = 0$ in block notation as

$$\begin{bmatrix} H_F & H_D \end{bmatrix} \begin{bmatrix} x_F \\ x_D \end{bmatrix} = \begin{bmatrix} 0 \end{bmatrix} \tag{3.12}$$

where H_D is an invertible sub matrix of H. That implies

$$x_D = -H_D^{-1} \; H_F \; x_F$$

Therefore, we can span the set of feasible solutions using just x_F with

$$\begin{bmatrix} x_F \\ x_D \end{bmatrix} = \begin{bmatrix} I \\ -H_D^{-1} \; H_F \end{bmatrix} \; \begin{bmatrix} x_F \end{bmatrix}$$

Now we substitute this into the initial formulation (3.11) obtaining

$$\min_{x_F} \left\| \begin{bmatrix} A \\ \sqrt{\epsilon_r} B \end{bmatrix} \begin{bmatrix} I \\ -H_D^{-1} H_F \end{bmatrix} \begin{bmatrix} x_F \end{bmatrix} - \begin{bmatrix} b \\ 0 \end{bmatrix} \right\|_2^2 =$$

$$= \min_{x_F} \left\| \begin{bmatrix} A_F - A_D H_D^{-1} H_F \\ \sqrt{\epsilon_r} \left(B_F - B_D H_D^{-1} H_F \right) \end{bmatrix} \begin{bmatrix} x_F \end{bmatrix} - \begin{bmatrix} b \\ 0 \end{bmatrix} \right\|_2^2 \tag{3.13}$$

Observe that H_D is diagonal, and H_F is very sparse. In fact, it has only one nonzero value on each row, so the same happens with the matrix $\begin{bmatrix} I \\ -H_D^{-1} H_F \end{bmatrix}$.

Renaming $\widetilde{x} = x_F$, $\widetilde{A} = A_F - A_D H_D^{-1} H_F$ and $\widetilde{B} = B_F - B_D H_D^{-1} H_F$ in (3.13) we get the unconstrained formulation

$$\min_{\widetilde{x}} \left\| \begin{bmatrix} \widetilde{A} \\ \sqrt{\epsilon_r} \widetilde{B} \end{bmatrix} \begin{bmatrix} \widetilde{x} \end{bmatrix} - \begin{bmatrix} b \\ 0 \end{bmatrix} \right\|_2^2 = \min_{\widetilde{x}} \|\widetilde{A}\widetilde{x} - b\|_2^2 + \epsilon_r \|\widetilde{B}\widetilde{x}\|_2^2 \tag{3.14}$$

Since often the matrix $\widetilde{A}$ obtained by the substitution procedure may still be ill conditioned the Tikhonov regularization term $\sqrt{\epsilon_r}\widetilde{B}$ plays an important role. In Appendix B all the results are formulated in terms of (3.14), with the $\widetilde{\ }$ dropped. The sparsity of the matrices involved for $\eta_{max} = \xi_{max} = 3$ can be observed in Figure 3.1. There we show from left to right a row permuted version of the matrices $\begin{bmatrix} A \\ \sqrt{\epsilon_r} B \end{bmatrix}$, $\begin{bmatrix} I \\ -H_D^{-1} H_F \end{bmatrix}$ and their product $\begin{bmatrix} A \\ \sqrt{\epsilon_r} B \end{bmatrix} \begin{bmatrix} I \\ -H_D^{-1} H_F \end{bmatrix} = \begin{bmatrix} \widetilde{A} \\ \sqrt{\epsilon_r} \widetilde{B} \end{bmatrix}$

The problem was solved in Matlab [27] using methods described in 2.2.4 and the differences encountered in the solutions were consistent with the error estimates given in theorem 3 and those included in Corollary 2 from Appendix A.

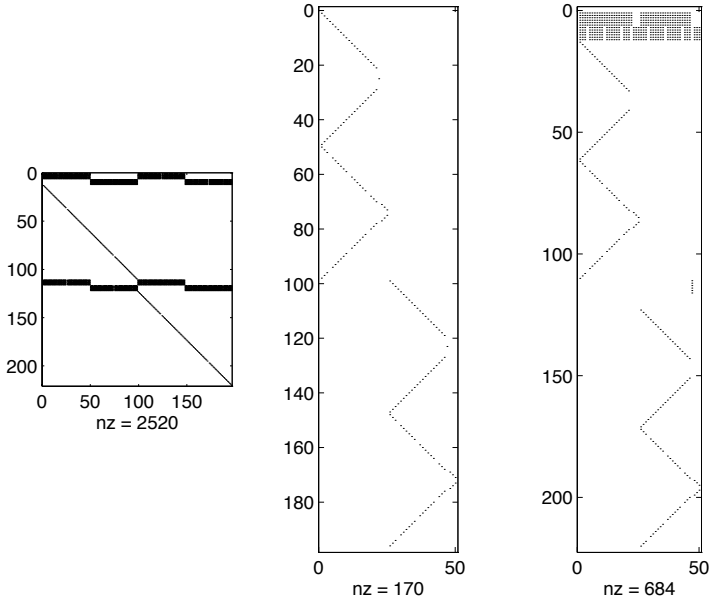

Figure 3.1: Uruguayan case with 6 station points. Sparse structure for the matrices of the LSQ with $\eta_{max} = \xi_{max} = 3$ and no imposed boundary conditions. Then number nz counts the nonzero elements in each matrix.

Chapter 4

Numerical examples

Here we include computational experiments in order to gain insight into the proposed method, as well as to motivate some way of choosing parameters, like for example the values of p and $N = \xi_{max} = \eta_{max}$. First we perform computations with model problems, trying to see the behaviour of the method in different situations, and also to compare the numerical solution with the exact one when it is available. Beside this, we include a comparison with the method used by López Vázquez [35], involving real data from the southern zone of Uruguay.

In all the cases, we make use of these notation:
$A_1x - b_1$: residual corresponding to data point conditions, $\|A_1x - b_1\|_2^2 = f_d(\mathbf{C})$.
A_2x: residual corresponding to homogeneous slip boundary conditions,
$\|A_2x\|_2^2 = f_b(\mathbf{C})$.
$Ax - b$: residual corresponding to both data point conditions and slip boundary conditions, that is

$$||Ax - b||_2^2 = \|A_1x - b_1\|_2^2 + \|A_2x\|_2^2 \qquad = f_d(\mathbf{C}) + f_b(\mathbf{C}) =$$
$$\frac{1}{N_d}\sum_{j=1}^{N_d} \|\varphi(P_j) - \hat{\varphi}(P_j)\|_2^2 \quad + \frac{1}{N_b}\sum_{h=1}^{N_b} \left(n(P_h), V(P_h)\right)^2$$

Bx: regularization term

$$\|Bx\|_2^2 = f_r(\mathbf{C}) = \sum_{\eta,\xi} \left(|\hat{U}_{\eta,\xi}|^2 + |\hat{V}_{\eta,\xi}|^2\right) (|\eta|^{2p} + |\xi|^{2p})$$

N_f : amount of wavenumbers present in the numerical solution,
$N_f = (2\xi_{max} + 1)(2\eta_{max} + 1)$
In some graphics we will use the names N_x, N_y instead of ξ_{max}, η_{max}

We study the sensitivity by means of three experiments, where we vary one of the parameters while keeping the others fixed (i.e),

1. Sensitivity with respect to ϵ_r. This experiment corresponds to the points in the L-curve introduced in section 2.2.3.

2. Sensitivity with respect to N. This is meant to find a suitable amount of wavenumbers in order to achieve small residuals.

3. Sensitivity with respect to p. As commented in section 3.1, p determines the smoothness degree of the solution and it must be greater than one for two dimensional problems. Nevertheless, it cannot be taken too large, as will be seen in the examples.

Numerical results of the evolution of the condition number $\kappa_2(M(\epsilon_r))$ of the least squares problem to be solved, as well as the effect on the spectrum of singular values are shown in the Figures to check theoretical predictions.

The results included in Chapter 2 and Appendix A justify that the condition number behaves like an approximate linear function of the inverse of the square root of the regularization parameter. The effect of the maximum wavenumber N or the smoothness parameter p on this condition number is less straigthforward altough some motivation can be given through the experiments. The reader will be also able to inspect directly the effect of the parameters in the computed velocity field, as well as the changes in $|\hat{U}_{\eta,\xi}|$ and $|\hat{V}_{\eta,\xi}|$ which are shown under the title " *Spectral energy distribution*". There one can check that the approximate flows can be constructed with a small number of terms.

4.1 Model problems

4.1.1 2D flow around a circular tube

This example has only one point with known velocity, and there is a solid boundary given by a tube wall, where the slip boundary condition holds:

$$(n(P), \varphi(P))|_{\text{solid wall}} = 0$$

All these can be seen in Figure 4.1. For the computations we have discretized the circle wall on $N_b = 100$ uniformly distributed points. The resulting flow can also be seen in Figure 4.1 and it corresponds to the following parameters:

$$p = 1.5, \quad N_b = 100 \quad \epsilon_r = 1e-4$$

Since our method defines an approximation on every point of the computational domain it will also define it inside of the tube. This will be of no importance since the tube wall acts as a streamline.

Sensitivity Results

1. Sensitivity with respect to ϵ_r. In Figures 4.3 and 4.4 we see that in this case the residual can be diminished to small values without almost no increase in the regularization term, and we are able to use Richardson

extrapolation to compute a smooth solution which interpolates the data. The results of the L curve experiment are shown in Figure 4.2.

2. Sensitivity with respect to N, shown in Figures 4.5 and 4.6.

   In Figure 4.5 we see that $\kappa(M(\epsilon_r))$ increases with the maximum wavenumber N. That can be explained by means of the bound (A.9) that indicates a growth with $\sqrt{6}\sqrt{1+3N}(2N+1)$.

   We also observe that $N \geq 2$ is enough to provide small residuals.

   The effect of N in the singular values can be seen by first looking at the operator B used for the regularization. When N increases, so does the number of freedom degrees in the problem, yielding new larger singular values in B, that behave like $\sqrt{|\eta|^{2p} + |\xi|^{2p}}$, while keeping all the old singular values approximately constant. This explains why the small singular values corresponding to the regularization looks essentially the same for different values of N (see Figure 4.5).

3. Sensitivity with respect to p, as shown in Figures 4.7 and 4.8. Let us see the dependence of $\kappa(M(\epsilon_r))$ shown in Figure 4.7. As p increases the diagonal matrix B increases its entries, which means that the singular values of $M(\epsilon_r; p)$ increase. This, depending on the relative size of ϵ_r will make the condition shrink or increase. The first happens when ϵ_r is relatively small, such that the singular values introduced by the regularization are much smaller than those originally present in the problem. In this case the maximum singular value of $M(\epsilon_r; p)$ will be basically unchanged, whereas the smallest increases. On the other hand, we can observe that the condition number increases with p when some of the singular values introduced by the regularization are of the same order as those originally present. Then the maximum singular value of $M(\epsilon_r; p)$ can increase with enough speed to make the condition number larger. Beside this, p affects the spectrum of singular values, changing the "power" profile, as seen in Figure 4.7.

As predicted before, $||Ax - b||$ decreases with N or as ϵ_r decreases. The dependence with respect to the smoothness parameter p is less simple, as can be seen in Figure 4.7. Recall that in section 3 it was pointed out that the value of p should be greater than 1 to have a well posed problem when we let $N \to \infty$. If that is not the case, even for small values of N, the solution will fit the measurements but vanish quickly away from them. That effect can be seen on the first plot in Figure 4.8. However, computational experience shows that the residuals increase when p is increased above some threshold level, and moreover, the solution may look wild as depicted on the rightmost of Figure 4.8, so it seems to be an optimal value of smoothness. In the present work we have taken $p = 1.5$.

With respect to the boundary condition at the solid wall, a question arises respect to the choice of the number of points in the discretized boundary. It seems tempting to try to add as much as possible points to improve the accuracy. However, the size of the problem will increase and we will face more

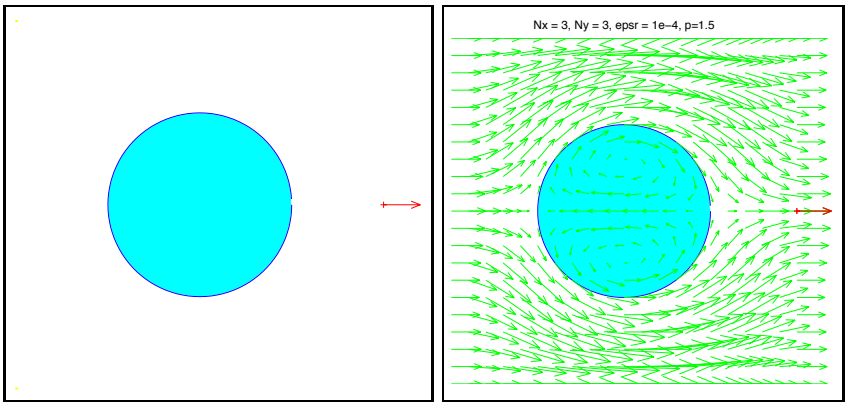

Figure 4.1: Numerical experiments with the tube problem.Left: Data for the problem. The circle wall has been discretized in $N_b = 100$ points and there exist only one flow measurement, shown in red. Right: Computed solution for $N = \xi_{max} = \eta_{max} = 3$,

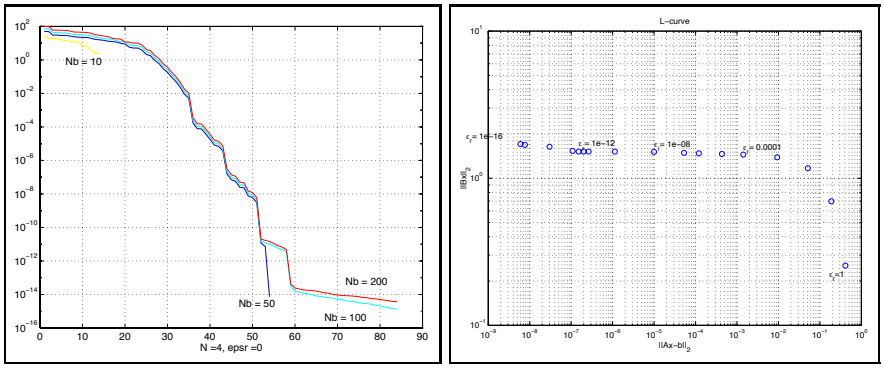

Figure 4.2: Numerical experiments with the tube problem. Left: Dependence of the spectrum of singular values w.r.t. N_b, the number of points in the discretized boundary. Right: L-curve plot of the residual and the regularization term.

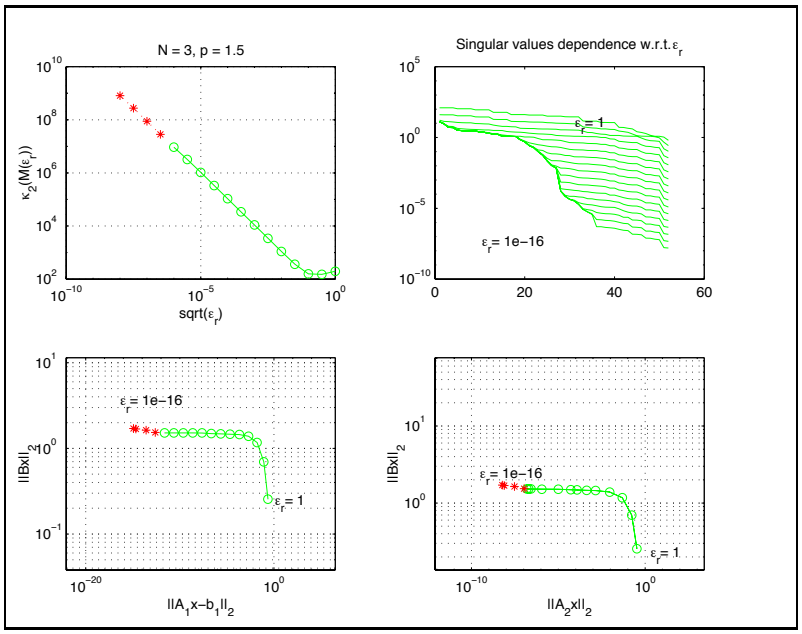

Figure 4.3: Numerical experiments with the tube problem. Dependence of the solution w.r.t. ϵ_r.

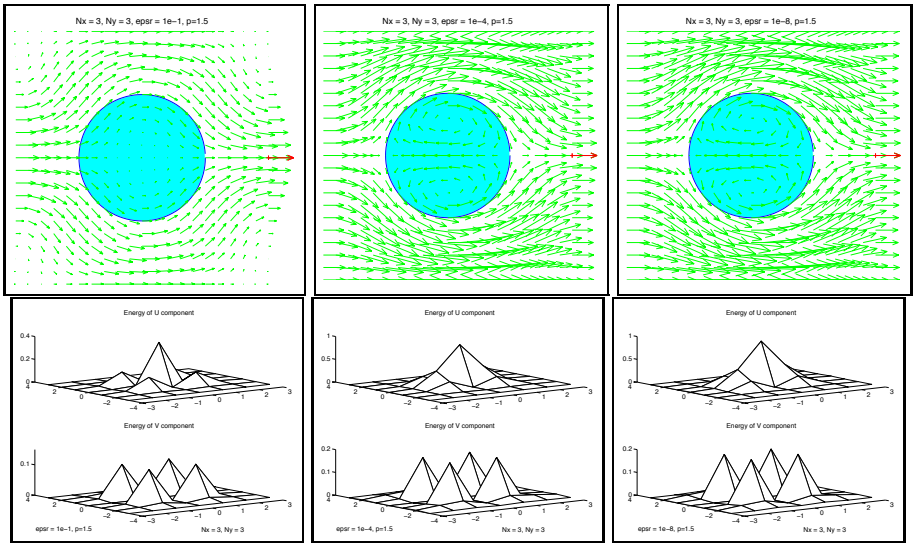

Figure 4.4: Numerical experiments with the tube problem. Dependence of the solution w.r.t. ϵ_r. Top:Flow results. Bottom:Spectral energy distribution

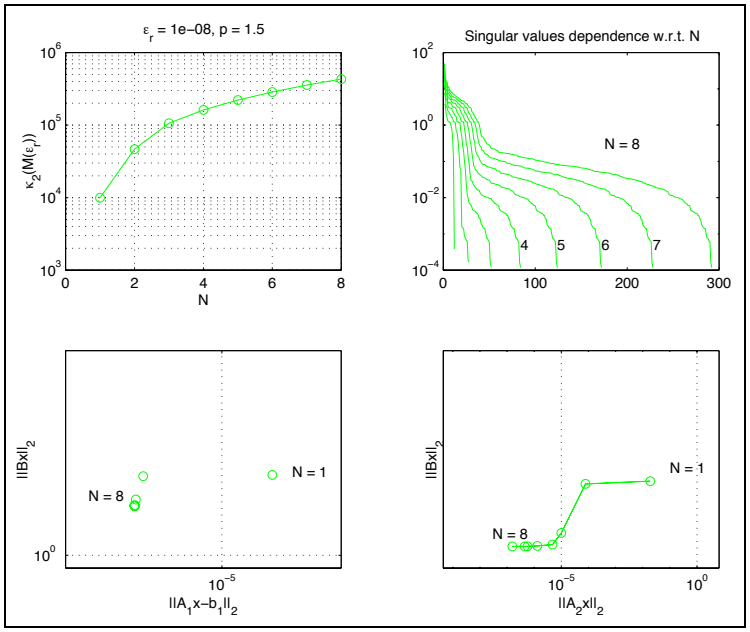

Figure 4.5: Numerical experiments with the tube problem. Dependence of the solution w.r.t. N.

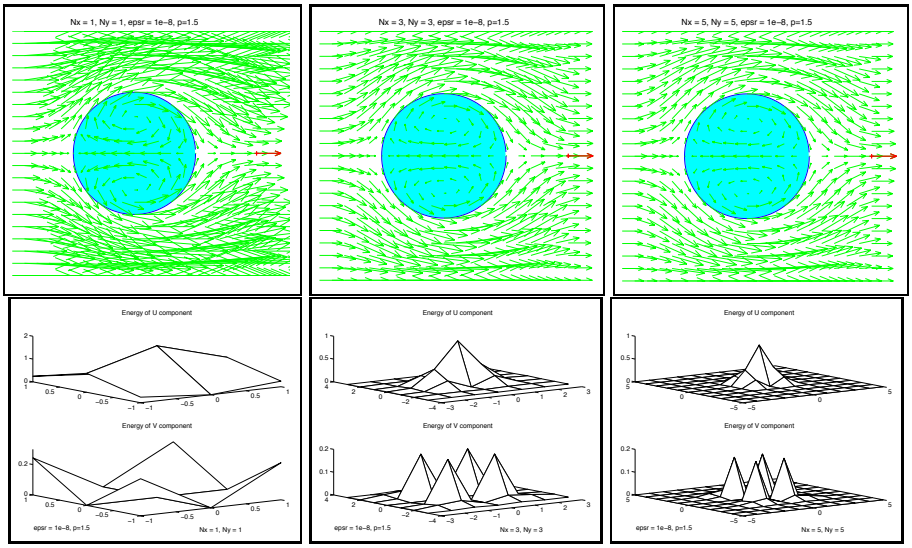

Figure 4.6: Numerical experiments with the tube problem. Dependence of the solution w.r.t. N. Top:Flow results. Bottom:Spectral energy distribution

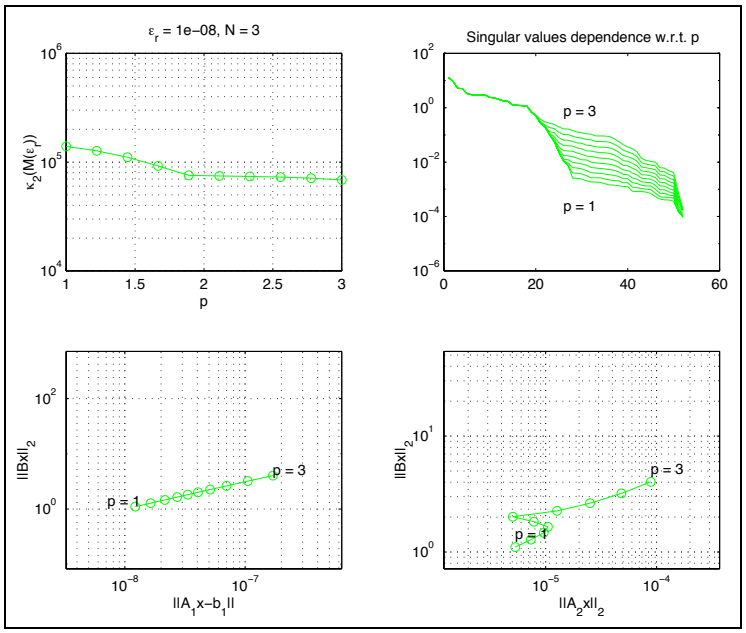

Figure 4.7: Numerical experiments with the tube problem. Dependence of the solution w.r.t. p.

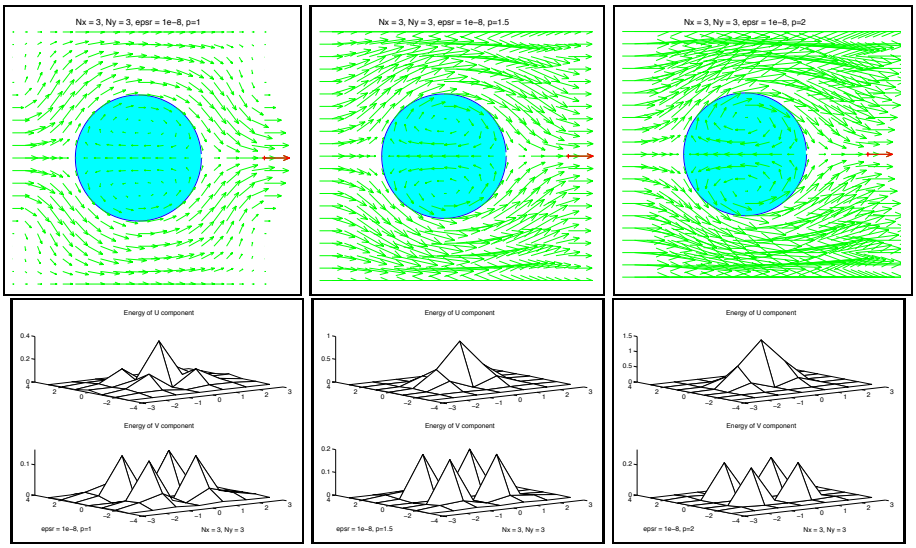

Figure 4.8: Numerical experiments with the tube problem. Dependence of the solution w.r.t. p. Top:Flow results. Bottom:Spectral energy distribution

computational effort Moreover, adding more points to the boundary discretization does not necessary imply a practical improvement in the accuracy in the numerical solution. Recall that

$$\|A_2 x\|_2^2 = \frac{1}{length(\partial D_1)} \int_{\partial D_1} (\varphi, n)^2 ds + \mathcal{O}\left(\frac{1}{N_b}\right) = \sum_{i=1}^{\min\{N_b, N_f\}} \sigma_i^2 (v_i^T x)^2$$

where $A_2 \in \mathbb{R}^{N_b \times N_f}$. Observe that both its singular values σ_i and right singular vectors v_i depend on N_b.

As N_b increases below N_f, the spectrum corresponding to large singular values are within $\mathcal{O}\left(\frac{1}{N_b}\right)$ of the spectrum that corresponds to the non discretized operator, while new small strictly positive singular values appear. Those are associated with ill-posedness, and do not provide any useful information.

Beside this, the error coming from the discretization of the boundary is just one of many, and it is not advisable trying to reduce it without keeping in mind that the others are still present and are possibly larger. Numerical results can be seen in Figure 4.2, where we show the computed singular values of matrix A for different number of points in the discretized boundary. There it can be seen that approximately 35 singular values are important. By important we mean above the regularization threshold, which is $\mathcal{O}(\sqrt{\epsilon_r})$.

In this particular example, there is almost no change in these singular values when we use 200 points or 100 in the discretization and the corresponding numerical result is practically the same.

4.1.2 2D flow over a ramp

In this example we have an incompressible flow with linear velocity profile over a ramp. We shall again see the effect of boundary conditions, and furthermore, how approximate is the numerical solution to the exact solution of the problem, which is available.

We have discretized the boundary wall by means of 100 uniformly distributed points and included 100 data points along the line segment

$$0 \leq x \leq 0.5, y = 0$$

as shown in Figure 4.9. The computational domain is $D_c = [0,1]^2$ and the parameters have been set to $p = 1.5$ and $\epsilon_r = 1e-4$. In Figure 4.9 we can see a typical numerical result, and in Figure 4.10 we show the residual components, both for the velocity conditions at the data points and the slip boundary condition. On the left we show the error in x and y velocity components (i.e.), the components of the vector $(\varphi - \hat{\varphi})(P_j)$ for $j = 1 \ldots N_d$.

On the rightmost graphic we show the value $(\varphi(P_h), n(P_h))$ for $h = 1 \ldots N_b$.

As in the tube flow example, all three sensitivity experiments have been carried out and the same sort of comments apply. However, this solution is less sensitive than the numerical solution of the tube problem, since there is more data available in this case.

1. Sensitivity with respect to ϵ_r. See Figures 4.11 and 4.12 for detailed results and Figure 4.17 for the L-curve experiment.

2. Sensitivity with respect to N, shown in Figures 4.13 and 4.14.

3. Sensitivity with respect to p, as shown in Figures 4.15 and 4.16.

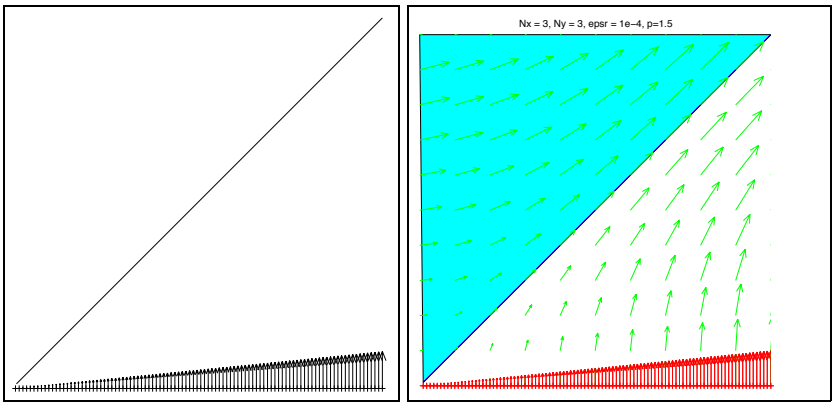

Figure 4.9: 2D flow over a ramp. Left: Boundary and data points. Right: Numerical solution

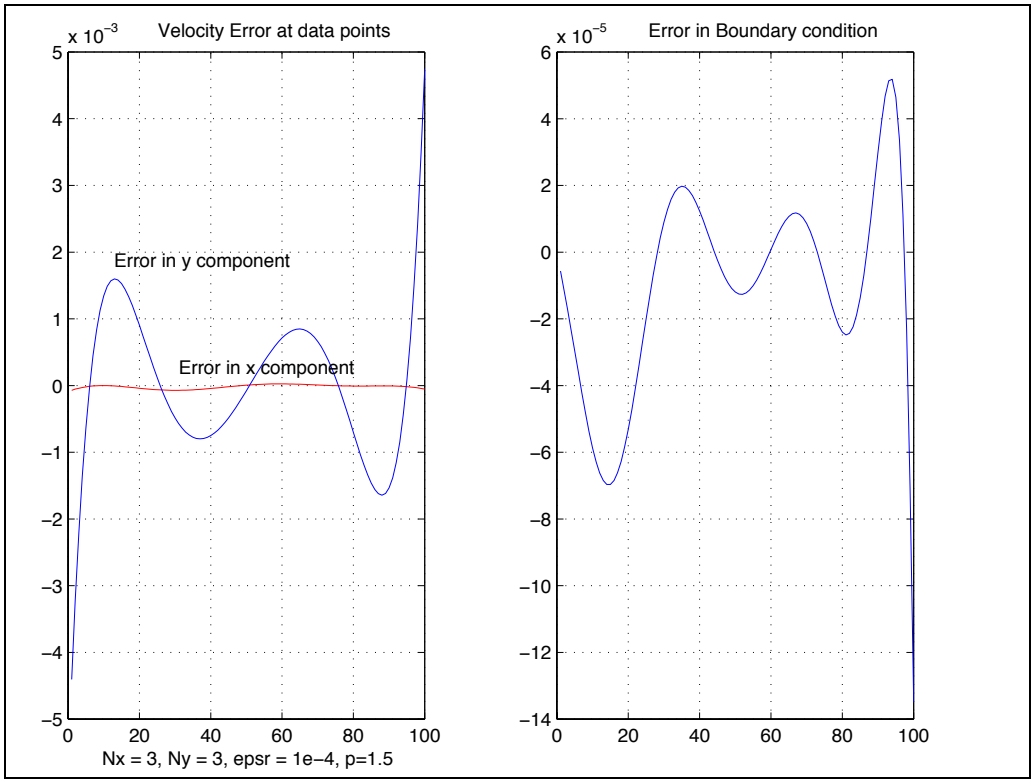

Figure 4.10: 2D flow over a ramp. Left: $A_1x - b_1$, residual at the data points Right: A_2x, residual of slip boundary condition at boundary points

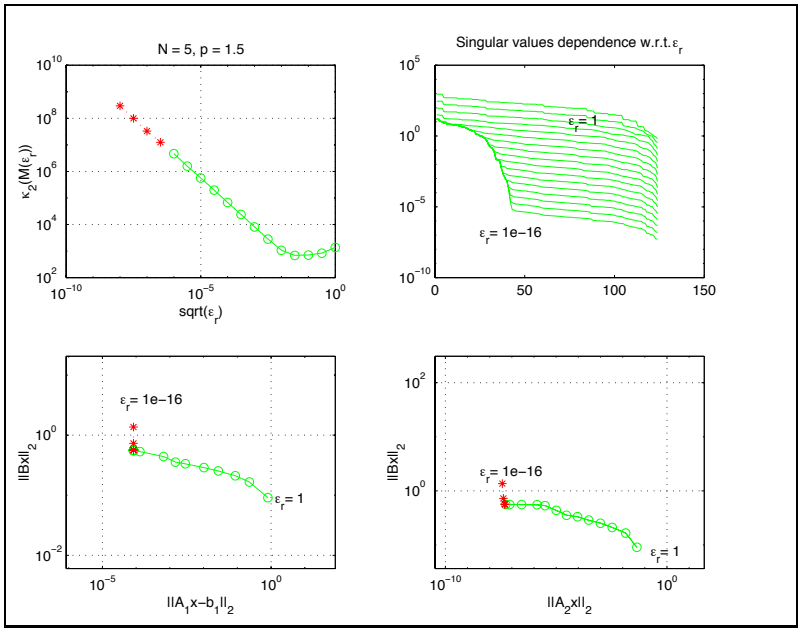

Figure 4.11: Dependence of the solution w.r.t. ϵ_r.

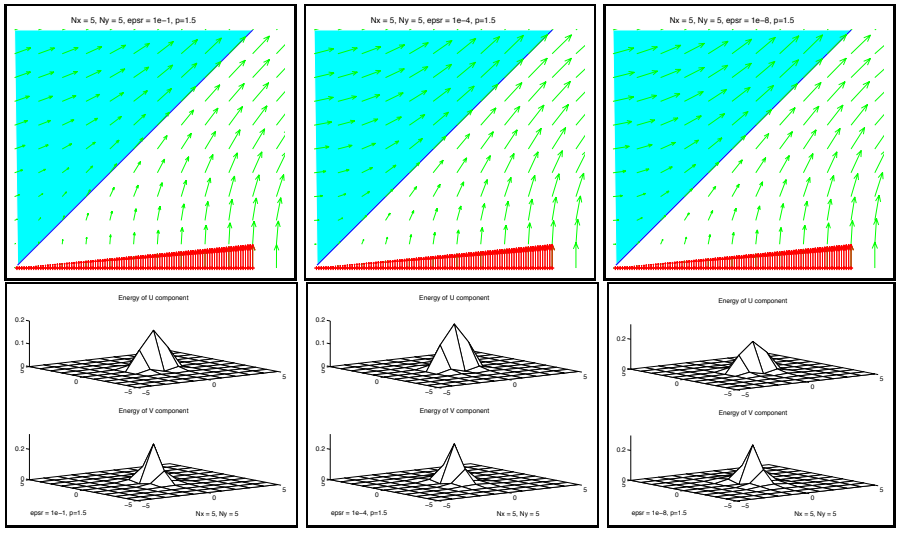

Figure 4.12: Dependence of the solution w.r.t. ϵ_r. Top:Flow results. Bottom:Spectral energy distribution

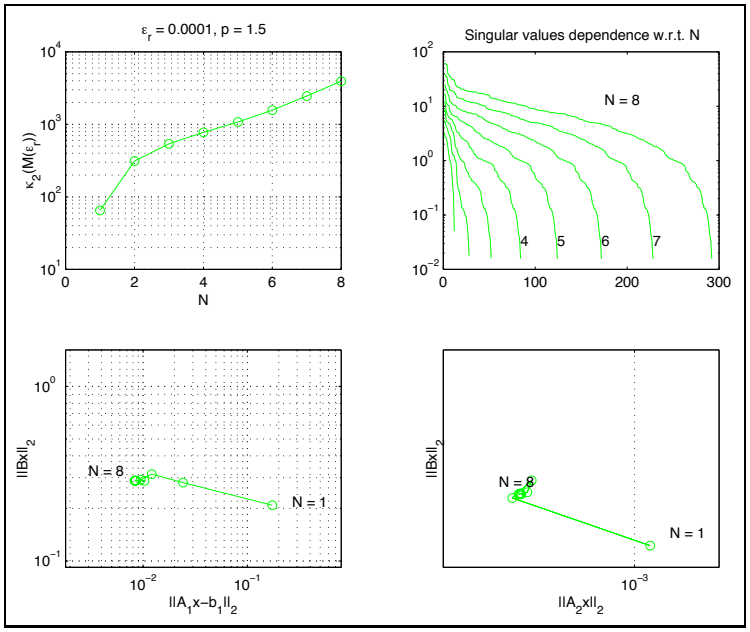

Figure 4.13: Dependence of the solution w.r.t. N.

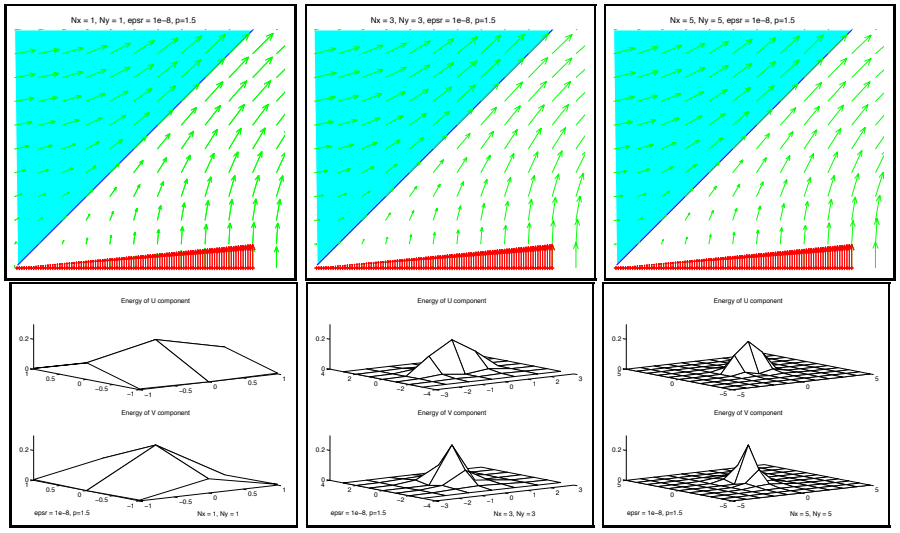

Figure 4.14: Dependence of the solution w.r.t. N. Top:Flow results. Bottom:Spectral energy distribution

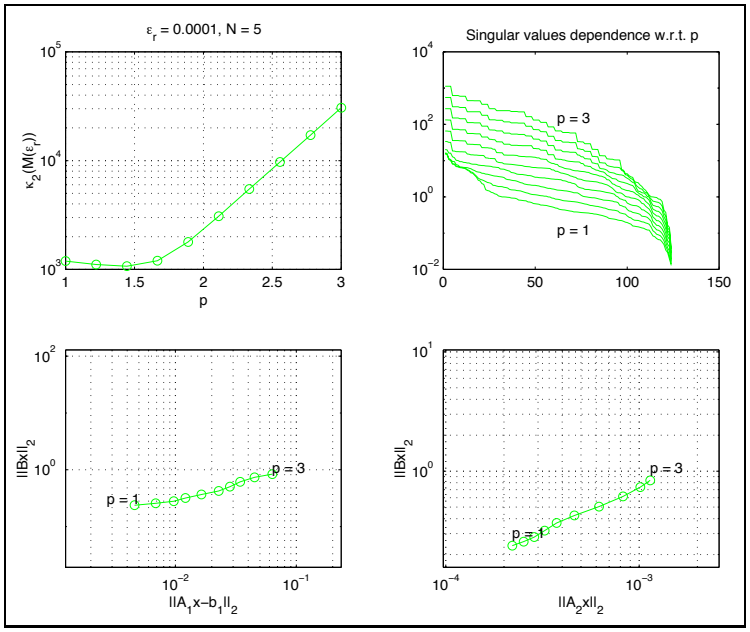

Figure 4.15: Dependence of the solution w.r.t. p.

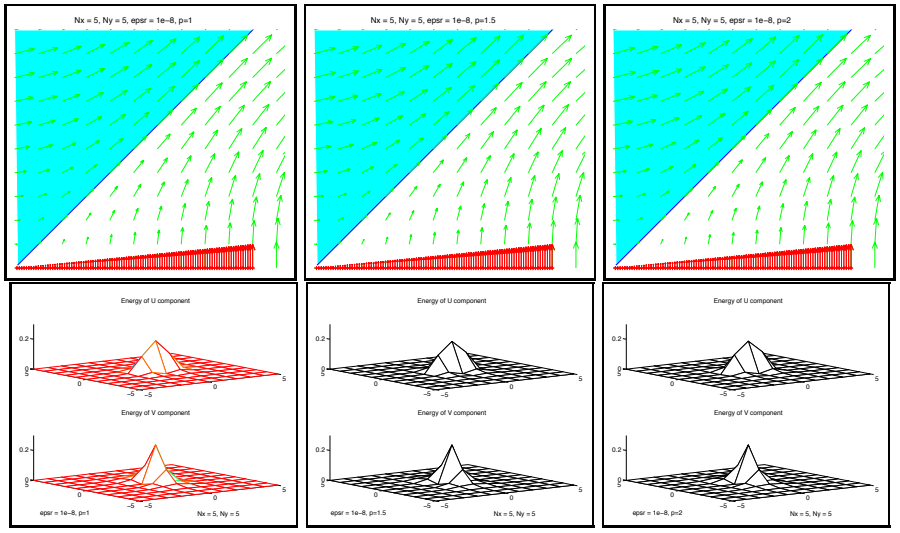

Figure 4.16: Dependence of the solution w.r.t. p. Top:Flow results. Bottom:Spectral energy distribution

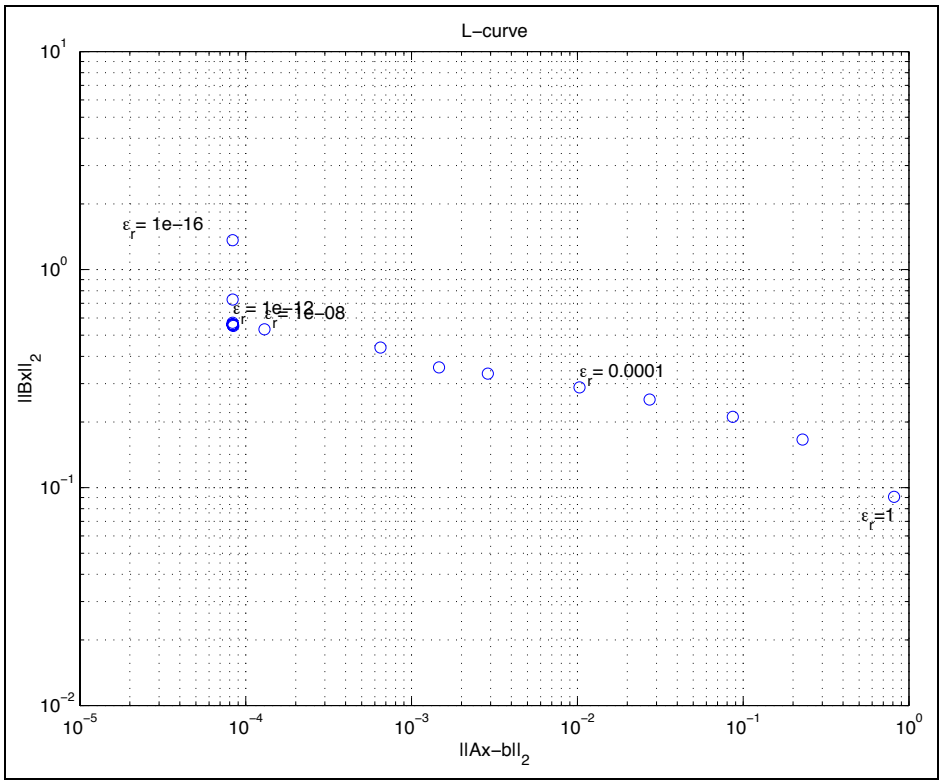

Figure 4.17: L curve for the ramp case.

4.1.3 Comparison with exact solution

As we said before, the exact solution is available in this example. Both the slip boundary condition and the data measurements are satisfied by the potential flow

$$\widehat{\varphi} = [y, x]$$

Now we compare this flow with the numerical solution, using a grid of points that is uniformly distributed on the region of interest:

$$\left\{(x, y) \in \mathbb{R}^2 : x \geq 0, x \geq y, x \leq 0.5\right\}$$

That grid can be seen in Figure 4.18, and the error function for $N = 2$ and $N = 3$ can be seen in Figure 4.19. There we see that $N = 2$ is enough for our purposes, since there is no gain in accuracy when using $N = 3$. To increase the accuracy one needs to use more data points, preferably away from the boundary where we have already imposed velocity data.

The same conclusion can be derived from Table 4.1 we show different norms of the error function on the grid of Figure 4.18, for values of $N = \xi_{max} = \eta_{max}$ ranging from 1 to 6.

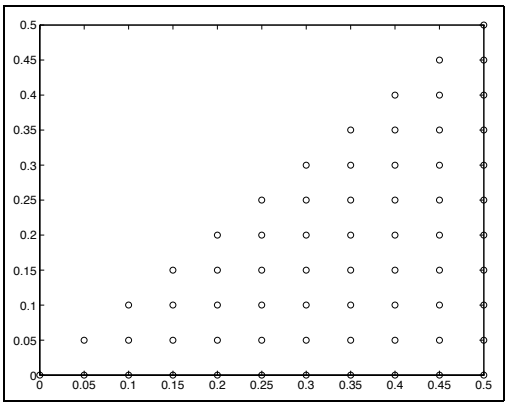

Figure 4.18: Grid of points used to measure the difference between the the exact solution and the numerical solution.

N	$\|\varphi - \hat{\varphi}\|_{\ell^2}$	$\|\varphi - \hat{\varphi}\|_{\infty}$
1	0.2863	0.0721
2	0.0577	0.0182
3	0.0854	0.0213
4	0.0546	0.0110
5	0.0545	0.0117
6	0.0550	0.0114

Table 4.1: Error norm on the grid of Figure 4.1 as a function of the maximum wavenumber.

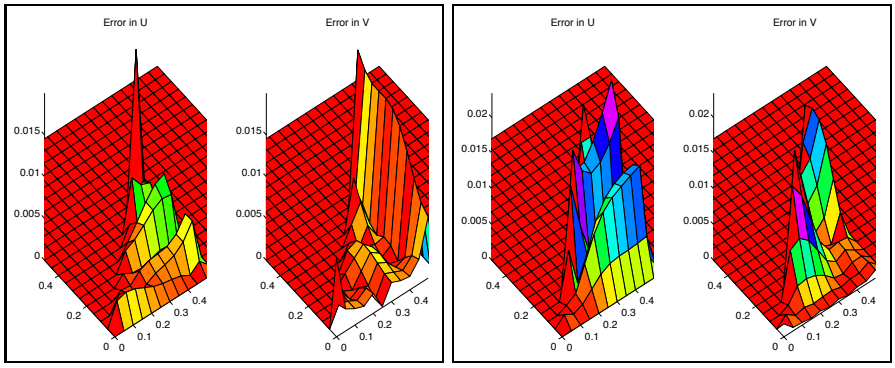

Figure 4.19: The mesh plot interpolates the values obtained at the grid from Figure 4.18. Left: Results for $N = 2$. Right: Results for $N = 3$.

4.1.4 2D Rankine vortex inside a tube

This example shows an application of the method to a confined flow. There exist 36 points with known velocity, and there is a solid boundary given by a tube wall, where the slip boundary condition holds. The velocity profile corresponds to a Rankine vortex, that is,

$$\hat{\varphi}(x,0) = (0, V(x)), \quad -R \leq x \leq R$$

where $R = .5$; and $V(x) = \begin{cases} \frac{5}{8x} & if\ |x| \geq 0.25 \\ 10x & if\ |x| \leq 0.25 \end{cases}$

All these can be seen in Figure 4.20. For the computations we have discretized the circle wall on $N_b = 100$ uniformly distributed points. The resulting flow can also be seen in Figure 4.20 and it corresponds to the following parameters:

$$p = 1.5, \quad N = 5 \quad \epsilon_r = 1e-4$$

Since our method defines an approximation on every point of the computational domain it will also define it outside of the tube. This will be of no importance since the tube wall acts as a streamline.

Sensitivity Results

Since most of the comments regarding sensitivity do apply in this example we do not repeat them, and content ourselves with a brief outline of the numerical results.

1. Sensitivity with respect to ϵ_r. In Figures 4.22 we see that in this case the residual remains in the order of 6 % of the velocity measurements. This slow convergence is due to the non-smoothness of the Rankine vortex. However, observe that the slip boundary condition is accurately fulfilled. The results of the L curve experiment are shown in Figure 4.21 and it justifies the approximate choice $\epsilon_r = 0.0001$.

2. Sensitivity with respect to N, shown in Figures 4.22, 4.24 and 4.23 We observe that the difference between the measurements and the numerical solution decreases as N increases, and that its maximum is clearly related with the radius $0,25$ where the Rankine vortex is non smooth.

3. Sensitivity with respect to p, as shown in Figure 4.25. Let us see the dependence of $\kappa(M(\epsilon_r))$ shown in Figure 4.25. This, depending on the relative size of ϵ_r will make the condition shrink or increase.

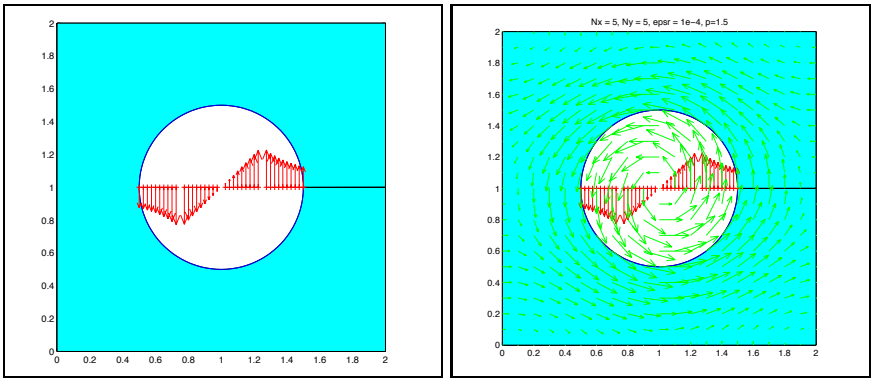

Figure 4.20: Numerical experiments with the Rankine vortex problem.Left: Data for the problem. The circle wall has been discretized in $N_b = 100$ points and there exist 36 flow measurements, shown in red. Right: Computed solution for $N = \xi_{max} = \eta_{max} = 5$,

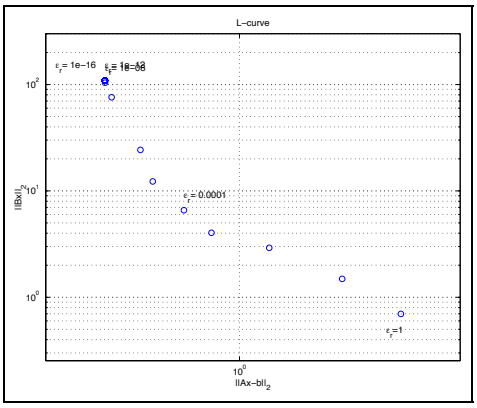

Figure 4.21: Numerical experiments with the Rankine vortex problem: L-curve plot of the residual and the regularization term.

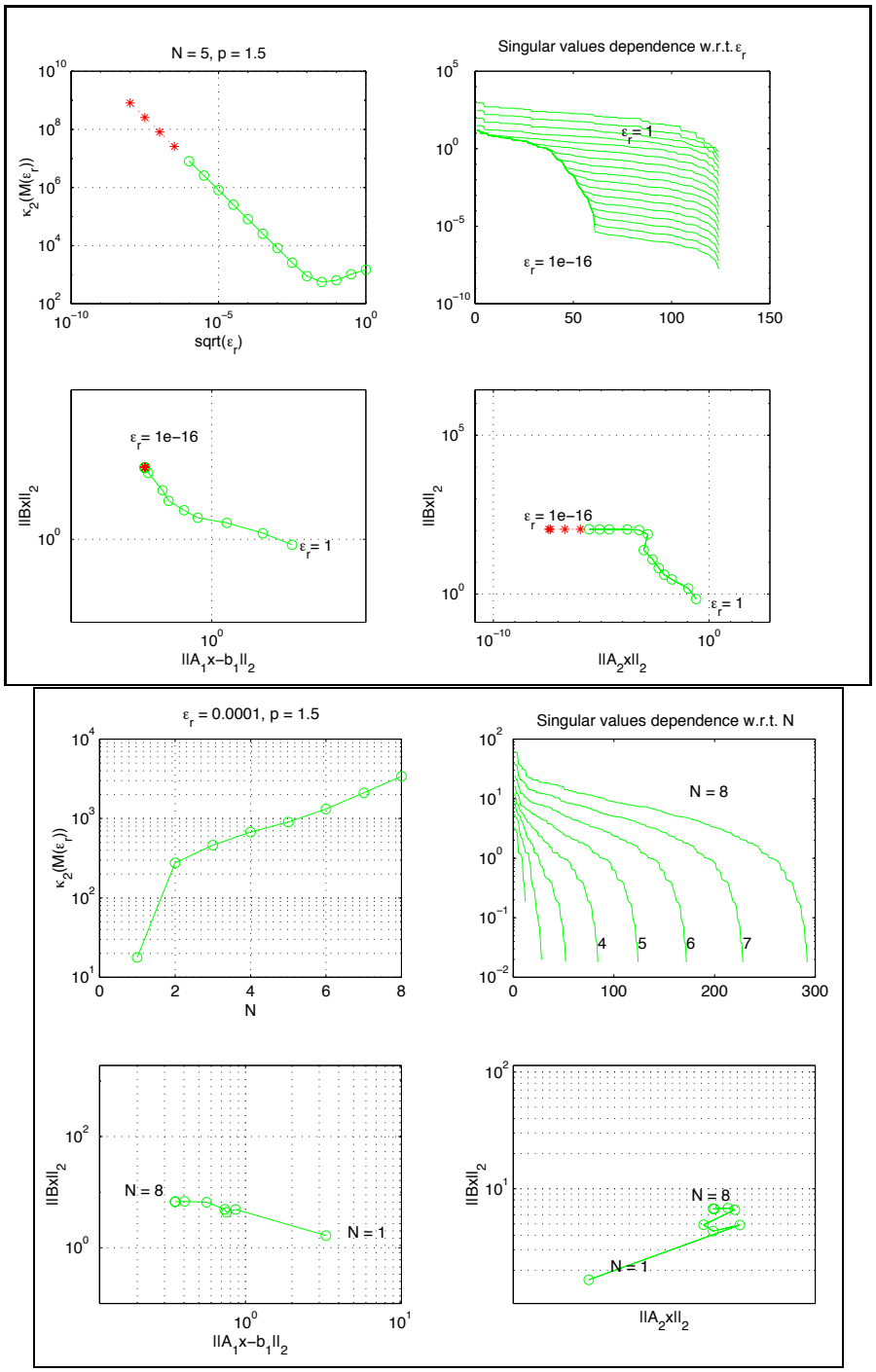

Figure 4.22: Numerical experiments with the Rankine vortex problem. Top:Dependence of the solution w.r.t. ϵ_r. Bottom: Dependence of the solution w.r.t. N.

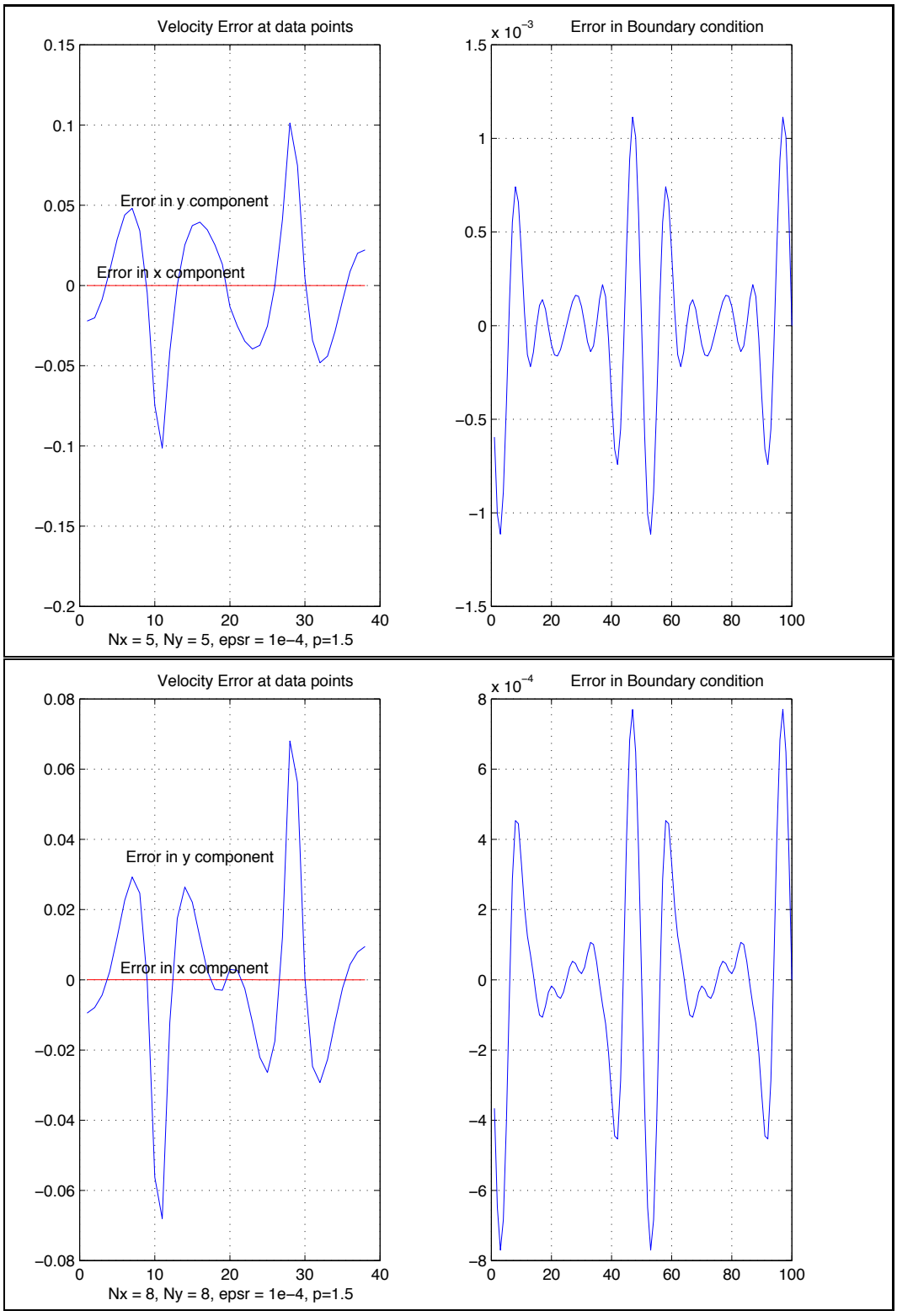

Figure 4.23: Residual plots in the Rankine vortex example. Above: Results with $N = 5$ Bottom: Results with $N = 8$

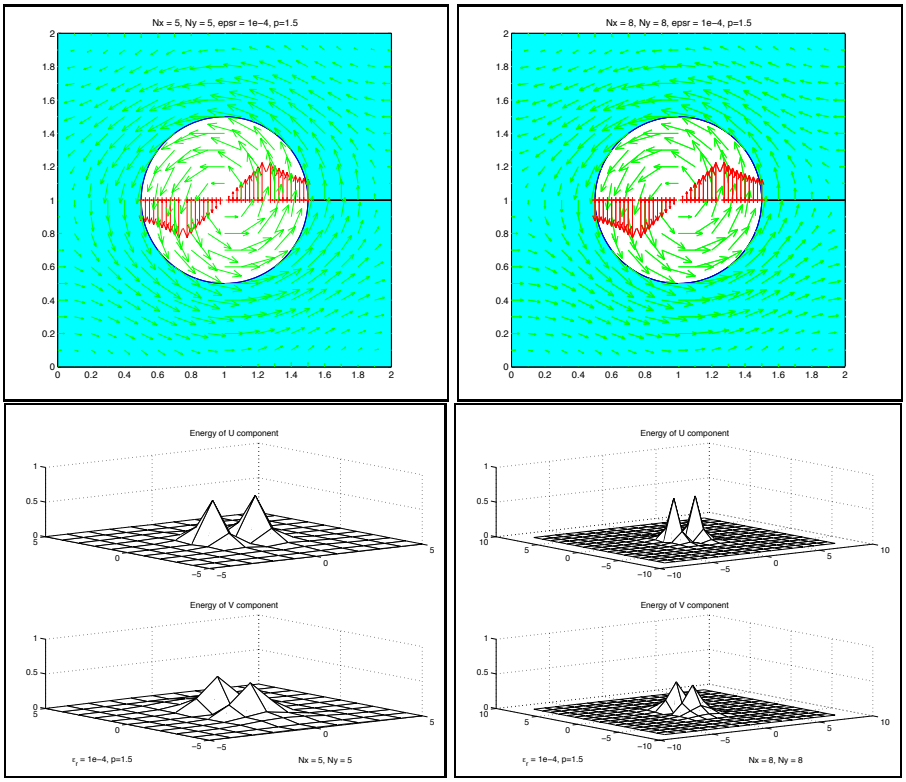

Figure 4.24: Numerical experiments with the Rankine vortex problem. Dependence of the solution w.r.t. N. Top:Flow results. Bottom:Spectral energy distribution.

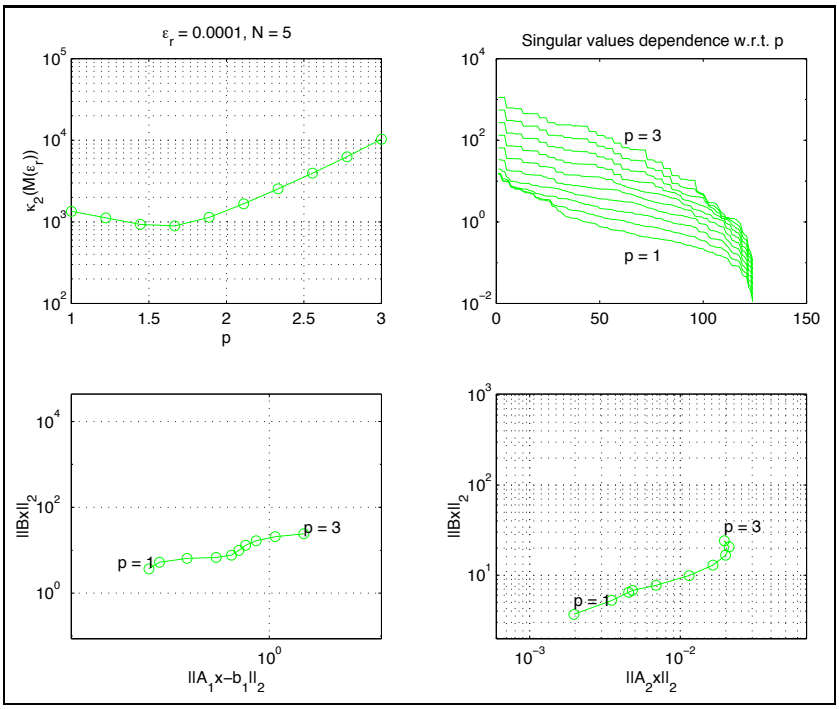

Figure 4.25: Numerical experiments with the Rankine vortex problem. Dependence of the solution w.r.t. p.

4.2 Wind field in the southern zone of Uruguay

Now we consider a problem with real data from the Southern zone of Uruguay. The same approximation problem was first studied by López Vázquez in his Master Thesis [35], where also a statistical analysis of time dependent measurements is done following the work of Ludwig [24] and Richman [29]. Precisely that Principal Components analysis is the data source for our example. Since we do not give the details of the statistical procedure the reader can directly refer to López Vázquez [35].

However, we sketch the result to provide an rough link between crude data measurements and the application of the numerical procedure described in this work. The original version of the problem can be stated as follows: given 6 velocity field measurements in an hourly basis, find an incompressible approximation for each time point. Instead of solving an approximation problem for each sample in time, an Principal Components expansion for the *measurements* is first computed.

$$\begin{bmatrix} \hat{\varphi}(t, P_1) \\ \vdots \\ \hat{\varphi}(t, P_{N_d}) \end{bmatrix} = \begin{bmatrix} \hat{\varphi}_m(P_1) \\ \vdots \\ \hat{\varphi}_m(P_{N_d}) \end{bmatrix} + \sum_k a_k(t) \begin{bmatrix} \hat{\varphi}_k(P_1) \\ \vdots \\ \hat{\varphi}_k(P_{N_d}) \end{bmatrix} \tag{4.1}$$

In this case, the contribution of the weights $a_k(t)$ decreases with k in such a way that with only a few (say in this case 3) terms, we have an acceptable approximation. This truncation procedure works as a low pass filter in time. Thus, we solve then the approximation problem for just each of the terms of the above expansion, and in this way, via 2 steps of approximation, the first in time and the second in space, we get $\varphi(t, P)$ extended to all the time-space domain

$$\varphi(t, P) = \varphi_m(P) + \sum_k a_k(t)\ \varphi_k(P).$$

This of course involves less computational effort than trying to solve for each time the incompressible approximation problem. Our model problem uses the data from the first principal component, (i.e.) $k = 1$. This data and a numerical solution can be seen in Figure 4.26. The remainder numerical results can be found in Appendix D.

1. Sensitivity with respect to ϵ_r. In Figures 4.27 and 4.28 we can see that the residual of the velocity measurements shrinks to zero when we reduce the regularization parameter. One very important feature of this example is the distinct gap in the singular values spectrum, which makes it easier to handle. Either we can use the Modified Truncated Singular Decomposition method directly or compute the solution using Richardson extrapolation. When an estimate of the error level present in the data is available, the bounds (A.9) devised in Appendix A can be used in the following way: Assume that we look for the unperturbed unregularized solution $x(0)$ If

we instead compute $x(\epsilon_r)$ the error will be approximately $x'(0)\epsilon_r$. In general, since the data is contaminated with error we obtain $\hat{x}(\epsilon_r)$ and an application of the bounds from the appendix yields

$$\frac{\|x(0) - x(\epsilon_r)\|_2}{\|x(0)\|_2} \approx \frac{(2N+1)\sqrt{6(1+3\rho)}E}{\sqrt{\epsilon_r}} + \frac{\|x'(0)\|_2}{\|x(0)\|_2}\epsilon_r$$

where the number E represents the relative error in the data measurements. In this case the quotient in the second term is of the order of $\frac{1}{\gamma_i^2}$ where γ_i is the smallest non zero generalized singular value, which is $\mathcal{O}(1)$. This yields the choice $\epsilon_r^* = (2N+1)^{2/3}(6+18\rho)^{2/3}E^{2/3}$. Therefore, the optimal error will be of order $(2N+1)^{1/3}E^{2/3}$.

Yet another possibility is to use the discrepancy principle described in Chapter 2.

2. Sensitivity with respect to N, shown in Figures 4.29 and 4.30. We observe that the difference between the measurements and the numerical solution can be made negligible for $N \geq 2$, something directly related with the amount of data.

3. Sensitivity with respect to p, shown in Figures 4.31 and 4.32.

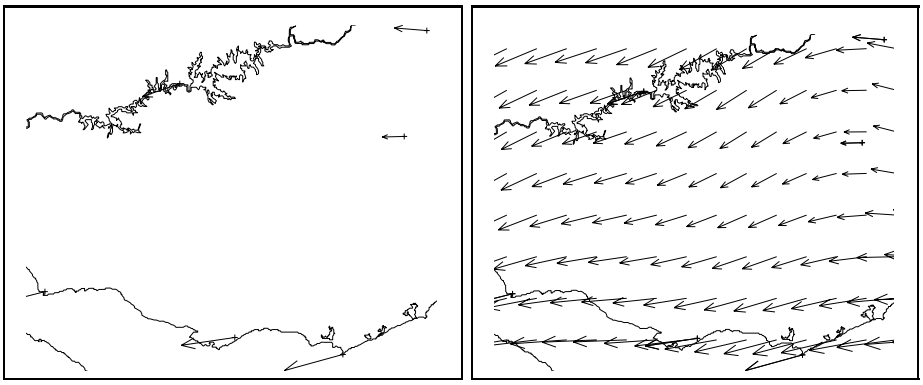

Figure 4.26: First Principal component example: Left: Available data. Right: Computational results.

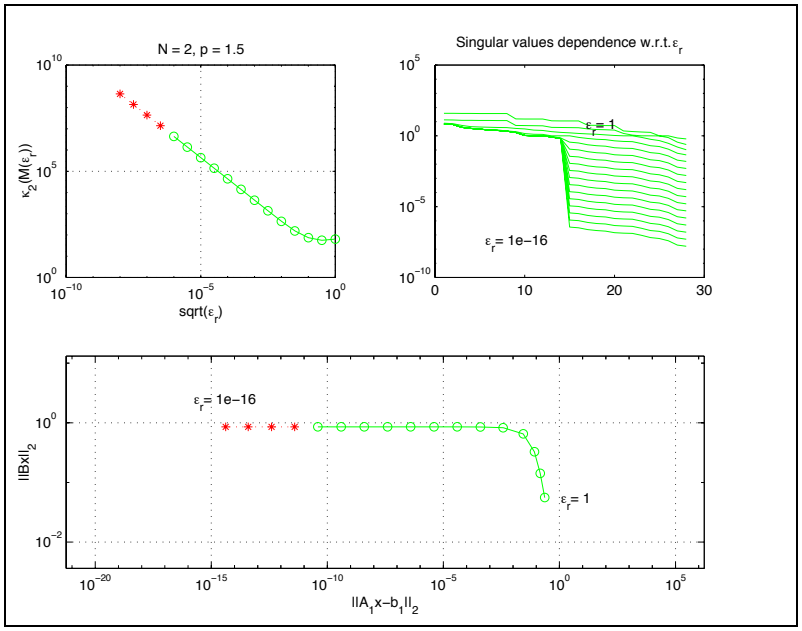

Figure 4.27: Dependence of the solution w.r.t. ϵ_r.

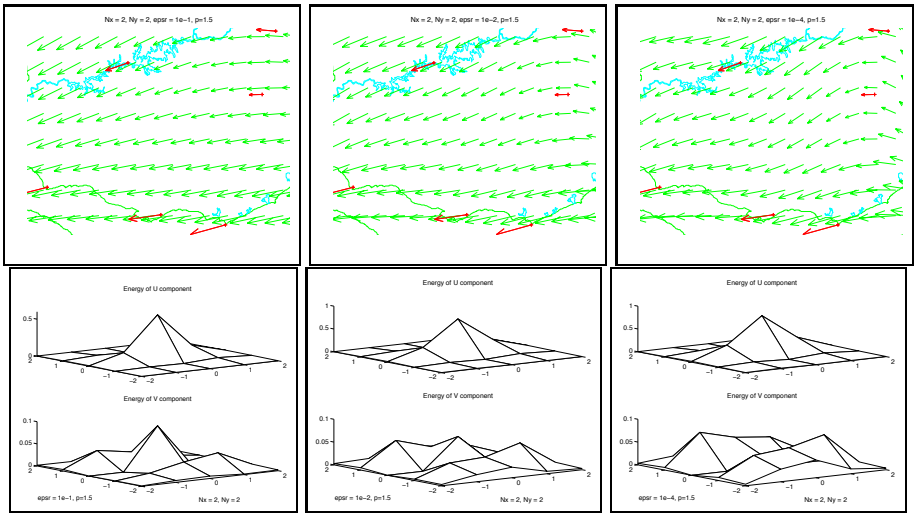

Figure 4.28: Dependence of the solution w.r.t. ϵ_r. Top:Flow results. Bottom:Spectral energy distribution

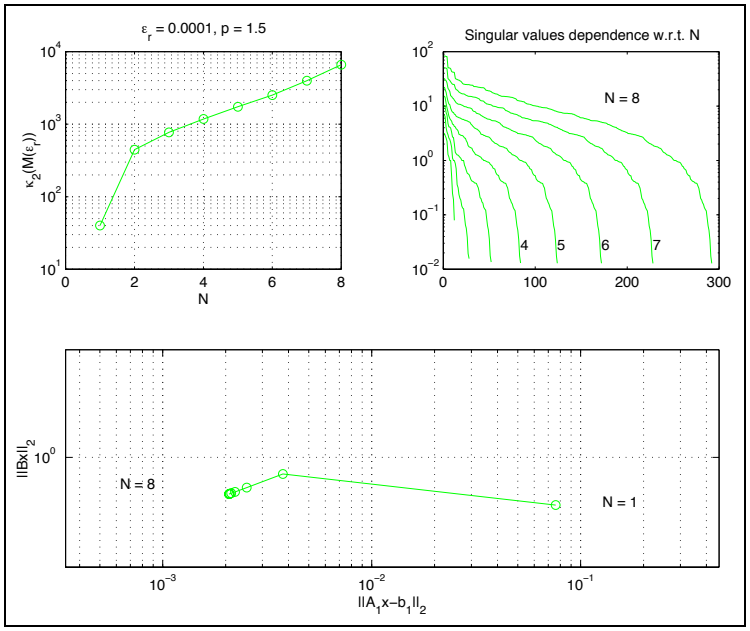

Figure 4.29: Dependence of the solution w.r.t. N.

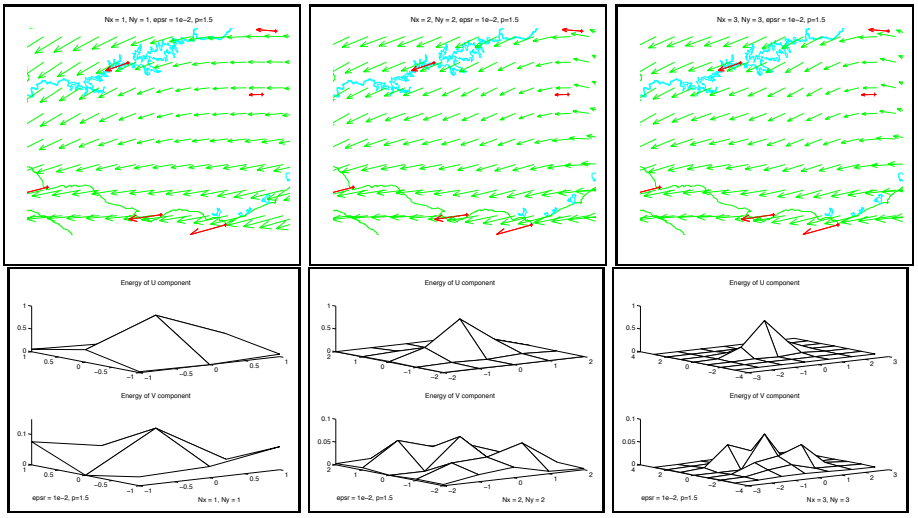

Figure 4.30: Dependence of the solution w.r.t. N. Top:Flow results. Bottom:Spectral energy distribution

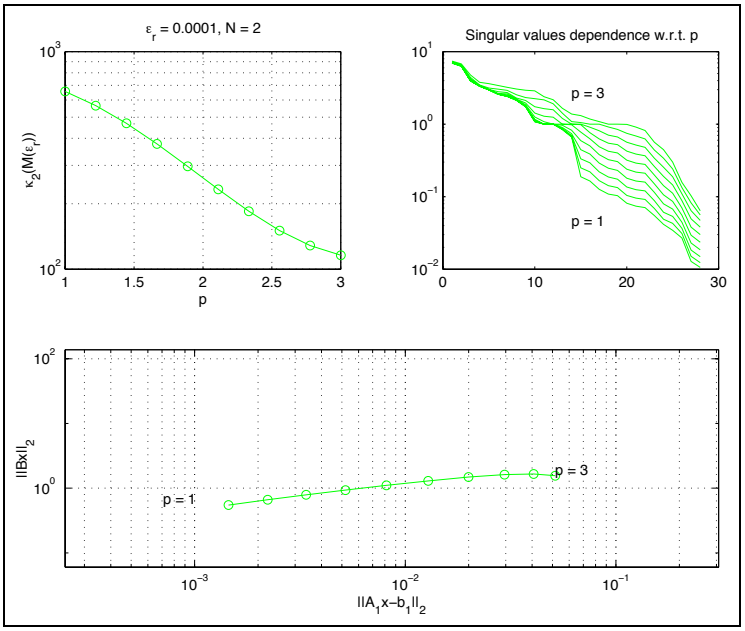

Figure 4.31: Dependence of the solution w.r.t. p.

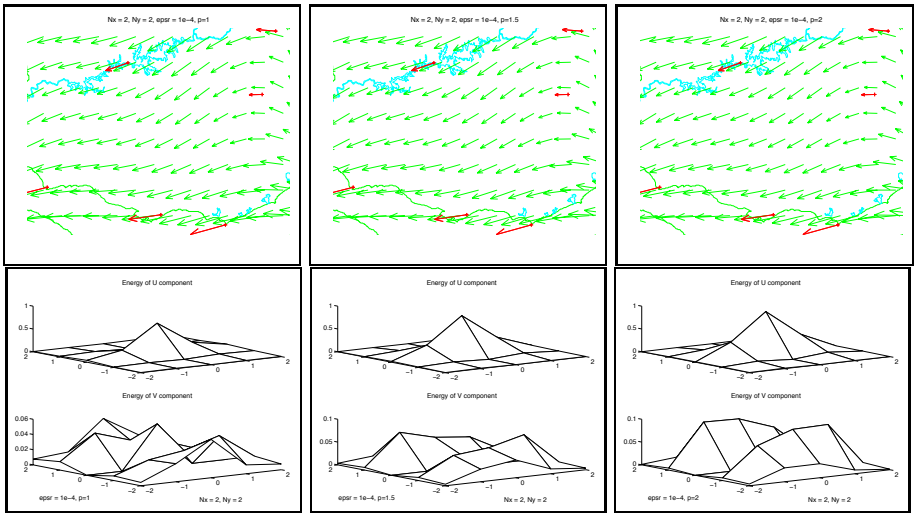

Figure 4.32: Dependence of the solution w.r.t. p. Top:Flow results. Bottom:Spectral energy distribution

4.2.1 Comparison with the results from [35]

As mentioned before, López Vázquez [35] closely follows Sasaki [30] and Sherman [31] solving the dual problem 2.6 for the Lagrange multiplier λ. This Partial differential equation has homogeneous Dirichlet boundary conditions when there exist free flow through the boundary, whereas the homogeneous Neumann boundary condition is used at solid walls, that is ∂D_1. We have seen in section 2 that this last B.C. introduces spurious solutions when α is not a multiple of the identity at the boundary ∂D_1. Unfortunately, this is the case in [35] since the scaling matrix α is chosen to be constant on the whole domain, and its diagonal coefficients are different.

The initial flow $\hat{\varphi}$ is generated by means of interpolation, which can be carried out in many possible ways.

On the other hand, since the approximation problem is posed in terms of the interpolated flow, that is

$$\min \|\alpha(\varphi - \hat{\varphi})\|_{L^2}$$

the data measurements will be treated in the same way as any other point in the domain, once the interpolant is generated.

Taking this last fact into account, a proposal due to Guo [13] is used. It involves adjusting a single constant c to minimize the residual at the data points, that is

$$c^* = arg \min_c \sum_{j=1}^{N_d} \|c\varphi(P_j) - \hat{\varphi}(P_j)\|_2^2$$

This correction cannot guarantee to what extent $c^*\varphi$ will approximate the data measurements, specially when the scaling matrix α is constant. This property is relevant for at least the mean value and the first principal component, since the incoming data has been already filtered by the principal components method, and those two components explain much of the variation of the measurements in time. As can be seen in Figure 4.33, the deviation from the data is particularly large at the stations of Punta del Este, while smaller deviations can be seen at the station of Melo and Carrasco. This does not happen with the proposed method, which is able to approximate the 6 data measurements up to a given tolerance taking $N \geq 2$. In addition, our method offers the flexibility to choose the regularization parameter either by an a priori knowledge of the error level or by an a posteriori procedure like the L curve method, adjusting the smoothing level in every case. That is relevant in the Principal component analysis, since the relative error level increases with the component number. In Figure 4.34 we show two numerical results, one with large regularization $\epsilon_r = 0.1$ which is very similar to the one depicted in Figure 4.33 and has deviations up to 15 % from the data measurements. That links the method presented in [35] with large values of regularization. In the same Figure we show a computation that has a negligible residual (of order 1e-4), and at the same time gives a smooth

flow. Furthermore, the fact that we can find a small residual with $N = 2$ means that we are able to represent the solution in space in a compact way, (i.e.) with just a few terms, which is in some sense complementary to the *compression in time* carried out by the Principal components method.

In [35], the Poisson equation for λ is solved by means of a Finite Element method with isoparametric functions, for elements with 8 nodes. The same method is applied for all the principal components, with no changes in the parameters.

Here the numerical procedure consists on solving an unconstrained least squares problem, and the amount of regularization can be adjusted to the amount of error present in each Principal Component.

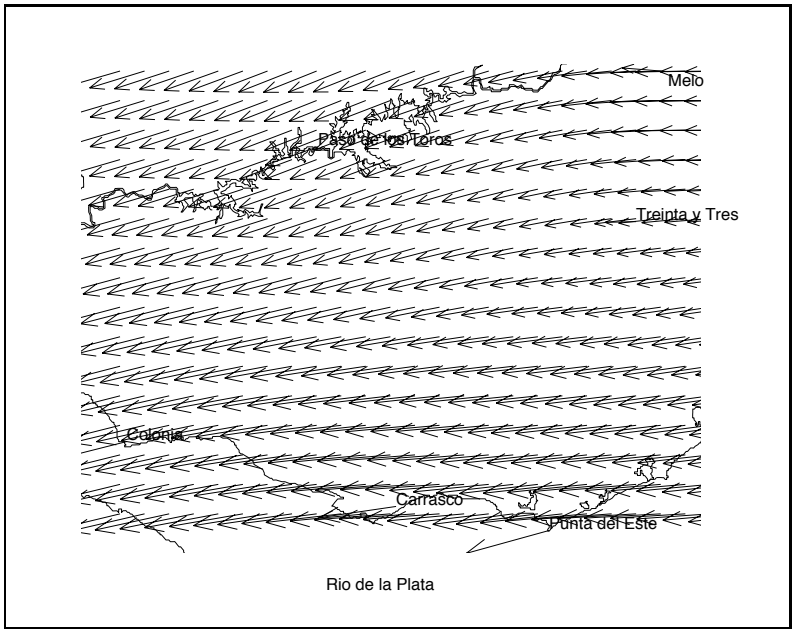

Figure 4.33: Results from [35], first principal component

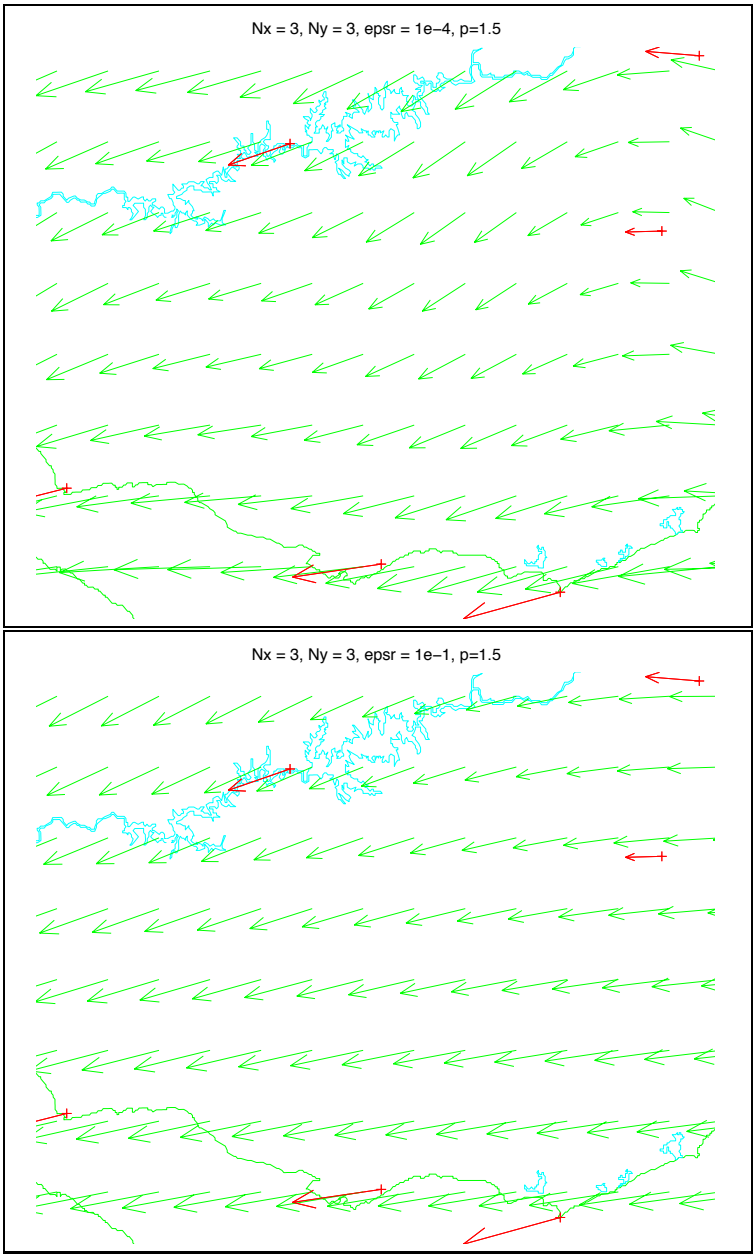

Figure 4.34: Results from the proposed method, first principal component

4.3 Effect of the parameters

Now, we summarize some features about the behaviour of numerical solutions with respect to various parameters used in the formulation.

Effect of η_{max} and ξ_{max}

As observed in the experiments, increasing the values of η_{max} and ξ_{max} yields a smaller residual and eventually, the unregularized problem can exhibit a null residual. That is the case in the Uruguayan example. On the other hand, the condition number $\kappa(M(\epsilon_r))$ increases mildly with the maximum wavenumber N, so is advisable to use as few wavenumbers as possible. Therefore, there is a tradeoff between small residuals and small condition number to consider in each case.

Effect of the size of the computational domain

In order to provide computational grounds for the relative choice of the Computational Domain, we have changed its size with respect to the physical one in the Uruguayan case. The column D_C in the next table shows the value of the magnification of the length side, and the residual at the data points. The values for the rest of the parameters are fixed to $\eta_{max} = \xi_{max} = 4$, $p = 1.5$, $\epsilon_r = 1e-8$. There are no important changes in the approximation, although the residuals at the data points increase when we magnify the computational domain. This is explained by the fact that the data will correspond to increasingly higher wave numbers in the larger domains, precisely those which with high penalization for its use. That effect can be observed in table 4.2. On the other hand, the computational domain has to be sufficiently large (so to avoid artificial discontinuities in the periodic boundary). This, if not treated with care, will cause the solution to be non smooth.

D_C	absolute $\|.\|_{L^2}$	absolute $\|.\|_\infty$
1	1.0740e-08	7.0188e-09
2	2.8212e-07	1.4813e-07
4	1.3199e-05	5.8180e-06

Table 4.2: L^2 norm of the residual at the data points when increasing the size of the computational domain

Effect of ϵ_r

The dependence of the solution with respect to ϵ_r has been analized throughout this work and the L curve method has been described and applied to provide an a posteriori choice for ϵ_r. In some cases where the perturbed problem also satisfies the discrete Picard condition an a priori estimate of the error level present in the data is needed to determine a sensible value for ϵ_r. An approximate value for

ϵ_r can be obtained from $\epsilon_r \approx \|E\|_2^{2/3}(2N+1)^{2/3}$, where $\|E\|_2$ is an estimate of the relative error level in the data. This choice corresponds to an approximate minimization of the relative error in the solution (i.e.),

$$\min_{\epsilon_r} \frac{\|x'(0)\|_2}{\|x(0)\|_2}\epsilon_r + \kappa_2(\epsilon_r)\|E\|_2$$

Here we also exemplify the use of Richardson extrapolation to verify the results predicted in Appendices A and B.

The extrapolated value can be computed as:

$$x^*_{extrp} = x^*(\epsilon_r/n) + \frac{x^*(\epsilon_r/n) - x^*(\epsilon_r)}{n-1} \tag{4.2}$$

The parameters were set to $n = 10$, $\epsilon_r = 1e-4$ All the other parameters are fixed to $p = 1.5$, $\eta_{max} = \xi_{max} = 2$.
Again we show the behaviour of the residuals at the data points.

ϵ_r	absolute $\|.\|_{L^2}$	absolute $\|.\|_\infty$
1e-4	3.9571e-05	2.3657e-05
1e-5	3.9578e-06	2.3661e-06
extrp.	8.9491e-10	4.3473e-10

Effect of p

The larger the value of p, the smoother the solution will be. That is obtained by imposing the pth derivative of the velocity field to belong to L^2. On the other hand, not any posivite value of p yields useful solutions. In section 3 it was pointed out that the value of p should be greater than 1 to have a well posed problem when we let $N \to \infty$. In other words, if we want to impose point values to the solution, the functional subspace where we minimize must contain only sufficiently smooth functions. If that is not the case, even for small values of N, the solution will fit the measurements but vanish quickly away from them. The importance of this effect will be greater for examples with only few data points.

However, computational experience shows that the residuals increase when p is increased above some threshold level, and moreover, the solution may look a bit wild, so it seems to be an optimal value of smoothness. In the present work we have taken $p = 1.5$.

Intuitively, for small values of ϵ_r there is no much difference between small values of $p > 1$, in the sense that the smoothing term only imposes an "order" between the frequencies, which is not altered by the different choices of p. Nevertheless, for this to hold they have to be small enough so the regularization term does not overrun the original data of the problem (i.e.), $\sqrt{\epsilon_r}N^p << 1$. In this work we take the value of $p = 1.5$

4.3.1 Experiments with noise in the data

In 2.2.2 and in Appendix A we predict that the data perturbations will be increasingly amplified as we shrink the regularization parameter. It is then the purpose of the following numerical experiments to show how this appears in practice, as well as how the regularization procedure can filter out the noise contribution.

The first experiment consists on adding uncorrelated and normally distributed noise to the velocity data, and then applying the method to filter out this contribution.

We perturbed all the data measurements randomly and observed the effect in the computed solution. The perturbations are independent, have normal distribution and their standard deviation is 0.1 of the velocity modulus at every measurement point. In other words

$$u_{pert}(P_j) = u(P_j) + eu_j * 0.1 * \sqrt{u^2(P_j) + v^2(P_j)}, \quad for\ j = 1 \dots N_d$$
$$v_{pert}(P_j) = v(P_j) + ev_j * 0.1 * \sqrt{u^2(P_j) + v^2(P_j)}, \quad for\ j = 1 \dots N_d$$

where $eu_j, eu_j \sim \mathcal{N}(0,1), \quad for\ j = 1 \dots N_d$. On the other hand, the boundary data has been kept unperturbed. As we can see in the following plots, the algorithm works well and the filtering procedure is successful, even with the small values of regularization parameter used here. A possible explanation of this behaviour is based on the fact that N, the maximum wavenumber has also a regularization effect. Its value bounds the highest frequency present in the numerical solution, therefore it precludes the unbiased uncorrelated error made of high frequency. Numerical results for both the ramp case and the Rankine vortex are shown in Figures 4.35 and 4.36 respectively.

The second experiment consists on shrinking the regularization parameter while keeping fixed the noise level. By means of this procedure, we are able to see how the numerical solution becomes more wiggly as it tries to approximate better noisy data. Our actual example is based on the Uruguayan example, since it is the example with least amount of data and that makes it more sensitive to perturbations. The noise has been generated in the same way as in the first experiment, and the results can be seen in Figure 4.37.

2D flow over a ramp with perturbed data

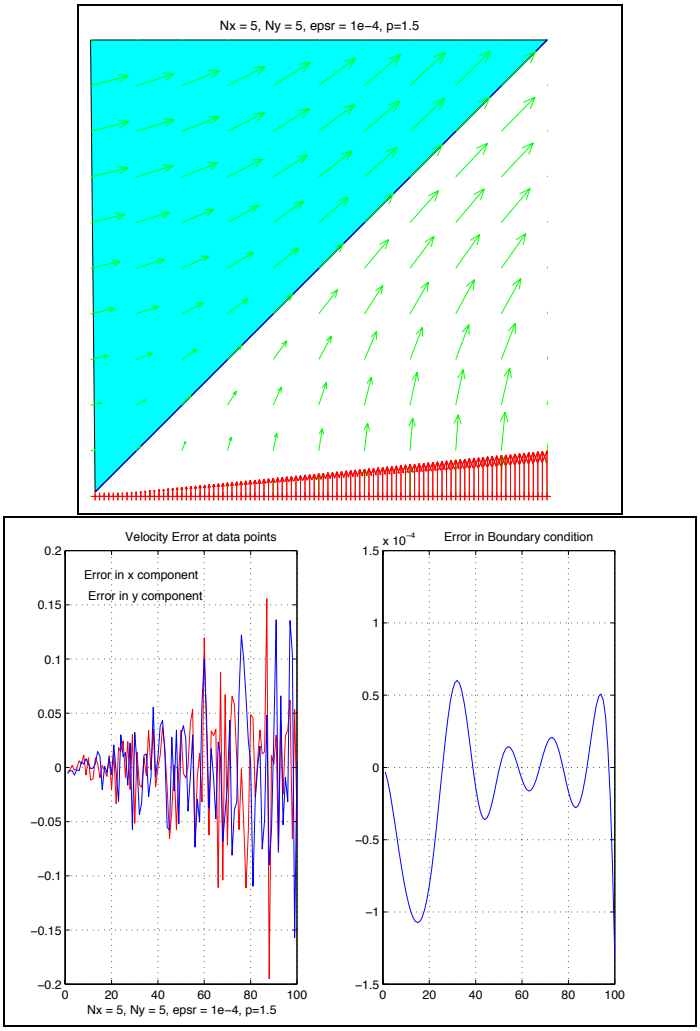

Figure 4.35: 2D flow over a ramp with random perturbations.Top: Numerical solution. Bottom: De-noising effect. Observe that the difference between the data and the numerical solution is made of scaled white noise, and that corresponds to the random perturbation that we introduced. On the other hand, there is no difficulty on handling the boundary condition, since it does not contain any perturbations.

2D Rankine vortex with perturbed data

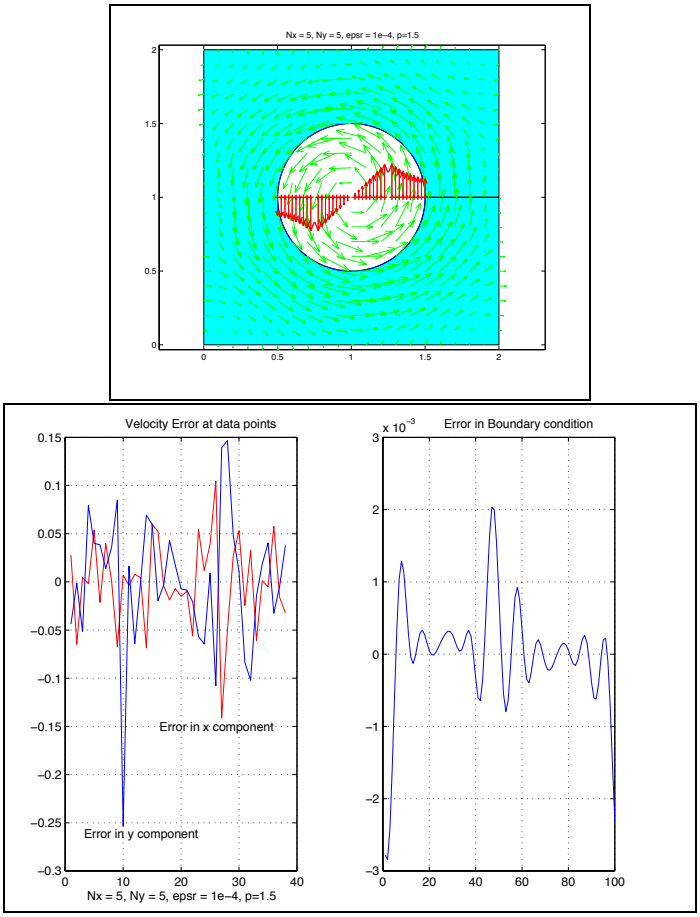

Figure 4.36: 2D Rankine vortex with random perturbations. Top: Numerical solution. Bottom: De-noising effect.Again, the difference between the data and the numerical solution is made of scaled white noise, and that corresponds to the random perturbation that we introduced. On the other hand, there is no difficulty on handling the boundary condition, since it does not contain any perturbations.

Uruguayan case with perturbed data and variable regularization

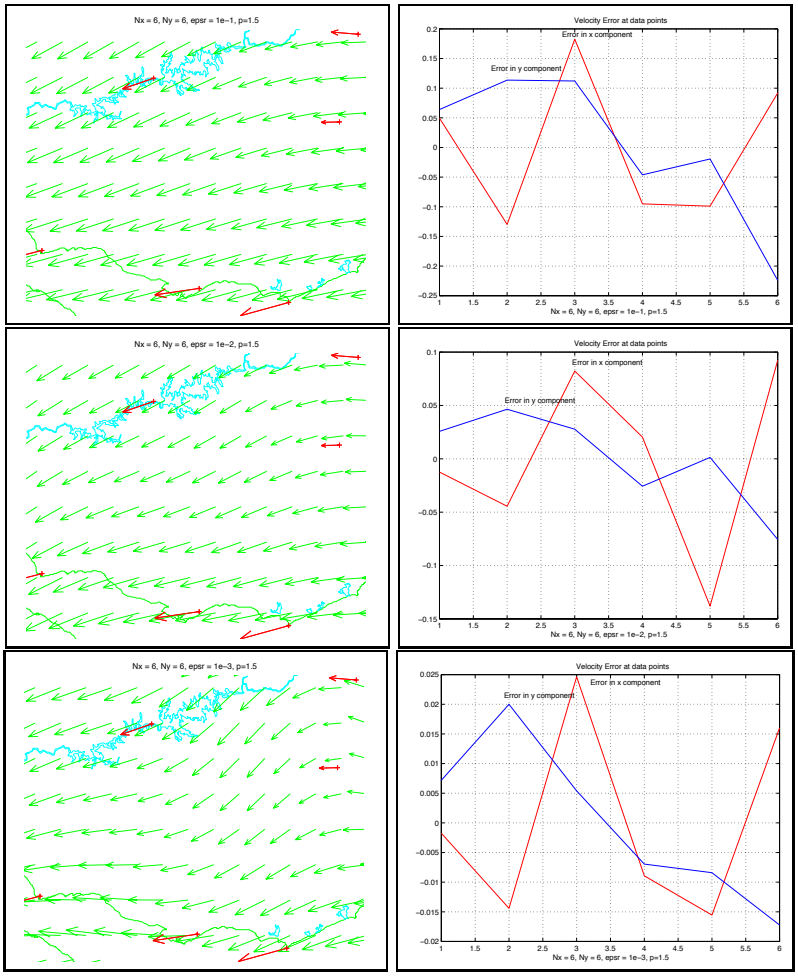

Figure 4.37: Numerical experiment with fixed noise level and different values of the regularization parameter. Decreasing the value of the ϵ_r parameter amplifies the error in the data and yields a wiggler solution. In addition, the pointwise residuals also shrink with ϵ_r. Since the L-curve criterion is not useful in this case, an a priori knowledge of the error is needed to provide a numerical solution

Chapter 5

Conclusions

Let us summarize the ideas that have been discussed throughout. When solving a flow estimation problem we often have a small number of data measurements, so additional information has to be included in order to find an useful solution. That sort of information can be the incompressibility condition, slip boundary conditions and some qualitative knowledge of the smoothness of the flow. The method presented in this work can handle all these conditions, and in addition, it can take into account the amount of noise present in the data, either in a posteriori way, like in the L curve method or with a priori information, minimizing an error bound of the solution. For that reason, it is useful to derive perturbation bounds relating the size of the regularization parameter and the error in the data with the corresponding perturbation in the solution.

Since we are able to substitute the incompressibility constraint, finding a numerical solution just involves an unconstrained linear least squares system, usually of small size.

Here Tikhonov regularization has been applied, but other methods mentioned in section 2 can be also applied. For example, when there is a distinct gap in the singular values spectrum, the MTSVD method (2.30) is very simple to use. An empirical choice of the smothness parameter p has been done, but a lower bound has been provided to guarantee that point conditions can be succesfully imposed.

The properties of convergence with respect to the number of data measurements common to spectral methods are present here, in the sense that the rate of convergence will be enhanced by the smoothness of the original flow. This means that in some cases, with very few components we are able to represent the numerical solution. as seen in our numerical experiments, both with model problems and real data.

Beside this, numerical results from this method have been compared with others from López Vázquez [35] in the Uruguayan case, yielding an interpretation of an equivalent regularization level used in that work. In other words, we can almost reproduce those results by choosing a large value of the regularization parameter and with just a small number of Fourier modes.

Requiring smoothness of the original flow seems to be a key limitation of the work, unless we are willing to face a large dimension least squares problem. For example, that is the case with boundary layers. However, one could "zoom in" into that zone of rapid variation, to obtain a local approximation that could be overlapped with the outer smooth solution. That implies an adaptive procedure which falls outside the scope of this thesis and can be the subject of future work.

Finally, a possible application which offers anoother view point of the algorithm is to use it to validate measurements. For example, With the help of a laser beam one can obtain a lot of velocity measurements in a planar section. A three dimensional version of this method could be used as a part of a statistical tool to reject poor quality measurements.

Appendix A

Singular values estimates

The purpose of this section is to provide bounds on the condition number of the matrix associated with Tikhonov regularization. First, we do the analysis in a general setting, with arbitrary A and B and then we restrict the results to the velocity field approximation problem discussed throughout the work. This as already seen in Chapter 2 is a vital issue to guarantee the stability of our computations. It is worth to mention that these results are close to those included in [15], but the proofs have been done independently and based on the Singular Value Decomposition instead of the Generalized Singular Value Decomposition.

As we shall see, we are able to control the condition number of the matrix from the least squares problem by choosing the value of ϵ_r. The condition number will be then $\mathcal{O}\left(1/\sqrt{\epsilon_r}\right)$.

In the following property we state the effect of ϵ_r on the singular values of a matrix associated with Tikhonov regularization, assuming that the regularization operator B is non singular.

Theorem 5 (Bounds of singular values) *Let the real valued matrix $A \in \mathbb{R}^{m\times n}$ have rank r, with singular values σ_i^A, $1 \leq i \leq r$ and define*

$$M(\epsilon_r) = \begin{bmatrix} A \\ \sqrt{\epsilon_r} B \end{bmatrix}$$

where $B \in \mathbb{R}^{n\times n}$ is an invertible matrix with singular values σ_i^B.
Then the singular values of $M(\epsilon_r)$ satisfy

$$\begin{aligned} \sigma_i(\epsilon_r) &= \sigma_i^A + \mathcal{O}(\epsilon_r), \text{ for all } 1 \leq i \leq r \\ \sigma_i(\epsilon_r) &= \mathcal{O}(\sqrt{\epsilon_r}), \text{ for all } r+1 \leq i \end{aligned}$$

Proof:

We use the fact that σ_i^2 are the eigenvalues of the symmetric matrix $M^T(\epsilon_r)M(\epsilon_r)$. Then, recalling the definition of the singular value decomposition of the matrix

A we have $A = U\Sigma V^T$ where U and V are orthogonal matrices and Σ is a diagonal matrix.
Therefore,

$$\Sigma^T\Sigma = diag((\sigma_i^A)^2) = V^T A^T AV, \tag{A.1}$$

Now, let $\sigma_i(\epsilon_r)$ denote the singular values of $M(\epsilon_r)$. Observe that the relation $\sigma_i(\epsilon_r)$ is well defined since the eigenvalues of a matrix are continuous functions of the matrix entries, which in this case are continuous functions of the regularization parameter ϵ_r.

Applying the same similarity transformation as in (A.1) to the matrix product $M^T(\epsilon_r)M(\epsilon_r)$ we arrive to

$$V^T M^T(\epsilon_r)M(\epsilon_r)V = \Sigma^2 + \epsilon_r V^T B^T BV$$

Then, Gerschgorin theorem (see [12], theorem 7.2.1, page 341) with suitable numbering of the singular values $\sigma_i(\epsilon_r)$ yields

$$|(\sigma_i^A)^2 - \sigma_i^2(\epsilon_r)| \leq m_i\ \epsilon_r \tag{A.2}$$

where $m_i = \|V^T B^T BV\ e_i\|_1$. This implies that $\lim_{\epsilon_r \to 0} \sigma_i(\epsilon_r) = \sigma_i^A$ and as a byproduct it yields

$$|\sigma_i^A - \sigma_i(\epsilon_r)| \leq \frac{m_i\ \epsilon_r}{\sigma_i^A + \sigma_i(\epsilon_r)} \tag{A.3}$$

Now, since $M(\epsilon_r)$ is constructed by appending extra rows to the matrix A we have $\sigma_i(\epsilon_r) \geq \sigma_i^A$, for all $1 \leq i \leq n$. This fact is a consequence of [2],theorem 3.5, page 476.
Recall that the rank of A is r. Thus, if $i \leq r$ then the singular value σ_i^A is strictly positive, and we get the bound

$$|\sigma_i^A - \sigma_i(\epsilon_r)| \leq \frac{m_i\ \epsilon_r}{2\sigma_i^A}, \text{ which is the first part of the theorem.} \tag{A.4}$$

To prove the other statement, let $i > r$. Then $\sigma_i^A = 0$, and (A.2) yields

$$\sigma_i(\epsilon_r) \leq \sqrt{m_i\ \epsilon_r}, \quad \forall i > r$$

The strategy to obtain a lower bound on the singular values is to use the non singularity of B, working with its smallest singular value.

$$\sigma_{min}^2(\epsilon_r) = \min_{\|x\|_2=1} \|Ax\|_2^2 + \epsilon_r\|Bx\|_2^2 \geq \epsilon_r \min_{\|x\|_2=1} \|Bx\|_2^2 = \epsilon_r(\sigma_{min}^B)^2$$

Now, since $\sigma_i^2(\epsilon_r) \geq \sigma_{min}^2(\epsilon_r)$, for all i from (A.2) we obtain

$\sqrt{\epsilon_r}\sigma_{min}^B \leq \sigma_i(\epsilon_r) \leq \sqrt{m_i\ \epsilon_r}$, which implies the second part of the theorem.□

In Figure A.1 we can see a numerical experiment showing the dependence of the singular values spectrum of $M(\epsilon_r)$ with ϵ_r. The matrix $A \in \mathbb{R}^{40\times 20}$ has rank equal to 7 and the regularization operator is $B = diag(1, 2^{1.5}, \ldots, 20^{1.5})$. The bound provided by theorem 5 is clearly identified in the graph, since the modified spectrum corresponding to the null space of A is just scaled by $\sqrt{\epsilon_r}$. In addition, observe that those perturbed singular values corresponding to non zero singular values of A remain almost constant. In the experiment, we have used
$\epsilon_r = 1e-4, 1e-5, \ldots, 1e-8$.

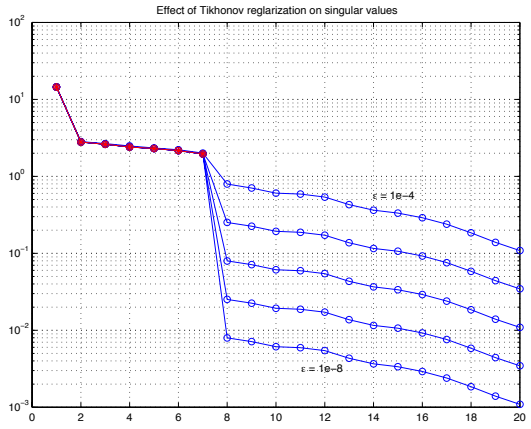

Figure A.1: Numerical example of the dependence of singular values of $M(\epsilon_r)$ with respect to ϵ_r

Using the last theorem we can now give a first estimate on the condition number of the regularized unconstrained LSQ problem.

Corollary 1 *With the same hypotheses as in theorem 5 we have*

$$\kappa_2\left(\begin{bmatrix} A \\ \sqrt{\epsilon_r}B \end{bmatrix}\right) \leq \frac{\|A\|_2\|B^I\|_2}{\sqrt{\epsilon_r}} + \sqrt{\epsilon_r}\kappa_2(B)$$

Proof:
It is just a matter of bounding the maximal and the minimal singular values of $M(\epsilon_r)$. The first singular value satisfies the inequalities:

$$\sigma_1(\epsilon_r) \leq \sqrt{\|A\|_2^2 + \epsilon_r\|B\|_2^2} \leq \|A\|_2 + \epsilon_r\|B\|_2$$

And as seen in the proof of the last theorem,

$$\left\|M(\epsilon_r)^I\right\|_2 \leq \frac{\|B^I\|_2}{\sqrt{\epsilon_r}}$$

□

The next property allows us to bound the condition of the matrix of the LSQ problem seen in 3.4.2. In that section we allow the diagonal matrix B from the regularization term to be singular, but keeping the assumption that the intersection of the null spaces $\ker(A)$ and $\ker(B)$ is trivial. For the velocity field problem this assumption of trivial intersection has been proved in corollary 4.

The next step is to allow a singular regularization operator B, but keeping the assumption of no intersection of null spaces.

A a direct consequence of [16],theorem 2.3. yields

$$\left\| \begin{pmatrix} A \\ \sqrt{\epsilon_r} B \end{pmatrix}^I \right\|_2 \leq \max \left(\frac{\|B^I\|_2}{\sqrt{\epsilon_r}}, \frac{1}{\inf\left(AP_{\ker(B)}\right)} \right) \tag{A.5}$$

where $P_{\ker(B)}$ is the orthogonal projection onto the null space of B and $\inf\left(AP_{\ker(B)}\right)$ denotes the minimum non zero singular value of $AP_{\ker(B)}$.

To be able to offer a geometric interpretation of the results, we first need to recall the notion of the angle between subspaces, and after that prove a simple bound.

Definition 1 *The angle θ^* between two subspaces V and W is defined by*

$$\cos(\theta^*) = \max_{\substack{\|x\|_2 = \|y\|_2 = 1, \\ x \in V,\ y \in W}} x^T\ y$$

Lemma 1 *Let θ^* be the angle between $\ker(A)$ and $\ker(B)$. Then*

$$\inf\left(AP_{\ker(B)}\right) = \min_{\|x\|_2=1,\ \ Bx=0} \|Ax\|_2 \geq \sin(\theta^*)(\sigma^A_{r_A}) = \frac{\sin(\theta^*)}{\|A^I\|_2}$$

Proof:
Let $x \in \ker(B)$ with $\|x\|_2 = 1$ and define the vector y as the orthogonal projection of x onto the Range of A^T.

$$y = P_{R(A^T)} x$$

Observe that the angle θ between x and $\ker(A)$ satisfies the relation

$$\|y\|_2^2 = \sin^2(\theta)$$

On the other hand, since by the above construction $x - y$ belongs to the null space of A we have $Ax = Ay$. Using the last relation and the inequality $\sin^2(\theta) \geq \sin^2(\theta^*)$,which comes directly from the definition of θ^*, we arrive to

$$\|Ax\|_2^2 = \|Ay\|_2^2 = \sin^2(\theta)\|Au\|_2^2 \geq \sin^2(\theta^*)(\sigma^A_{r_A})^2$$

The last assertion holds since $u = \frac{y}{\sin^2(\theta)} \in Range(A^T),\ \|u\|_2 = 1.$ □

Now let

$$A_k = \sum_{i=1}^{k} \sigma_i u_i v_i^T, \quad with\ 1 \leq\ k \leq rank(A)$$

be a truncated SVD expansion of A. Define θ_k as the angle between $\ker(B)$ and $\ker(A_k)$. Since

$$\inf\left(AP_{\ker(B)}\right) \geq \inf\left(A_k P_{\ker(B)}\right),\ for\ \ 1 \leq\ k \leq rank(A)$$

then by means of lemma 1 we arrive to

$$\inf\left(AP_{\ker(B)}\right) \geq \max_{1 \leq k \leq rank(A)} \left\{ \frac{\sin(\theta_k)}{\|A_k^I\|_2} \right\}$$

We remark that both $\sin(\theta_k)$ and $\|A_k^I\|_2$ do not decrease as k increases. Thus, it is reasonable to expect that the maximum of $\left\{ \frac{\sin(\theta_k)}{\|A_k^I\|_2} \right\}$ will occur at an intermediate value $1 < k^* < rank(A)$.

The next corollary is just the generalization of 1 for B singular.

Corollary 2 *With the same hypotheses as above,*

$$\kappa_2\left(\begin{bmatrix} A \\ \sqrt{\epsilon_r} B \end{bmatrix}\right) \leq$$

$$\max\left(\frac{\|A\|_2 \|B^I\|_2}{\sqrt{\epsilon_r}} + \sqrt{\epsilon_r}\kappa_2(B), \min_{1 \leq k \leq rank(A)} \left\{ \frac{\kappa_2(A_k)}{\sin(\theta_k)} + \epsilon_r \frac{\|A_k^I\|_2 \|B\|_2}{\sin(\theta_k)} \right\} \right) \quad \text{(A.6)}$$

□

From corollary 2 we see that if the minimum of $\left\{ \frac{\sin(\theta_k)}{\|A_k^I\|_2} \right\}$ is small enough then it makes sense to apply the Tikhonov regularization. This has the following geometric interpretation: *the subspace associated with relatively small singular values of A should be near orthogonal to the null space of B.*
The above can be seen as a condition for the choice of the regularization operator B, since A generally given from the physical model. We can think of the above statement as the numerical counterpart of the requirement $\ker(A) \cap \ker(B) = \{0\}$. If that happens the condition number will be approximately controlled by $\frac{\|A\|_2 \|B^I\|_2}{\sqrt{\epsilon_r}}$. To find satisfactory results we also need the right hand side b to satisfy the discrete Picard condition commented in section 2.2.2.

As remarked in the numerical examples, the angle between the null spaces of A and B may shrink when the number of wave numbers present in the solution increases, so it may be useful to also add a small penalization to the mean value components in the solution to make B invertible and keep the result from theorem 5.

In what follows, we particularize the sensitivity results to the case of the velocity field estimation. For that reason, recall the quantities N_{Dep} (number

of dependent variables) and N_{free} (number of dependent variables) defined in section 3.4.2.

The next property gives a bound in the "substitution" matrix used in section 3.4.2 to achieve an unconstrained formulation. It shows that the substitution matrix is indeed very well conditioned.

It uses the fact that $N_{Dep}/N_{free} \leq 3$, which can be easily verified by the reader.

Property 1 *Recall the definition of the matrices H_D and H_F given in (3.12). Then the following bound on the condition number of the substitution matrix holds:*

$$1 \leq \left\| \begin{bmatrix} I \\ -H_D^{-1} H_F \end{bmatrix} \right\|_2 \leq \sqrt{1+3\rho} \tag{A.7}$$

where $\rho \leq \max(\eta_{max}, \xi_{max})$. Moreover, there exists a choice of the set of free variables such that $\rho \leq 3$ This is accomplished by looking at constraint 3.7 and choosing as independent the variables

$$\begin{cases} \hat{U}_{\eta,\xi} & if |\eta| \leq |\xi|, \ and \ |\xi| > 0 \\ \hat{V}_{\eta,\xi} & if |\eta| > |\xi| \\ \hat{U}_{\eta,\xi} \ and \ \hat{V}_{\eta,\xi} & if \eta = \xi = 0 \end{cases} \tag{A.8}$$

Proof: Just consider the definition of the 2-norm:

$$\left\| \begin{bmatrix} I \\ -H_D^{-1} H_F \end{bmatrix} \right\|_2^2 = \max_{\|x\|_2=1} \|x\|_2^2 + \left\| H_D^{-1} H_F x \right\|_2^2$$

Now let ρ be the maximum absolute value of the entries in the rectangular matrix $H_D^{-1} H_F$. Beside this, recall that $H_D^{-1} H_F$ has at most one nonzero element per row and that for every independent variable there are at most 3 dependent variables

Therefore, we arrive to

$$\left\| \begin{bmatrix} I \\ -H_D^{-1} H_F \end{bmatrix} \right\|_2^2 \leq 1 + 3\rho$$

To conclude observe that $\rho \leq \max\{\xi_{max}, \eta_{max}\}$ for any choice of independent variables and that if (A.8) holds $\rho \leq 1$

□

In what follows, we provide a bound on the first singular value of the matrix A that contains information about both the station points and the slip boundary conditions. For that reason, let A_1 be the matrix associated with condition (3.2) via the least squares formulation (3.3). In a similar way, let A_2 be associated with the slip boundary condition in ∂D_1 as explained in (3.4) and (3.5).

Property 2 *Let* $A = \begin{bmatrix} A_1 \\ A_2 \end{bmatrix}$ *with* A_1 *and* A_2 *as above and let*

$$N_f = (2\xi_{max} + 1)(2\eta_{max} + 1)$$

Then $\|A_1\|_2^2 \leq 2N_f$, $\|A_2\|_2^2 \leq 4N_f$ *and*

$$\|A\|_2 \leq \sqrt{6N_f}$$

□

Finally, by means of the preceding properties, we are able to give a bound for the condition number of the matrix for the constrained problem discussed in 3.4.2. In order to emphasize the important terms in the bound, we have used the $\mathcal{O}$ notation.

Property 3 *Let*

$$\hat{M}(\epsilon_r) = \begin{bmatrix} A \\ \sqrt{\epsilon_r} B \end{bmatrix} \begin{bmatrix} I \\ -H_D^{-1} H_F \end{bmatrix}$$

Then

$$\kappa_2(\hat{M}(\epsilon_r)) \leq \sqrt{1+3\rho}\ \max\left(\frac{\sqrt{6N_f}}{\sqrt{\epsilon_r}} + \mathcal{O}(\sqrt{\epsilon_r}), \min_{1 \leq k \leq rank(A)} \frac{\kappa_2(A_k)}{\sin(\theta_k)} + \mathcal{O}(\epsilon_r) \right) \quad \text{(A.9)}$$

□

Since the regularization operator B is diagonal with entries $\sqrt{\eta^{2p} + \xi^{2p}}$ its kernel is spanned by constant flows, and $\sigma_{r_B}^B = 1$. That simplifies the bounds in property 3. If we also add a small penalization δ in the entries that correspond to $\eta = \xi = 0$ we are able to preclude any "closeness" between the null spaces represented by a small value of $\sin(\theta^*)$ in (A.9).

Now, keeping the same notation as in property 3 and applying (2.13)we have the following perturbation bound in the Euclidean norm:

$$\|x(\epsilon_r) - \hat{x}(\epsilon_r)\| \leq \frac{\kappa_2(\hat{M}(\epsilon_r))}{1 - \kappa_2(\hat{M}(\epsilon_r)) \frac{\|\delta A\|}{\|A\|}} \left(\frac{\|\delta A\|}{\|A\|} \|x(\epsilon_r)\| + \frac{\|\delta b\|}{\|A\|} + \kappa_2(\hat{M}(\epsilon_r)) \frac{\|\delta A\|}{\|A\|} \frac{\|r(\epsilon_r)\|}{\|A\|} \right)$$

Appendix B

Convergence as $\epsilon_r \to 0^+$

The goal of this section is to analyze what happens when we let $\epsilon_r \to 0^+$, assuming exact arithmetic and no errors in the data.

We now introduce some notation that will be used on what follows. Let A be a $m \times n$ matrix, with $rank(A) = r < n$. Let Z be a basis for $\ker(A)$, represented as a $n \times (m - r)$ matrix. Analogously, let N be a $n \times r$ matrix such that its columns make a basis of $Ker(A)^{\perp} = Range(A^T)$. Observe that $N^T Z = 0$ and $AZ = 0$. Then, any arbitrary x can be written uniquely as $x = Zx_Z + Nx_N$. We shall also make use of the following notations: $B_Z = BZ$, $B_N = BN$, $A_N = AN$.

The following property gives useful results about the dependence of the solution of a rank deficient linear least squares problem, showing that there exist a limit value $x(0)$, and that only the null space component of $x(0)$ depends on B.

Property 4 *Consider the Linear Least Squares Problem from Tikhonov regularization:*

$$x(\epsilon) = argmin_x \ \|Ax - b\|_2^2 + \epsilon \|Bx\|_2^2 \tag{B.1}$$

where the matrix A is $m \times n$, $rank(A) = r < n$. Let Z be a basis for $\ker(A)$, *and assume that BZ has rank $n - r$. Then*

$$\lim_{\epsilon \to 0^+} x(\epsilon) = \left\{ N - Z \left(B_Z^T B_z \right)^{-1} B_Z^T B_N \right\} \left(A_N^T A_N \right)^{-1} A_N^T b$$

□

To prove this property we shall use the optimality conditions for (B.1) which are widely known as the normal equations, and work with the components in $\ker(A)$ and its orthogonal subspace $Range(A^T)$. Beside this, we also use that the matrix $A_N^T A_N$ is invertible.

Proof:
First observe that B_Z has full column rank, so $B_Z^T B_Z$ is non singular, and the same happens with the inverse of $A_N^T A_N$. Beside this, the minimizer of (B.1) is the solution of

$$(A^T A + \epsilon B^T B)x(\epsilon) = A^T b \tag{B.2}$$

Now decompose the vector $x(\epsilon)$ into null space and the range of A^T:

$$x(\epsilon) = Z x_Z(\epsilon) + N x_N(\epsilon)$$

Therefore, from (B.2) we arrive to

$$\epsilon B^T B Z x_Z(\epsilon) + (A^T A + \epsilon B^T B) N x_N(\epsilon) = A^T b$$

Multiplying the last equation from the left by Z^T yields:

$$B_Z^T B_Z x_Z(\epsilon) + B_Z^T B_N x_N(\epsilon) = 0 \tag{B.3}$$

and multiplying from the left by N^T we get

$$\epsilon B_N^T B_Z x_Z(\epsilon) + [A_N^T A_N + \epsilon B_N^T B_N] x_N(\epsilon) = A_N^T b \tag{B.4}$$

From (B.3) and (B.4) we easily conclude that

$$lim_{\epsilon \to 0^+} x_N(\epsilon) = (A_N^T A_N)^{-1} A_N^T b$$

and

$$lim_{\epsilon \to 0^+} x_Z(\epsilon) = -(B_Z^T B_Z)^{-1} B_Z^T B_N (A_N^T A_N)^{-1} A_N^T b$$

which finishes the proof. □

The vector $x(0)$ can be expressed by means of the GSVD of the matrix pair (A, B) taking the limit in expression (2.17)

$$x(0) = X \begin{pmatrix} \Sigma^+ & 0 \\ 0 & I_{n-q} \end{pmatrix} U^T b = \sum_{i=1}^{q} \frac{u_i^T b}{\sigma_i} x_i + \sum_{i=q+1}^{n} (u_i^T b) x_i$$

This corresponds to a particular choice of the matrices N and Z described above.

If we are interested to enforce as much as possible the interpolation conditions it is useful to reduce the effect of the regularization term, (i.e) compute $x(0)$. That is numerically easier if one knows a priori that an extrapolation on the vanishing parameter can be done. In this case, Richardson extrapolation [4] can be applied.

Corollary 3 *Richardson extrapolation can be used to compute* $x(0)$

Proof:
It is enough to observe that the solution can be expanded as a power series for sufficiently small values of ϵ :

$$x(\epsilon) = x(0) + a_1\epsilon + a_2\epsilon^2 + ...$$

To conclude we use the following result (see [12] lemma 2.2.3, page 59):

if $\|H\| < 1$ for some operator norm, then

$$(I - H)^{-1} = I + H + H^2 + H^3 + ...,$$

Keeping this in mind, is sufficient to take

$$H = \epsilon(A_N^T A_N)^{-1} B_N^T (I - B_Z (B_Z^T B_Z)^{-1} B_Z^T) B_N$$

with $\epsilon < \epsilon_0 = \|(A_N^T A_N)^{-1} B_N^T (I - B_Z (B_Z^T B_Z)^{-1} B_Z^T) B_N\|^{-1}$ in (B.4). □

The result of the extrapolation can be also expressed by means of the GSVD. For example

$$x_{extrap}(\epsilon) = x(\epsilon) + (x(\epsilon) - x(2\epsilon)) =$$

$$X \begin{pmatrix} F_{extrap} & 0 \\ 0 & I_{n-q} \end{pmatrix} U^T b = \sum_{i=1}^{q} f_i^{extrap} \frac{u_i^T b}{\sigma_i} x_i + \sum_{i=q+1}^{n} (u_i^T b) x_i$$

where $F_{extrap} = diag(f_i^{extrap})$ and the filter factors from Richardson extrapolation are given by

$$f_i^{extrap}(\epsilon) = \frac{1}{1 + \frac{\epsilon}{\gamma_i^2}} \frac{1 + 3\frac{\epsilon}{\gamma_i^2}}{1 + 2\frac{\epsilon}{\gamma_i^2}} = f_i^{Tikh} \frac{1 + 3\frac{\epsilon}{\gamma_i^2}}{1 + 2\frac{\epsilon}{\gamma_i^2}} > f_i^{Tikh}$$

which shows that the extrapolated solution has less regularization.

Let us now discuss the behaviour of the filter factors from the extrapolation. For small values of $\frac{\epsilon}{\gamma_i^2} << 1$ we have that

$f_i^{extrap}(\epsilon) = 1 - \mathcal{O}\left((\frac{\epsilon}{\gamma_i^2})^2 \right)$

which basically implies that there is almost no regularization error in components associated with large generalized singular values.
Conversely, for large values of $\frac{\epsilon}{\gamma_i^2} >> 1$ corresponding to relatively small γ_i we have
$f_i^{extrap}(\epsilon) \approx \frac{3}{2} f_i^{Tikh} = \mathcal{O}\left(\frac{\gamma_i^2}{\epsilon} \right)$ which implies a bit less regularization than Tikhonov's.

In Figure B.1 we plot the filter factors coming from Tikhonov regularization and those from the described extrapolation as a function of $\frac{\epsilon}{\gamma_i^2}$.

Another implication of property 4 is that the there exist a limit value for the solution of the velocity problem (3.10) as we shrink the regularization parameter.

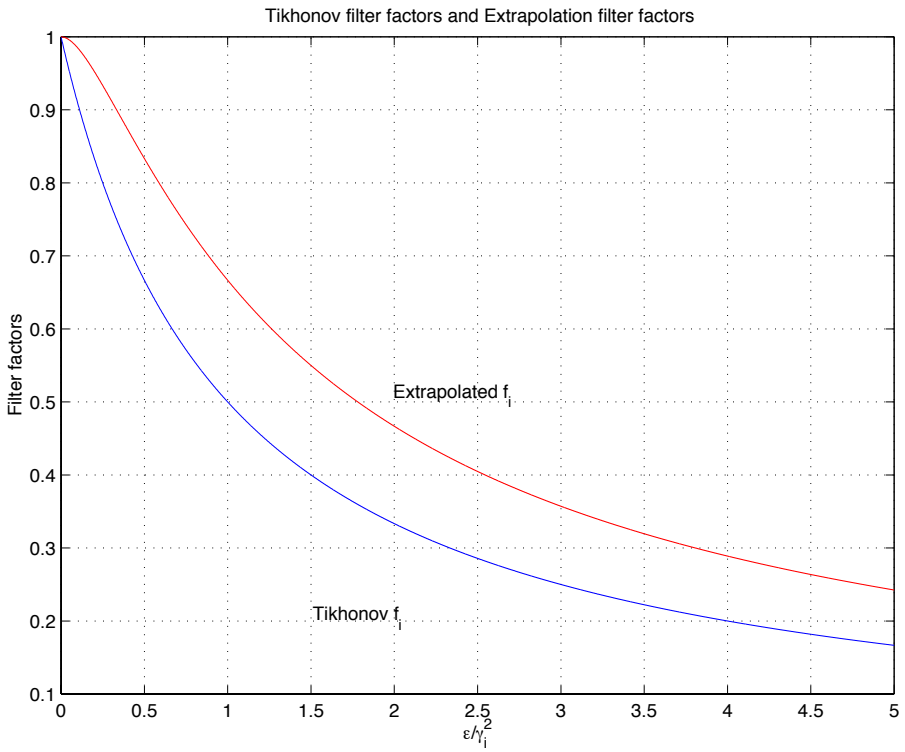

Figure B.1: Filter factors of Tikhonov regularization and its extrapolation. The extrapolation offers larger filter factors, leading to less regularization.

Corollary 4 *The solution of (3.10) has a well defined limit as* $\epsilon \to 0^+$.

Proof:
We use property 4. Observe that problem (3.10) can be written with the structure (3.11) once reformulated in real arithmetic. In this particular case, the term $\epsilon_r f_r(C)$ is equal to $\epsilon_r \|Bx\|^2$ from property 4. This means that the only hypothesis to check is that B_Z is full column rank (i.e.) $rank(A) \cap rank(B) = \{0\}$ Recall that associated to each x real vector there exists a unique $\mathbf{C}$ complex valued vector containing the Fourier components. If $Bx = 0$ then $f_r(\mathbf{C}) = 0$ and then all $C_{\eta,\xi} = 0$, $\eta \neq 0$, $\xi \neq 0$ which is equivalent to say that the only non zero Fourier components are those from the mean value: $\hat{U}_{0,0}$ and $\hat{V}_{0,0}$.

Therefore, $\|Ax\|_2^2 = 0$ implies

$$\frac{1}{N_d} \sum_{i=1}^{N_d} \left(\hat{U}_{0,0}\right)^2 + \left(\hat{V}_{0,0}\right)^2 = 0$$

and

$$\frac{1}{N_b} \sum_{i=1}^{N_b} \left(\hat{U}_{0,0} n_x(P_h) + \hat{V}_{0,0} n_y(P_h)\right)^2 = 0$$

yielding $\hat{U}_{0,0} = \hat{V}_{0,0} = 0$, what we wanted to prove. □

The next property is the analogous of the characterization of the MTSVD solution defined in (2.30) and can be used to prove that with η_{max}, ξ_{max} sufficiently large the approximate solution obtained from the limit process will interpolate the data.

Property 5 *With the same hypothesis of property 4 let* $x(0) = \lim_{\epsilon \to 0+} x(\epsilon)$. *Then*

$$\begin{array}{rl} x(0) = & arg\min \|Bx\|_2 \\ & s.t. \\ & \min \|Ax - b\|_2 \end{array} \tag{B.5}$$

Proof:
To prove the desired result, we pose the optimality conditions for (B.5) which is equivalent to

$$\begin{cases} \min_x \ 1/2\|Bx\|_2^2 \\ s.t. \\ A^T Ax = A^T b \end{cases}$$

Its optimality conditions are

$$\begin{bmatrix} B^T B & A^T A \\ A^T A & 0 \end{bmatrix} \begin{bmatrix} x \\ \lambda \end{bmatrix} = \begin{bmatrix} 0 \\ A^T b \end{bmatrix}$$

Using the same notation as before, we write $x = Zx_Z + Nx_N$ and multiply the last equation from the left by the nonsingular matrix

$$\begin{bmatrix} Z^T & 0 \\ 0 & N^T \end{bmatrix}$$

obtaining

$$\begin{aligned} (B_Z^T B_Z)x_Z + B_Z^T B_N x_N &= 0 \\ A_N^T A_N x_N &= A_N^T b \end{aligned}$$

which is the set of equations that uniquely determine $x(0)$ as seen in property 4. □

If we do not take the limit of $x(\epsilon)$ (i.e), fix $\epsilon > 0$ and moreover $b \in Range\epsilon(A)$ then we have $\|b - Ax(\epsilon)\|_2 = \mathcal{O}(\epsilon)$. The last assert can also be seen directly from relation (2.18).

Appendix C

Reduction to the 2D case for flat topology

The flow has 3 components (u, v, w) which depend on (x, y, z). Then, assuming flat topology and either constant geostrophic wind or potential law extrapolation in z direction, the 3D problem of estimating the flow is reduced to a 2D subproblem on a certain layer at 10 meters height.

The only physical boundary conditions to satisfy are at $z = 0$ (null velocity) and $z = H$ where we can choose between the geostrophic wind (whenever it is available) and a potential law extrapolation. If we assume flat topology, and neglect the effect of the third component from the wind flow we get $\varphi(x, y, z) = (u(x, y, z),\ v(x, y, z),\ 0)$ and the incompressibility relation simplifies to $u_x(x, y, z) + v_y(x, y, z) = 0$. Moreover, if we use an extrapolation law in the vertical direction of the form

$$\begin{aligned} u(x, y, z) &= u(x, y, z_0)(z/z_0)^n \\ v(x, y, z) &= v(x, y, z_0)(z/z_0)^n \end{aligned} \tag{C.1}$$

it is enough to ensure that $u_x(x, y, z_0) + v_y(x, y, z_0) = 0$ to get an incompressible approximation. Thus, our velocity problem is reduced to 2 dimensions, and we have to solve it in the layer where the measurements have been taken.

On the other hand, if we use the geostrophic wind as a boundary condition at $z = H = z_G$ then our approximation will be

$$\begin{aligned} u(x, y, z) &= u(x, y, z_0) + (u_G(x, y) - u(x, y, z_0))\frac{log(z) - log(z_0)}{log(z_G) - log(z_0)}, \quad \forall z \in [z_0, z_G] \\ v(x, y, z) &= v(x, y, z_0) + (v_G(x, y) - v(x, y, z_0))\frac{log(z) - log(z_0)}{log(z_G) - log(z_0)} \quad \forall z \in [z_0, z_G] \end{aligned} \tag{C.2}$$

and the potential law (C.1) for $z \in [0, z_0]$. If the geostrophic is assumed to be 2D divergence free (a constant geostrophic is a particular case of this hypothesis) then $u_x(x, y, z_0) + v_y(x, y, z_0) = 0$ is enough to ensure the incompressibility of the 3 dimensional flow.

Appendix D

Other results in the Uruguayan case

D.0.2 Flow results

In this section we present the results for the mean value and the first two principal components of the wind field in the Southern part of Uruguay. At the same time, we reproduce (with permission) the results from [35].

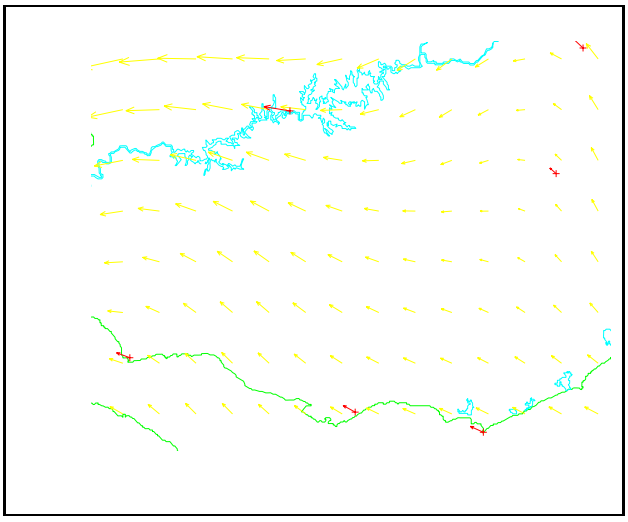

Figure D.1: Results from the proposed method, mean value component

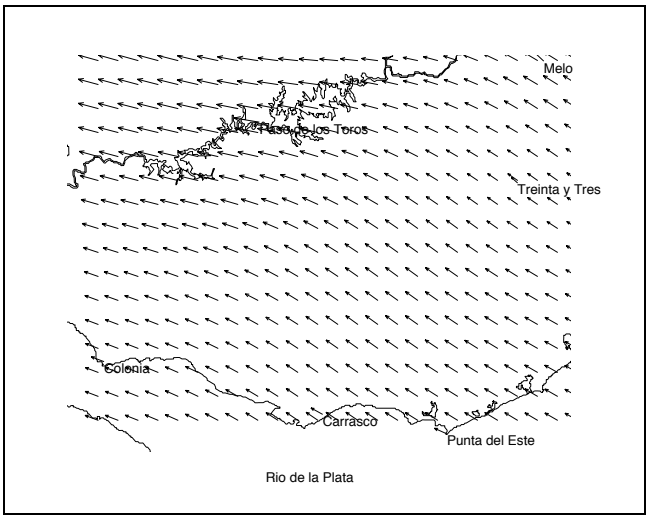

Figure D.2: Results from [35], mean value component

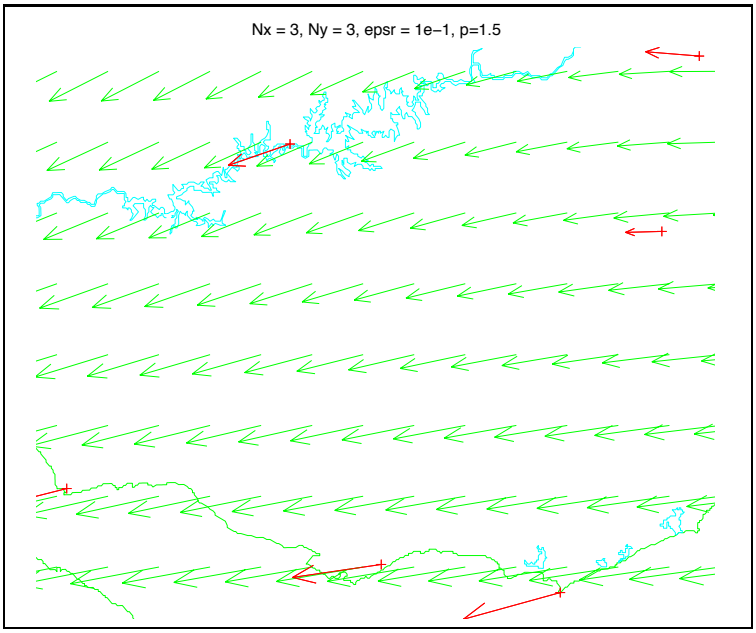

Figure D.3: Results from the proposed method, first principal component

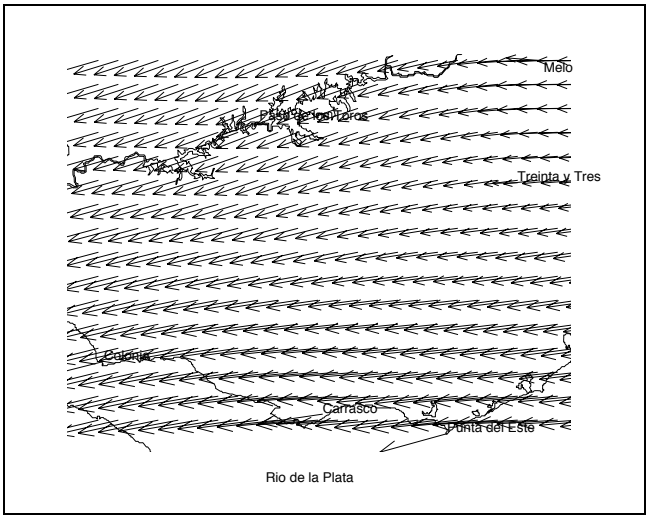

Figure D.4: Results from [35], first principal component

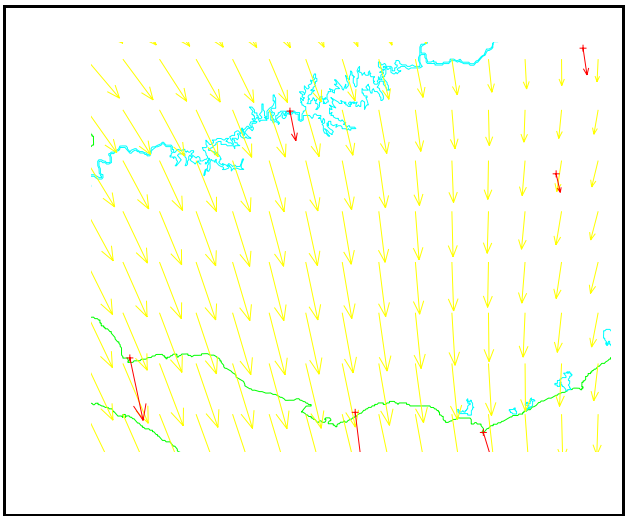

Figure D.5: Smoothed results from the proposed method, second principal component $\epsilon_r = 1e-2$

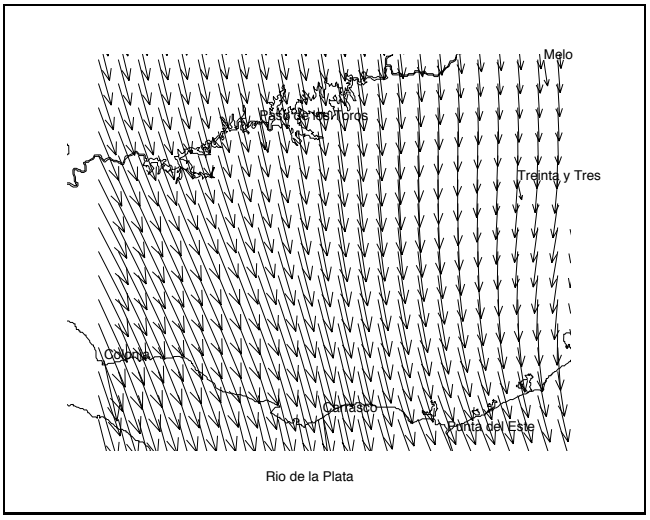

Figure D.6: Results from [35], second principal component

Bibliography

[1] G. Anger. *Inverse Problems in Differential Equations.* Plenum Press, New York and London, 1990.

[2] Å. Björck. Least squares methods. In P.G. Giarlet and J. L. Lions, editors, *Handbook of Numerical Analysis*, volume 1, pages 467–651. North Holland, 1990.

[3] Å. Björck. *Numerical methods for least squares problems.* SIAM, Philadelphia, 1996.

[4] G. Dahlquist and Å. Björck. *Numerical methods.* (New edition, to appear), 1998.

[5] M.H. Dickerson. Mascon. a mass consistent atmospheric flux model for regions with complex terrain. *Applied Meteorology*, 17(3):241–253, March 1978.

[6] M. P. Ekstrom and R. L. Rhodes. On the application of eigenvector expansions to numerical deconvolution. *Journal of Computational Physics*, 14:319–340, 1974.

[7] L. Eldén. Algorithms for regularization of ill-conditioned least squares. *BIT*, 17:134–145, 1977.

[8] R. M. Endlich, F. L. Ludwig, C. M. Bhumralkar, and M. A. Estoque. A diagnostic model for estimating wind energy. *Applied Meteorology*, 21:1441–1454, 1982.

[9] R.M. Endlich and J. Lee. An improved diagnostic model for estimating wind energy. Technical report, Pacific Northwest Laboratory, 1983. PNL4256.

[10] P. C. Hansen G. H. Golub and D. P. O'Leary. Tikhonov regularization and total least squares. August 1997.

[11] O. Gil and R. Tempone. On the existance and uniqueness of minimizers arising from the approximation and interpolation of divergence free flows. December 1998.

[12] G.H. Golub and C.F. van Loan. *Matrix Computations, second edition.* Johns Hopkins, 1988.

[13] X. Guo and J.P. Palutikof. A study of two mass- consistent models: Problems and possible solutions. *Boundary layer meteorology*, 53:303–332, 1990.

[14] J. Hadamard. *Lectures on Cauchy's Problem in Linear Partial Differential equations.* Yale University Press, New Heaven, 1923.

[15] P.C. Hansen. Perturbation bounds for discrete tikhonov regularization. *Inverse Problems*, 5:41–44, 1989.

[16] P.C. Hansen. Regularization, gsvd and truncated gsvd. *BIT*, 29:491–504, 1989.

[17] P.C. Hansen. The discrete picard condition for discrete ill-posed problems. *BIT*, 30:658–672, 1990.

[18] P.C. Hansen. Truncated svd solutions to discrete ill-posed problems with ill determined numerical rank. *SIAM Journal Sci. Stat. Computations*, 11:503–518, 1990.

[19] P.C. Hansen. Analysis of discrete ill posed problems by means of the l-curve. *SIAM review*, 34:561–580, 1992.

[20] P.C. Hansen. *Rank deficient and Discrete Ill-Posed problems. Numerical Aspects of Linear Inversion.* SIAM, Philadelphia, 1997.

[21] P.C. Hansen, T.C. Sekii, and H. Shibahashi. The modified truncated svd method for regularization in general form. *SIAM Journal Sci. Stat. Computations*, 13:1142–1150, 1992.

[22] C.L. Lawson and R. J. Hanson. *Solving Least Squares Problems.* Prentice-Hall, Englewood Cliffs, 1974.

[23] C. Y. Liu and W. R. Goodin. An iterative algorithm for objective wind field analysis. *Monthly Weather Review*, 104:784–792, June 1976.

[24] F. L. Ludwig and G. Byrd. An efficient method for deriving mass-consistent flow fields from wind observations in rough terrain. *Atmos. Environment*, 14:585–587, 1980.

[25] Hino M. and Yang Men. Stereoscopic imaging technique for instantaneous 3-dimensional velocity fields form sparse and insufficient velocity data. application to turbulent structure and oscillatory flow. Madrid, Spain, 1991. 24^{th} IAHR Congress,. 8 pages.

[26] Hino M., Yang Meng, and Masaaki Murayama. An attempt at estimating the instantaneous velocity field of a nonstationary flow from velocity measurements at few points. *Fluid Dynamics Research*, 7:101–108, 1990.

[27] The Mathworks Inc., Natick, Mas. USA. *MATLAB User's Guide*, 1992.

[28] K. Miller. Least squares methods for ill-posed problems with a prescribed bound. *J. Math. Anal.*, 1:52–74, 1970.

[29] M.B. Richman. Rotation of principal components. *J. Climatology*, 6:293,335, 1986.

[30] Y. Sasaki. Some basic formalisms in numerical variational analysis. *Mon. Weather Review*, 98(12):875–883, December 1970.

[31] C. Sherman. A mass consistent model for wind fields over complex terrain. *Journal of applied meteorology*, 17, 312-319 1978.

[32] G. Strang. *Introduction to applied mathematics.* Wellesley - Cambridge Press, 1986.

[33] A. N. Tikhonov and V. Y. Arsenin. *Solutions of Ill-Posed Problems.* Winston and sons, Washington, D.C., 1977.

[34] R.M. Traci, G.T. Phillips, and P.C. Patnaik. *Developing a site selection methodology for wind energy conversion systems.* Science Applications Inc., September 1978. Prepared for the United States Department of Energy.

[35] C. López Vazquez. Predicción de la serie temporal del campo de velocidad del viento sobre topografía compleja.
Aplicación a la zona sur del Uruguay. Master's thesis, Facultad de Ingeniería, Universidad de la República, Uruguay, July 1993. In Spanish.